INTRINSIC DEGRADATION MECHANISMS OF BARIUM TITANATE BASED MULTILAYER CERAMIC CAPACITORS

by

J.N. Schunke

Thesis submitted to the faculty of

Virginia Polytechnic Institute and State University

in partial fulfillment of the requirements for the degree of

MASTER OF SCIENCE

in

Materials Engineering

APPROVED:

L.C.Burton, Chairman

J.L. Lytton

R. H. Zallen

June 1985.

Blacksburg, Virginia

INTRINSIC DEGRADATION MECHANISMS OF BARIUM TITANATE BASED MULTILAYER CERAMIC CAPACITORS.

by

J.N. Schunke

ABSTRACT

A study was conducted into the intrinsic degradation behavior of X7R and Z5U capacitors. The major goals of this research were:

1) to determine current-voltage, activation energy and leakage current characteristics for such capacitors.
2) to investigate how these characteristics change with degradation;
3) to investigate possible correlations between observed behavior and capacitor microstructure or composition.

Examination of capacitor microstructures revealed large differences in grain morphology and electrode spacings. The development of a color gradient between positive and negative electrodes with degradation was observed in one type of capacitor.

Compositional studies using EDAX, AUGER, and microprobe analyses failed to detect gradients in dielectric

composition in degraded capacitors indicating that gradients are less than 0.1 atomic percent. Current-voltage studies showed a 3/2 power dependance, at voltages above one volt for X7R capacitors indicating space charge limited current. This dependance was attributed to point emission from electrode protuberances. The 3/2 dependance was observed to shift to a square law behavior with degradation. This change was attributed to a increase in conductivity of the dielectric near the cathode, blunting the effect of electrode protuberances. Z5U capacitors were found to have ohmic behavior. No Schottky or Poole Frenkel currents were observed.

Degradation studies were carried out on capacitors at 2 to 8 times the rated voltage, and at temperatures from 100 to 150^{o}C. Leakage currents in actively degrading capacitors were observed to rise exponentially with time. This rise was accompanied by a gradual decrease in activation energy. A model is proposed to explain the observed current vs degradation behavior.

ACKNOWLEDGMENTS

The author would like to express his sincerest gratitude to Dr. L. C. Burton for his contributions and suggestions throughout this research effort. His time and support are deeply appreciated.

The author would also like to extend his thanks to Dr. R. Zallen and Dr. J. L. Lytton for their helpful suggestions and for serving on his committee. Financial support of the is also acknowledged.

A special thanks is in order for two people, my wife and a friend for their typing, proofreading and encouragement throughout this research effort. I would also like to express my thanks to for the EDAX and most of the SEM photography, for Auger analysis and to for the operation of the microprobe. Finally I would also like to express my sincere thanks to for all their assistance with the secretarial work during the authors tenure in graduate school.

TABLE OF CONTENTS

LIST OF FIGURES

LIST OF TABLES

LIST OF SYMBOLS

I	Current
V	Voltage
T	Temperature
t	Time
ρ	Resistivity
ε	Dielectric constant
μ	Drift mobility
ϕ	Activation energy
A	Cross-sectional area
L	Layer thickness
k	Boltzmann's constant
q	Charge on an electron
n	Carrier concentration
N_c	Density of states - conduction band
N_t	Trap density
ΔE	Trap energy - below conduction band edge
E	Electric field
ϕ_{BO}	Zero voltage barrier hieght
E_F	Fermi energy
E_C	Conduction band energy
N_{GB}	Density of states - conduction band

Chapter I

INTRODUCTION

Recent increases in demand have greatly expanded the ceramic capacitor industry. Sales increased by 43% in 1983 and approximately 39% in 1984. This year (1985), sales of multilayer ceramic capacitors (MLC's) are expected to exceed 700 million dollars with over 10 billion MLC capacitors being sold[1].

With the rise in use of MLC's there has been an increasing emphasis placed on reliability, especially for defense applications where reliability is crucial. Failures in MLC's may be divided into two categories, intrinsic failure and extrinsic failure: extrinsic failures are caused by defects induced during processing. Most infant mortalities may be ascribed to extrinsic defects. Intrinsic failures are those due to the inherent chemistry and physics of the capacitor itself. Activity in quality control has emphasized extrinsic failure mechanisms and as a result this area is fairly well understood. Tests have been developed to screen out parts with extrinsic defects (i.e. delaminations, cracks, voids) with fairly high accuracy[2-4].

Comparatively little research has been done in the area of intrinsic failure mechanisms. Intrinsic failures are due to the inherent chemistry and physics of the MLC and not due to faulty manufacture. Mechanisms for intrinsic failure include ionic and vacancy migration from electrodes, segregation or phase separation and generally require long term service to show up. Intrinsic failure mechanisms are just as important as processing defects in long term high reliability applications and will become much more important as the dielectric thickness is decreased.

The requirements for capacitors are primarily electrical in nature. Compositions are not specified and any material composition that will achieve the desired properties may be used. As a result, capacitor compositions vary widely from one manufacturer to another. The composition used by any given company for a particular capacitor type is proprietary. Even if the exact compositions were known, variables in powder production and sintering treatments would prevent exact duplication of capacitor characteristics. That these compositions, which have been developed on a totally experimental basis, work so well is a tribute to the individuals who developed them.

Since the raw materials for $BaTiO_3$ are only about 99% pure, manufacturers have to deal with a host of impurities already present (Table 1.1), and add various elements and compounds to produce the desired properties. Dopants are added for a large number of reasons: increasing capacitor lifetime, modifying the dielectric constant, increasing the voltage stability, altering the Curie temperature, lowering the temperature dependence of the dielectric constant, reducing dielectric losses, preventing reduction, inhibiting grain growth, and lowering the sintering temperature. Some of the elements used to modify barium titanate based dielectrics for capacitors are listed in Table 1.2. Some of the major uses of these elements are:

a) Lowering the sintering temperature - oxides of bismuth, boron, copper cadmium, silicon, zinc and lead (also added as $Pb_5Ge_3O_{11}$) are used as glass formers[6,7].

b) Lowering the temperature dependance of the dielectric constant - bismuth and neodymium are commonly used [8].

c) Reducing grain growth - niobium, dysprosium, lanthanum, samarium and manganese [9-12].

d) Inhibiting reduction during firing in reducing atmospheres - manganese, iron, gallium, chromium and magnesium [13-16].

TABLE 1.1 Some impurities found in Barium Titanate raw material.(Analysis for one supplier[5])

Na	0.0006	-	0.006	wt %
Al	0.0005	-	0.005	
Si	0.00004	-	0.0004	
Fe	0.001	-	0.01	
Co	0.0006	-	0.006	
Cu	0.00005	-	0.0005	
Mg	0.00006	-	0.0006	
Cr	0.0008	-	0.008	
B	0.001	-	0.01	
Be	0.0004	-	0.004	
Ge	0.0005	-	0.005	
W	0.001	-	0.01	
Ni	0.0005	-	0.005	
V	0.0005	-	0.005	

TABLE 1.2 Some elements which may be used in doping Barium Titanate for MLC applications

Pb	Bi
Sr	Dy
Sm	Ca
Sb	Zn
La	Zr
Nb	Ga
Ag	Cr
Y	Mg
Gd	Na
Fe	Ni
Mn	Cu
P	Ge
Co	Si
Nd	Cd

e) Lowering the Curie point - iron, nickel, zinc, strontium, lanthanum, zirconium and niobium [13,17-19].

f) Increasing the voltage stability - calcium and strontium[20].

In addition to these additives, anti-ferroelectrics such as $NaNbO_3$ may be added to reduce dielectric saturation problems[21].

Besides the various dopants, initial powder sizes, polymer binders, electrode type and composition, sintering times and sintering temperatures will all affect the dielectric properties of the ceramic capacitor. With this large number of variables it would be impossible to determine the ideal composition and manufacturing process for any given capacitor application by simple trial and error. An understanding of the degradation mechanisms is therefore important. If the intrinsic failure mechanism for a given capacitor were understood, the composition and processing could be modified to improve capacitor lifetime, thus increasing the capacitor's reliability and allowing use under more severe conditions (higher field strengths and higher temperatures). It is hoped that by understanding the intrinsic failure mechanism(s) of barium titanate based dielectrics, $BaTiO_3$ based thick films may be developed for

commercial applications. The present day compositions for such applications are not reliable.

Chapter II

LITERATURE REVIEW

Research has shown that small changes in capacitor composition can change capacitor lifetime and dielectric properties by orders of magnitude. While it is known that dopants and impurities affect capacitor lifetimes, it is unclear how (mechanistically) dopants and impurities alter capacitor properties.

The emphasis of this review is placed on known indicators of long term reliability and on characteristics which change with degradation.

2.1 The relationship between stoichiometry and resistivity

Dielectric constant and resistivity are the two most basic attributes of a capacitor material. In addition to its effect on charge storage, resistivity appears to be a good indicator of capacitor lifetime. The higher the resistivity of the dielectric, the longer the lifetime of the capacitor. The effect of doping on $BaTiO_3$ has been studied by a number of authors and two stages have been observed. Pure barium titanate is an insulator. Adding

small amounts of dopants causes an increase in conductivity and the ceramic becomes semiconductive. As the dopant level increases further, conductivity drops back down and the ceramic becomes insulating again (Figure 2.1). Such trends with impurity levels have been found for Nb, Sb, Sm, La, Y, Ca and Ag[19,22,24,26-28]. The increase in resistivity has been attributed to a lower anion vacancy concentration as predicted by the mass action law. Dopants with an excess positive charge tend to improve capacitor lifetimes. This is especially apparent in accelerated life test studies where both voltage and temperature are increased. For example, the addition of 0.4 wt. % of MnO_2 to high purity $BaTiO_3$ (99.8%) increases resistivity by half an order of magnitude and increases capacitor lifetime by over three orders of magnitude[16]. Raising the level of Mn to 0.6% by weight further increases capacitor lifetime.

2.2 Relationship between dielectric properties and grain size

Reducing grain size has been shown to improve the dielectric properties and lifetime of capacitors. The increase in resistivity with doping levels can be directly correlated to reduction in grain size.

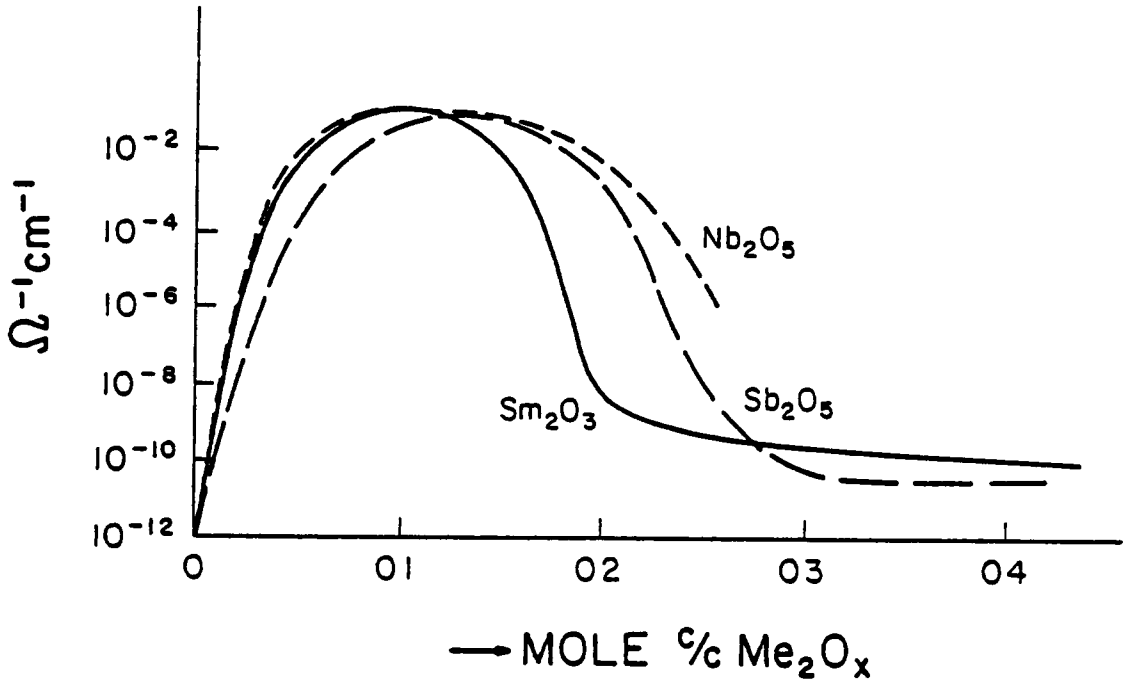

Figure 2.1 Conductivity versus doping concentration[22-26].

Intermediate levels of doping with niobium (≈0.2%) produces a heterogeneous microstructure with some sections having a small grain size (~1μm) interspersed with large grains (20-30 μm). Kahn[29] examined this phenomena and found the large grains were semiconducting, having a conductivity approximately ten orders of magnitude higher than the small grains. Similar results have been found for yttrium doped $BaTiO_3$[28]. The correlation between fine grain size and increased resistivity has also been found for Dy, La, and Mn[11,22,24,30]. Further it has been shown that for the same composition, increased sintering time decreases with the dielectric strength. This has been strongly correlated with an increase in the grain size[31].

Work on polycrystalline $BaTiO_3$ has shown that potential barriers exist at grain boundaries[32-35]. At present the actual nature of the potential barrier is open to discussion and may vary with capacitor composition. Three possible potential energy diagrams for grain boundaries are shown in Figure 2.2. Grain boundary resistances ten times greater than the resistance in the grain itself have been reported in large grained $BaTiO_3$[31]. A very important aspect of doping is the inhomogeneous distribution of the dopants. Studies have shown that most additives to $BaTiO_3$ are concentrated at the grain boundaries. The classic experiment

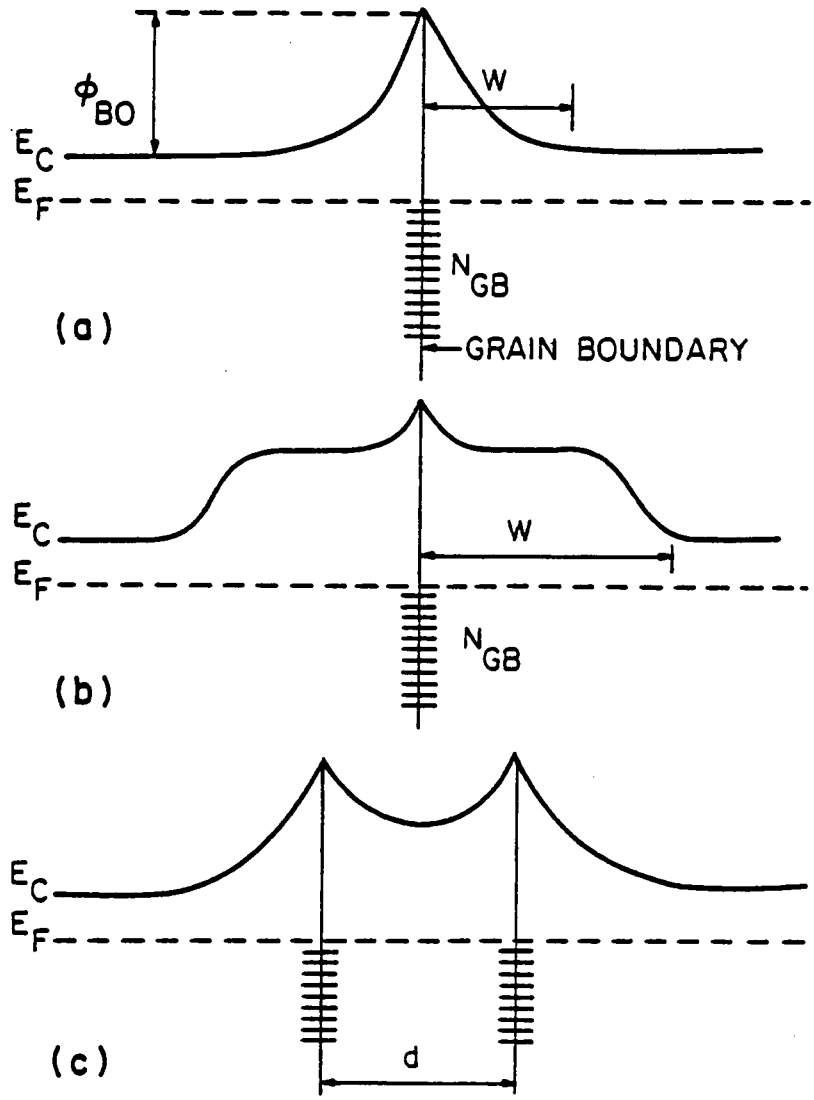

Figure 2.2 Grain Boundary Potential Barrier. Potential energy diagrams for three possible cases: (a) uniform donor density and thin boundary region, (b) intrinsic region near the grain boundary, (c) thin layer of second phase separating grains.

showing how dopants at the grain boundaries affect capacitor lifetimes was performed by Lehovic and Shirn[36] who diffused bismuth oxide vapor along the grain boundaries of $BaTiO_3$ ceramic (Figure 2.3). It would appear that the dopants affect the height of the potential barrier at the grain boundaries and do not greatly affect the width of the barrier.

2.3 Changes in field distribution with time (degradation)

Two methods have been used to study the changes in field distribution with degradation in $BaTiO_3$. Goto and Kachi[37] used the Kerr effect to optically study changes in field distribution with time. Lehovic and Shirn[36] used a movable probe and voltmeter to measure voltage distribution across $BaTiO_3$ ceramic as a function of time. In the optical study on $BaTiO_3$, single crystals showed a striking change in field distribution with time (Figure 2.4a). The field strength at the anode first increased and then gradually decreased. Comparison of the capacitor leakage current (Figure 2.4b) and the field distribution revealed that the initial increase in resistivity appeared to begin when the field strength at the cathode began decreasing and that the

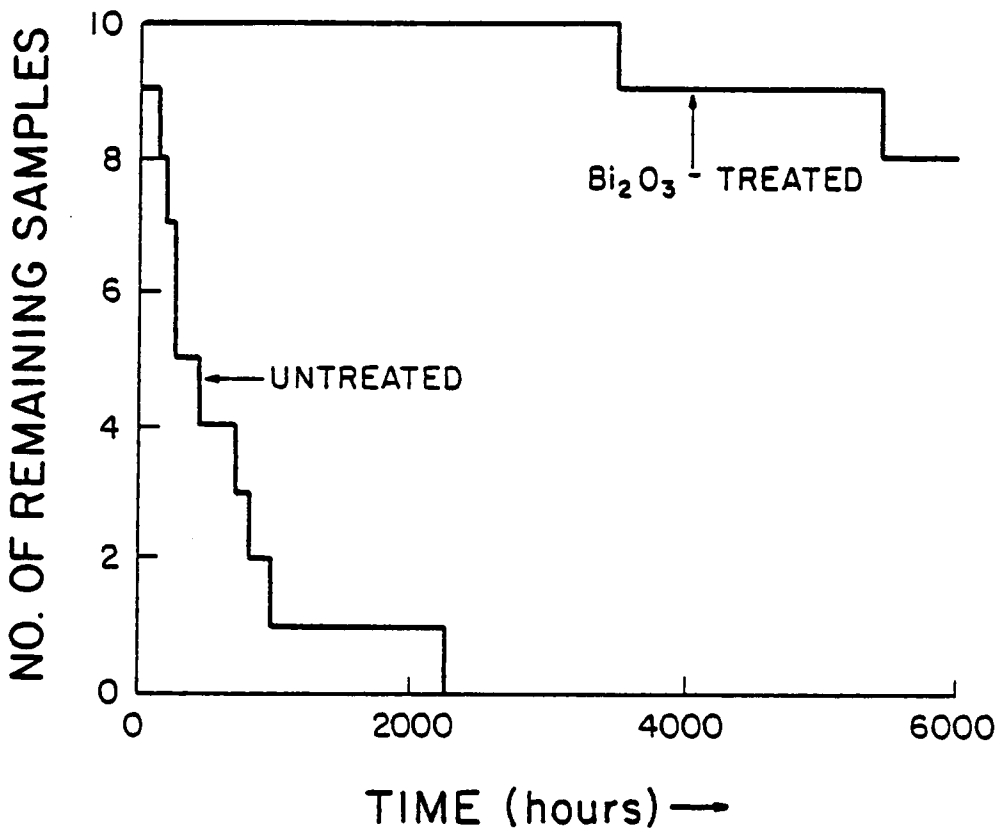

Figure 2.3 Comparative Life Test of Ba_2O_3 treated and untreated capacitors[35].

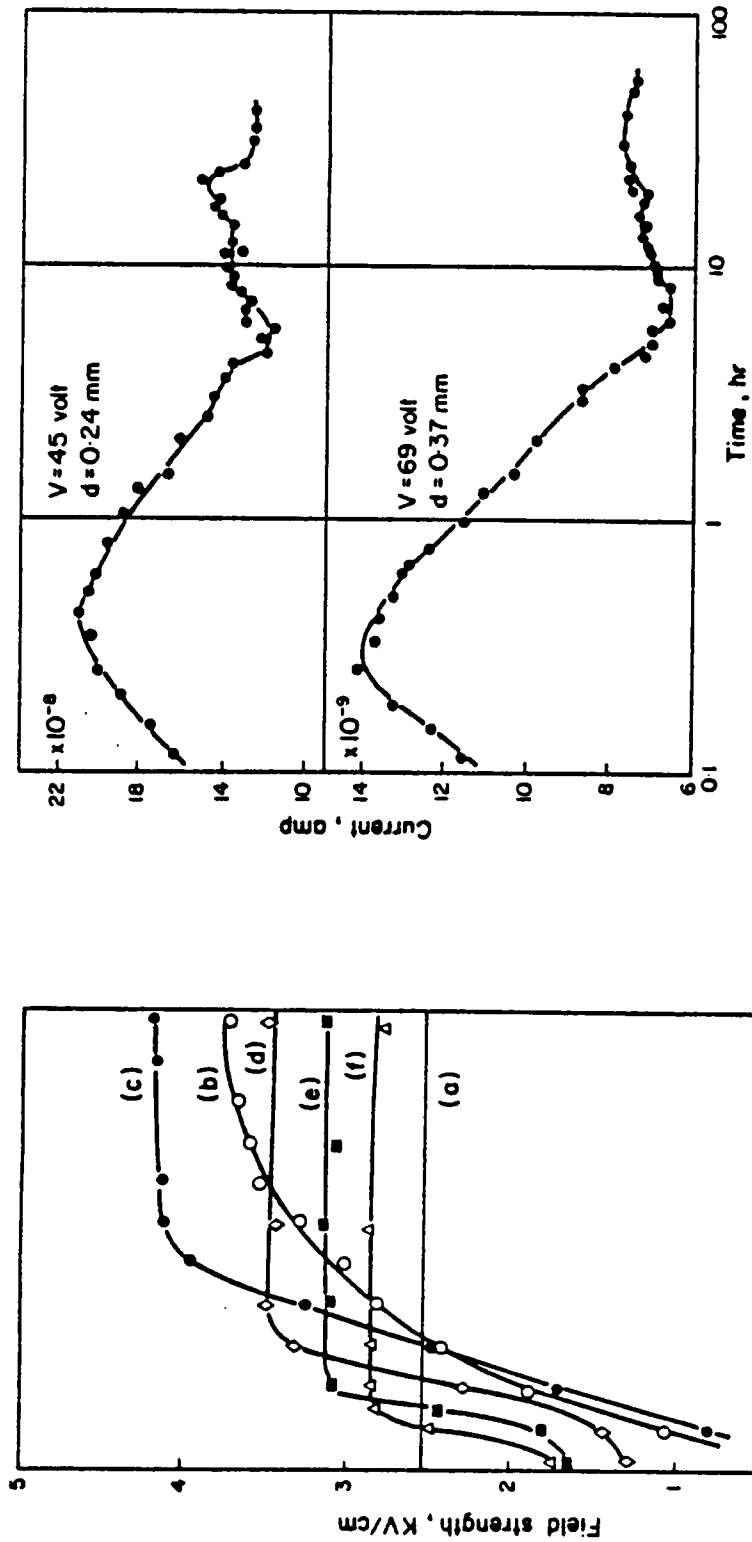

Figure 2.4 Changes in field strength distribution and leakage current with time for $BaTiO_3$ single crystals[37].
Times on field strength diagram: a=10 sec, b=1.5 hr, c=7.5 hr, d=10 hr, e=18 hr, f=24 hr.

resistivity began dropping as the field strength at the cathode increased. These results were similar to previous data on polycrystalline $BaTiO_3$. Lehovic and Shirn[36] used a movable probe to determine the potential distribution for polycrystalline $BaTiO_3$ as a function of time. By calculating the distribution field strength from these results it was found that initially a high conductivity region was being injected from the cathode and a low conductivity region from the anode. As degradation time increased, the low conductivity region moved closer to the cathode in a manner similar to the results shown for single crystal $BaTiO_3$. Comparison with a plot of leakage current vs. time revealed that the initial drop in conductivity occurred with the presence of an inflection point in the potential distribution curve (high resistivity region shifting away from the anode). The following rise in conductivity occurs when the inflection point disappears (high resistivity region reaches the cathode).

The most widely accepted intrinsic failure mechanism is oxygen vacancy migration[6,36,38-41]. To date oxygen vacancy migration is only a proposed mechanism. Models have not yet been developed to explain where exactly the oxygen vacancies form (grain boundaries vs anode), how they move through the dielectric (grain boundaries, grains, or a

combination of the two) and cause failure to occur. Electromigration of Pd electrode material is considered here as an extrinsic failure mechanism, since electromigration of Pd requires both salt contamination and filing of voids between the electrodes with water[42].

One phenomenological result of electrical degradation is the appearance of a color change of the dielectric in certain cases[36,43-45]. This color change has been observed in both single crystal and polycrystalline samples degraded under a DC voltage stress[44-46]. It appears that capacitor composition determines if the ceramic will or will not change in appearance with degradation. Similar darkening occurs due to oxygen depletion[47]. It has been proposed that the darkening is due to F centers - electrons trapped at oxygen vacancies[48,49].

2.4 Effect of temperature and voltage stress.

Studies have shown that capacitor lifetime under a DC voltage stress is inversely proportional to the exponential of temperature[50]. Research has also indicated that lifetime is inversely proportional to n^{th} power of field strength where n varies depending on capacitor composition. These results have been shown to hold for both DC and AC

applications[16,39]. Relative mean times to failure have been modelled according to the empirical equation[51]:

$$t_1/t_2 = (V_2/V_1)^n \quad \exp\,[\phi/K\,(\,1/T_1-1/T_2\,)]$$

where ϕ is an activation energy. This equation has shown itself useful for numerous capacitor compositions, at least at lower voltages. As voltage is increased, a "knee" tends to appear in the curve of ln lifetime vs 1/T. There appears to be two voltage stress regimes. At lower voltages values of n tend to range from 2.5 to 4.0[16,39,51-53]. The high voltage regime was found more recently and values of n>10 have been reported[16]. No theory has been put forward yet to explain why degradation times follow this equation or why a knee would appear in the curve. There is gradual change in the type of failure mode that should be noted. As voltage stress is increased a larger percentage of capacitors fail in the avalanche breakdown mode indicating failure due to extrinsic defects. Whether a capacitor has failed intrinsically or extrinsically may be determined by its leakage current versus degradation (time) curve. Capacitors which fail due to extrinsic defects, have relatively shorter lifetimes, fail at lower leakage currents and show a discontinuous rise in the leakage current. This type of failure is termed avalanche breakdown (ABD) where the capacitor fails with an abrupt burst of current and

contrasts to capacitors which fail due to intrinsic mechanisms. Intrinsic failure is characterized by thermal runaway or TRA. These capacitors have failed by self heating caused by the magnitude of the current (Joule heating). Comparison of the two types of failure modes is shown in Figure 2.5.

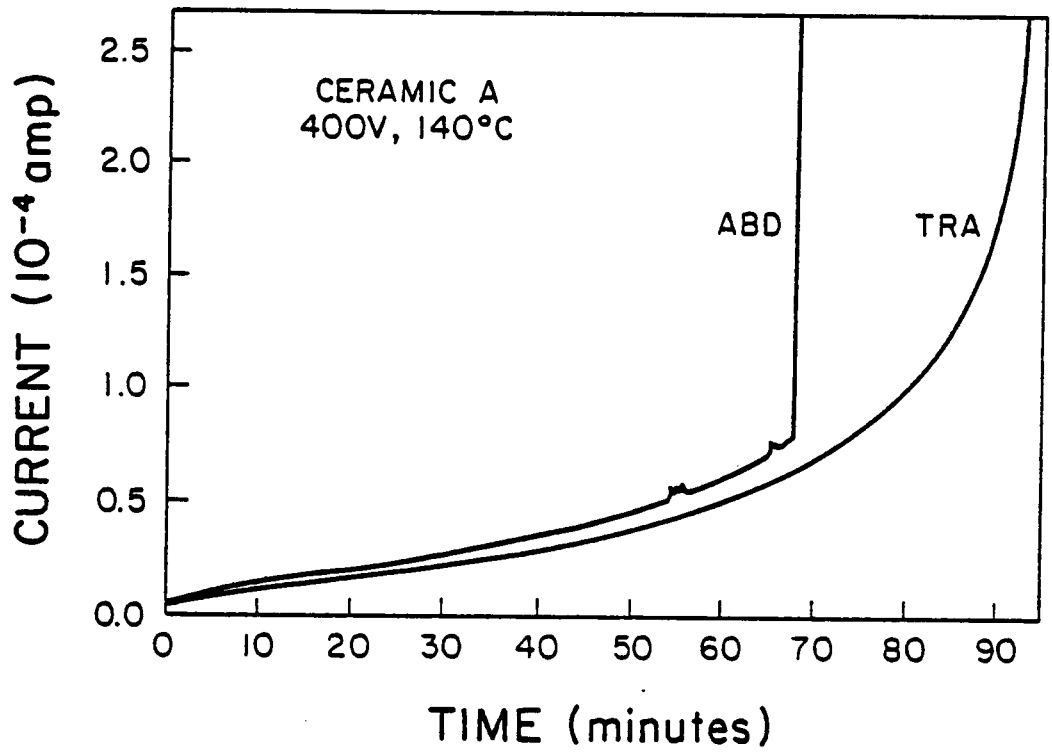

Figure 2.5 Comparison of leakage current versus time for capacitors that fail by thermal runaway as compared to avalanche breakdown[53].

Chapter III

RESEARCH OBJECTIVE

Ceramic capacitors are imperfectly understood at best. Researchers are not in agreement about the conduction mechanism or even the charge carrier in $BaTiO_3$ based capacitors. The main objective of this research was to obtain a better understanding of degradation mechanisms in $BaTiO_3$ based MLC's using materials, compositional and electrical techniques. To develop a model for electrical degradation a number of questions were posed:

1) Is oxygen movement analytically observable? Is there any other ion movement?
2) Is there a visual difference between new and degraded capacitors?
3) What fraction of the leakage currents is ionic?
4) How do leakage currents change with degradation?
5) How do activation energies change with degradation?
6) How do I-V curves change with degradation?
7) What is the charge carrier mobility?
8) Does capacitor microstructure affect the observed characteristics?

It was felt that by answering these questions, enough information would be obtained to determine the predominant charge carrier and develop a model which would explain how capacitors degrade with time under voltage. These questions were approached from several directions:

a) commercially manufactured capacitors (mainly X7R and Z5U types) were degraded using accelerated life testing, typically at 150°C and four to eight times the rated voltage. Current voltage characteristics and activation energies were checked at various degrees of degradation as judged by insulation resistance.

b) New and degraded capacitors were cross sectioned and examined using optical and scanning electron microscopy.

c) Compositional measurements were made on cross sectioned samples of new and degraded capacitors using energy dispersive x-ray analysis (EDAX), Auger electron spectroscopy (AES) and electron beam microprobe.

d) X7R and Z5U capacitors were degraded using accelerated life test methods. Activation energies, I-V curves, and leakage currents were monitored during the degradation process.

e) Hall effect measurements were made on new and hydrogen reduced X7R type ceramic in an effort to determine carrier type and mobility.

Commercially manufactured X7R and Z5U capacitors were chosen for this research due to their widespread use. (X7R capacitors are commonly specified for military applications, an area where high reliability is desired.)

The Electronic Industries Association specifications for these two capacitor types are as follows:

X7R ±15% capacitance change from +25°C reading over the temperature range -55°C to +125°C.

Z5U +22% -56% maximum capacitance change from +25°C reading over the temperature range +10°C to +85°C.

No compositional requirements are specified.

Chapter IV

THEORETICAL BACKGROUND

This chapter presents the theoretical background necessary to understand the results of the electrical experiments. The various types of current that have been proposed to flow in MLC's are reviewed, and the controlling variables are discussed.

4.1 Ohmic Conduction.

In ohmic conduction, the metal-insulator junction does not present a potential barrier to current flow. The steady state of electrical behavior is controlled by the bulk properties of the insulator, and the relationship between current and voltage may be expressed as:

$$I = \Sigma\ n\ q\ \mu\ V\ A\ /\ L$$

Current may consist of both electronic and ionic contributions. The temperature dependance of I is often of the form:

$$I = I_o\ e^{-\phi/kt}$$

where ϕ is a thermal activation energy. In MLC's this activation energy may be due to grain boundaries or small polaron hopping.

4.2 Space Charge Limited Current

The space charge limited current (SCLC) case occurs when the injected carrier concentration exceeds the bulk carrier concentration. This results in a "space charge" build up of uncompensated electrons at the cathode (ion injection from electrodes is considered unlikely in MLC's) which alters the local field. For this type of conduction mechanism the current-voltage relation depends on electrode geometry. Normally MLC's are considered to have planar,or near planar, electrodes. For this case[54]

$$I = \frac{9}{8}\,\theta\,\varepsilon\,\mu\,V^2\,A/L^3$$

where θ is a trapping parameter defined as

$$\theta = \frac{N_c}{2N_t}\,e^{-\Delta E/kT}$$

For the case of a point electrode emitting to a roughly planar anode the current voltage relation may be written as[55]:

$$I = \frac{2\pi\sqrt{2}}{3}\,\mu\,[\theta q\varepsilon n]^{1/2}\,V^{3/2}$$

This case may pertain to MLC's considering the possibilities of forming electrode protuberances from ink flowing into pores and between grains in the dielectric sheet. If protuberances are present they will act as point emitters since the electric field will be much larger at the tip than along the rest of the electrode (Figure 4.1).

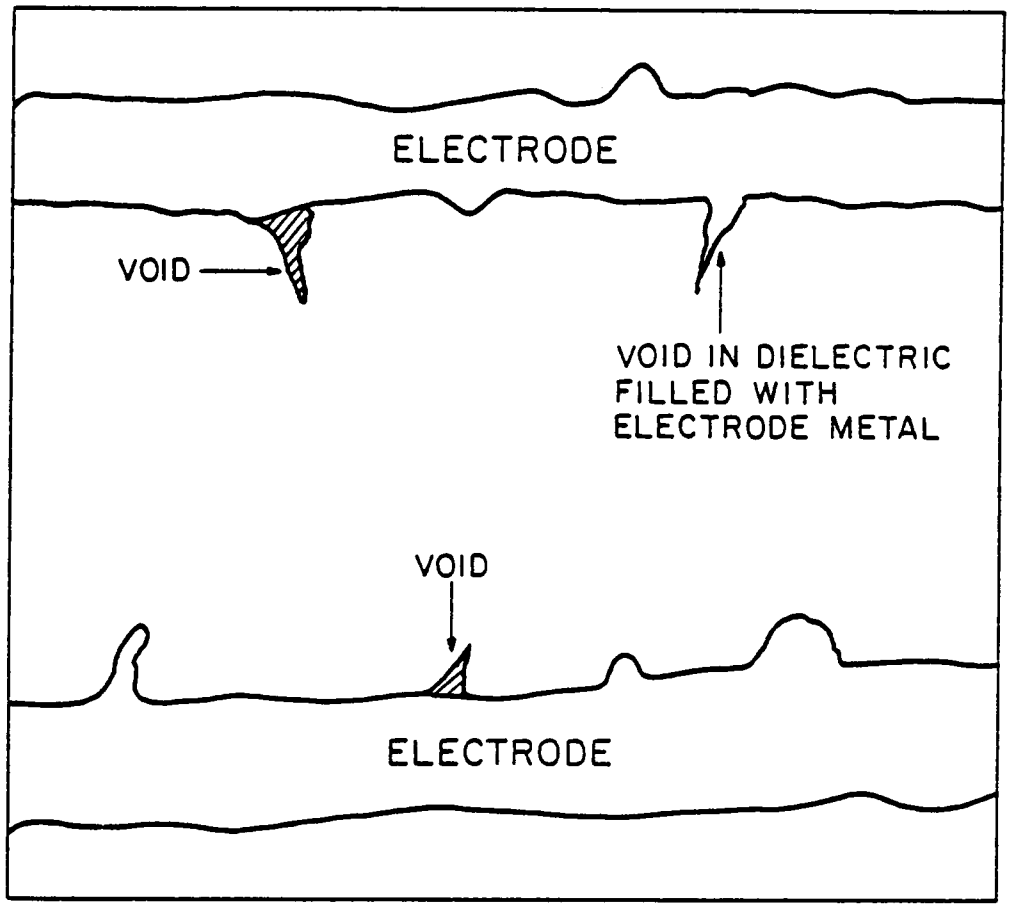

Figure 4.1 Electrode protuberances - a potential source of enhanced electron injection.

4.3 Schottky Current

Schottky current arises from electron emission across a barrier as a result of field effects lowering the potential barrier. Schottky current has an exponential dependance on the field strength and may be expressed by the equation[56]:

$$I = I_o \exp[\frac{B}{T}(E/k)^{1/2}]$$

where B is a constant. Whether this type of current will arise from rectifying contacts at the electrode (Schottky emission), or potential barriers at traps and grain boundaries (Poole-Frenkel current), is open to discussion. While rectifying contacts may seem unlikely in MLC's it has been suggested that a surface depletion layer may cause rectification[57]. A detailed list and explanation of the variables affecting the observed current-field behavior for Schottky emission is presented in Anderson and Days work[58].

Plots of current vs voltage for ohmic, SCLC and Poole-Frenkel currents are shown in Figure 4.2 and illustrate I-V plots with all other factors taken as constants. In reality, the mobility and dielectric constant may be voltage (field) dependant. The field dependance of the dielectric constant for $BaTiO_3$ based capacitors is well known. Whether this will cause a noticeable deviation from

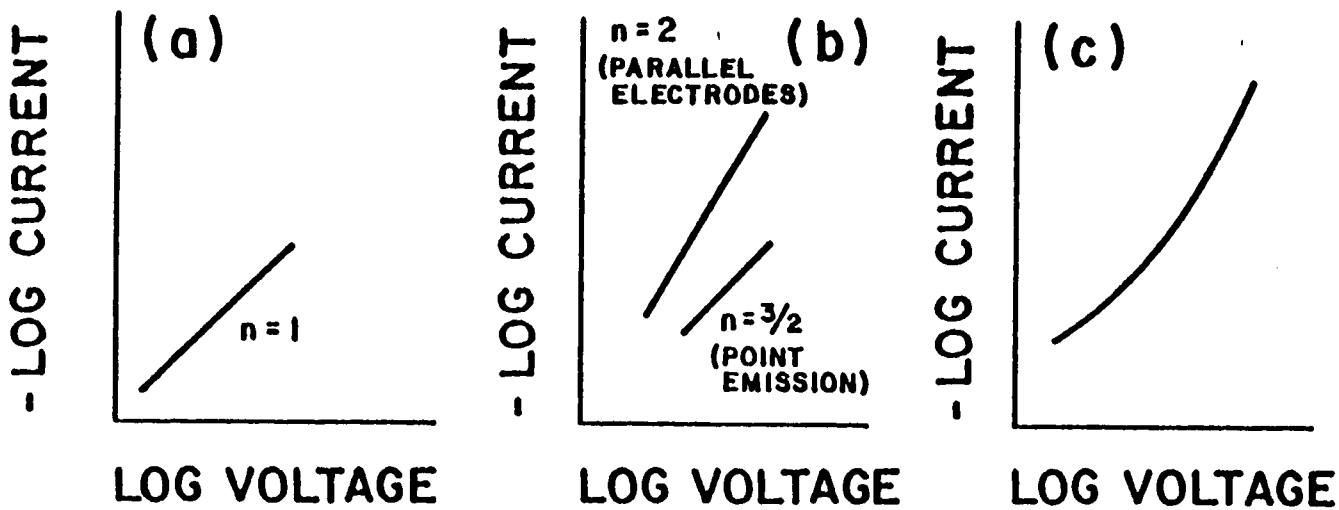

Figure 4.2 Generic I-V curves for ohmic, space charge limited and Poole-Frenkel currents.
(a) Ohmic, (b) SCLC, (c) Poole-Frenkel.

the linearity depends on the particular composition and its voltage sensitivity. Field emission (tunneling) was not discussed in this section since it requires very high fields ($>10^6$ V/cm) and would not appear without Schottky emission appearing first (at lower fields).

Chapter V

EXPERIMENTAL METHODS AND MATERIALS

5.1 Materials

5.1.1 Types of Capacitors used

Several types of commercial capacitors were used for this work. Up to this point the word "type" has been used to signify between different classes of capacitors X7R, Z5U, COG, etc. Due to the large differences in degradation behavior (found here) from one manufacturer to another, the word type will now be used to differentiate between manufacturers. The majority of the results published here are the result of tests on X7R and Z5U capacitors from three different manufacturers. Table 5.1 gives the capacitor classes, voltage rating, nominal capacitance, and the designation used for each in this paper.

5.1.2 Specimen Preparation

The procedure used here differed from the EIA standard RS-469[2] in two important respects:

1) Decapsulation, and

2) hand grinding versus rotary wheel grinding.

Table 5.1. Capacitor classes, ratings and designations.

Designation	Capacitor class	Capacitance	Voltage Rating	Manufacturer
X7R type A	X7R	100nF	50 V	Corning
X7R type B	X7R	1µF	50 V	Sprague
Z5U type A	Z5U	1µF	50 V	Sprague
Z5U type B	Z5U	1µF	50 V	Centralab

Initial studies of decapsulated capacitors showed that chemically decapsulating capacitors (using dimethylformamide) caused a permanent color change in the dielectric. Subsequent cross-sectioning of capacitors with their coatings intact revealed that satisfactory results could be obtained without removing the plastic coatings provided care was taken in the grinding steps. The rotary grinding steps were subsequently changed to hand grinding when tests showed a much lower degree of ceramic pullout for hand grinding.

New and degraded capacitors were prepared for examination using the following procedure:

a) Capacitors were mounted in epoxy for cross-sectioning perpendicular to the electrodes and end terminations. Struers epoxy was used for the mounting material. The epoxy was cured at room temperature.

b) Rough grinding through the plastic coating on the capacitor was performed on a rotary grinding wheel using 180 mesh grit. After the electrodes were reached, hand grinding on 240 grit paper was used to reach the approximate depth desired. Finish grinding was then performed using 320, 400 and 600 grit paper. All grinding steps were "wet".

c) Polishing was accomplished in two stages: rough polishing on microcloth (from Buehler Ltd.), using a slurry of 1 micron alumina and fine polishing on a syntron vibratory polisher using 0.05 micron alumina.

d) Etching: Certain prepared samples were etched with a solution containing 0.5% by volume hydrofluoric acid and 5 % hydrochloric acid for 8 to 30 seconds (depending on the capacitor type) to bring out the microstructure.

5.1.3 Microscopy and Compositional Analysis.

Microstructural characterization was performed on a Reichert optical microscope and an AMR 900 scanning electron microscope. Qualitative compositional analysis was initially performed on the AMR 900 using an EDAX 9100 energy dispersive analyzer. Further compositional analysis was performed on a model 550 PHI Auger/ESCA unit and a ARL SEMQ electron microprobe. Either gold-palladium alloy or carbon were used to improve the surface conductivity for examination in the scanning electron microscope and the microprobe. To ensure that the specimen polishing steps did not induce cross contamination, fractured samples were also examined and their localized compositions checked against those of the polished samples.

5.2 Accelarated Life Testing.

Multilayer ceramic capacitors are designed for long term service. As a result accelerated life testing is required to degrade capacitors in a reasonable time span. Two factors were used to accelerate degradation in this study; increased voltage stress (2 to 8 times rated voltage), and increased temperature (100 to 180^{o}C).

In this study the accelerated life test set up (shown in Figure 5.1), utilized an Hewlett Packard voltage supply (model 6116A) with a fluke digital multimeter (model 6018) to insure voltage accuracy. Leakage currents were measured using a Keithly digital electrometer (model 616). To insure temperature stability, capacitors were placed in an insulated glass tube with a copper constantan thermocouple, before being placed into a Tenney oven (model TJR). This furnace is designed to maintain a given temperature to within +0.25^{o}C over a 24 hour period. Temperature was monitored with a Omega 410B temperature indicator which reads to the nearest tenth of a degree. To minimize electrical noise, coaxial cables were used outside the furnace. Only teflon coated wire was used inside the oven. To test and monitor the leakage currents from multiple

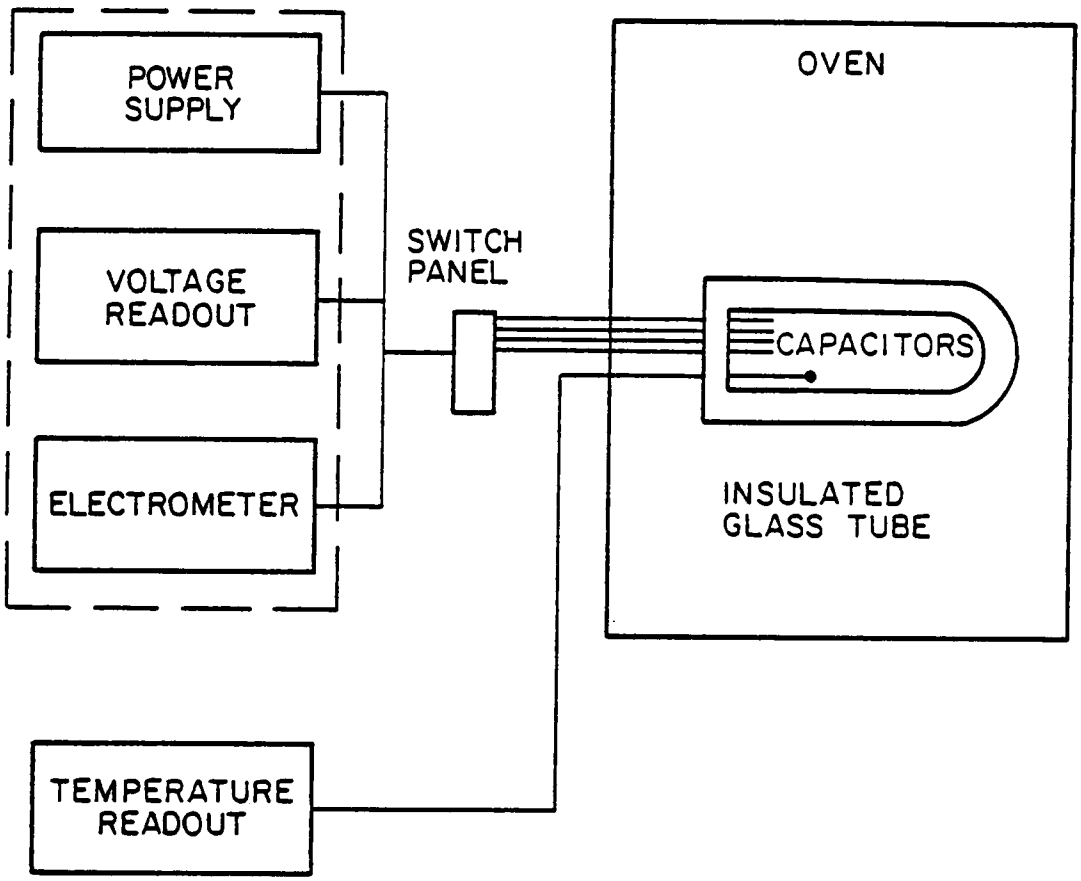

Figure 5.1 Accelerated Life Testing Set-up.

capacitors, a switching system was set up (Figure 5.2) using two series of switches. Normally the low potential leads on all capacitors were switched (on) to ground. To make a measurement on a particular capacitor, the low potential lead was switched (on) to the electrometer and then the circuit to ground was switched (off). After taking a reading the switching procedure was followed in reverse order. The switching sequence is shown schematically in Figure 5.3. This set up allowed readings to be taken on multiple capacitors without inducing spurious effects caused by momentarily disconnecting the ground. DC was used for the voltage stress in this research since the majority of applications involve DC voltage. (One very common application of capacitors is in computers where a small AC signal is superimposed on a DC bias.)

5.3 Measurement Techniques.

5.3.1 Grain Size Determination.

The grain sizes of the capacitors were determined from SEM and optical micrographs using the line intersect method. Normally two photographs were used and three lines were drawn through each photo. Average grain diameter was then determined from the number of grains intersected divided by the line distance divided by the magnification.

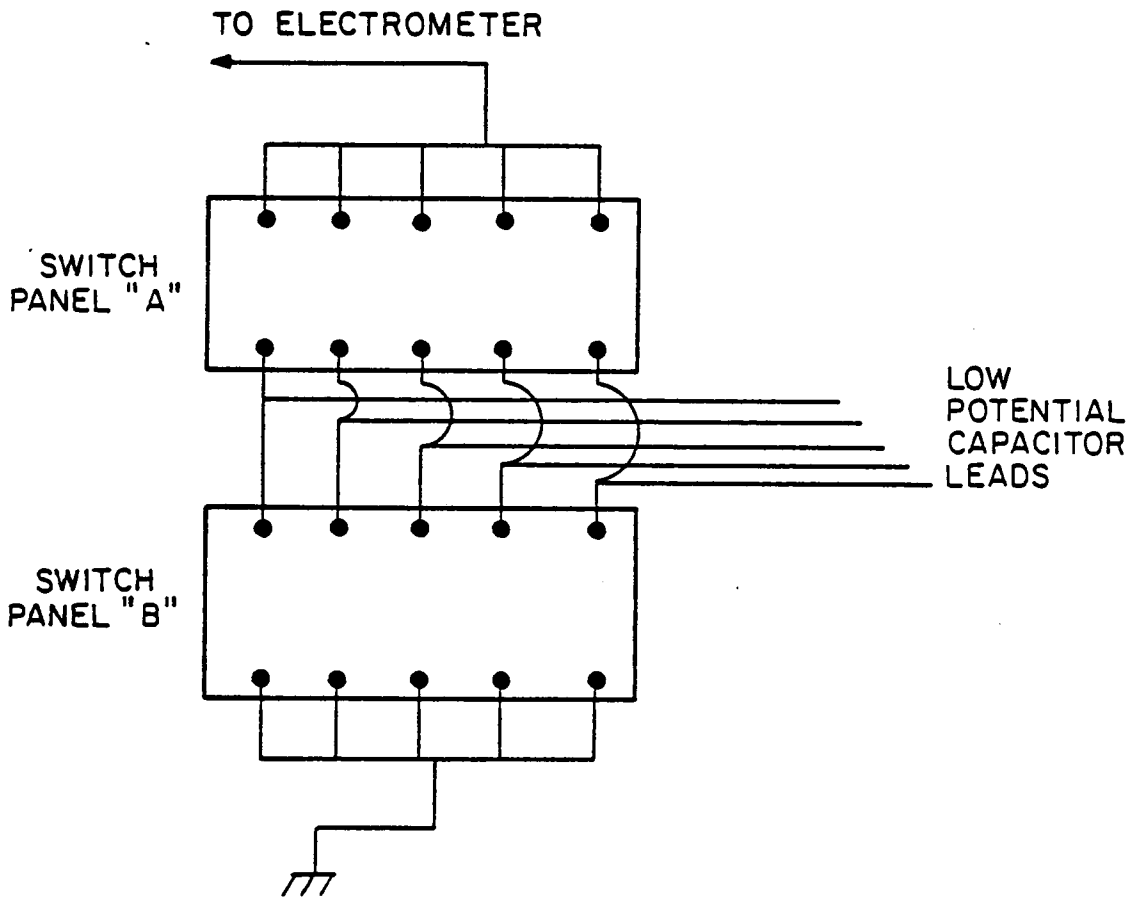

Figure 5.2 Switching set-up used for measurements on multiple capacitors.

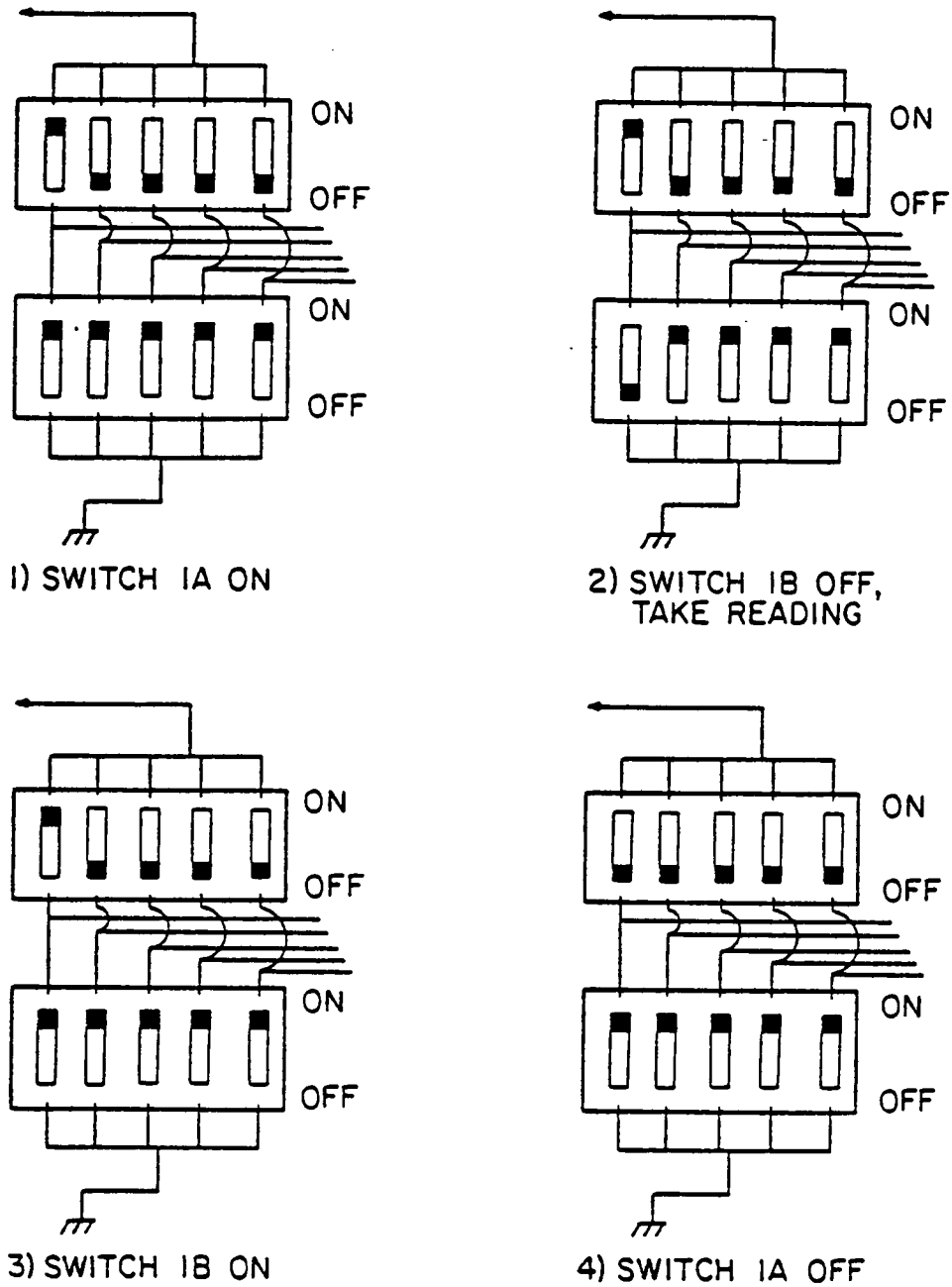

Figure 5.3 Switching sequence used to prevent spurious readings.

5.3.2 Leakage Current Studies.

The principal failure criteria for MLC's is low resistance. One mega ohm is considered a dead short. Exploratory studies showed that there are three difficulties encountered when trying to measure the resistivity of $BaTiO_3$ based capacitors at room temperature: long time periods required for current stabilization, voltage dependant capacitance and extremely low leakage currents. By increasing the temperature to 100°C (or higher) all three of these problems are overcome; current decay times substantially decrease, capacitance is no longer voltage dependant and leakage currents increase. For these reasons, leakage current measurements were performed at elevated temperatures, typically at 100°C to 150°C. The same test setup used for accelerated life testing was used to measure current.

5.3.2.1 I-V Curves.

Leakage currents were measured as a function of the applied voltage for both new and degraded devices to see how I-V characteristics change with degradation. Initially current versus time plots were made at each voltage tested to find the time required for stabilization of the leakage

current. From the results of these initial studies the following stabilization times were determined for new X7R devices: for applied voltages of 1 volt - 12 hours, for 1 to 20 volts - 1 hour, for voltages between 20 and 100 volts - 30 min, and above 100 volts - 15 minutes. Severely degraded devices required less time to stabilize. Z5U capacitors required a minimum of 1 hour at all voltages.

5.3.2.2. Leakage Current versus Degradation Time.

Leakage currents were also measured as a function of time during accelerated life test studies using the same test setup. Applied voltage stress and temperature were varied for different samples to alter the severity of the life test.

5.3.2.3. Activation Energies.

Thermal activation energies were determined from leakage current measurements by maintaining a constant voltage and changing the temperature. Activation energies were calculated from the slope of ln I vs K/T curves using linear regression for the most probable fit. Initial studies of Ln I vs 1/T revealed a nearly linear response over a broad

temperature range. Consequently activation energies were calculated from leakage currents measured at 150, 145, 140, 135 and 130°C for all capacitors except Z5U type B. Z5U type B capacitors were found to degrade quite rapidly at temperatures higher than 130°C, therefore activation energies were calculated from leakage currents measured at 100, 95, 90, and 85°C. A typical plot of current versus time for downward temperature shifts is shown in Figure 5.4. Due to the pyroelectric nature of the capacitors tested, capacitors were allowed to stabilize for one hour at each temperature before a reading was taken. Pyroelectric effects were found to diminish with degradation.

5.3.3 Hall Effect Measurements.

Hall mobility measurements were attempted on new and hydrogen reduced X7R ceramic from room temperature to 200°C. Since hall mobilities have been reported in the range of 1 X 10^{-4} to 0.5 $cm^2/V \cdot sec$ for various compositions of $BaTiO_3$[42,59], a standard DC 4 point probe, Van der Pauw setup was initially used for hall mobility measurements (Figure 5.5). Reduced ceramic samples were prepared by reduction in forming gas for 40 hours at three temperatures,

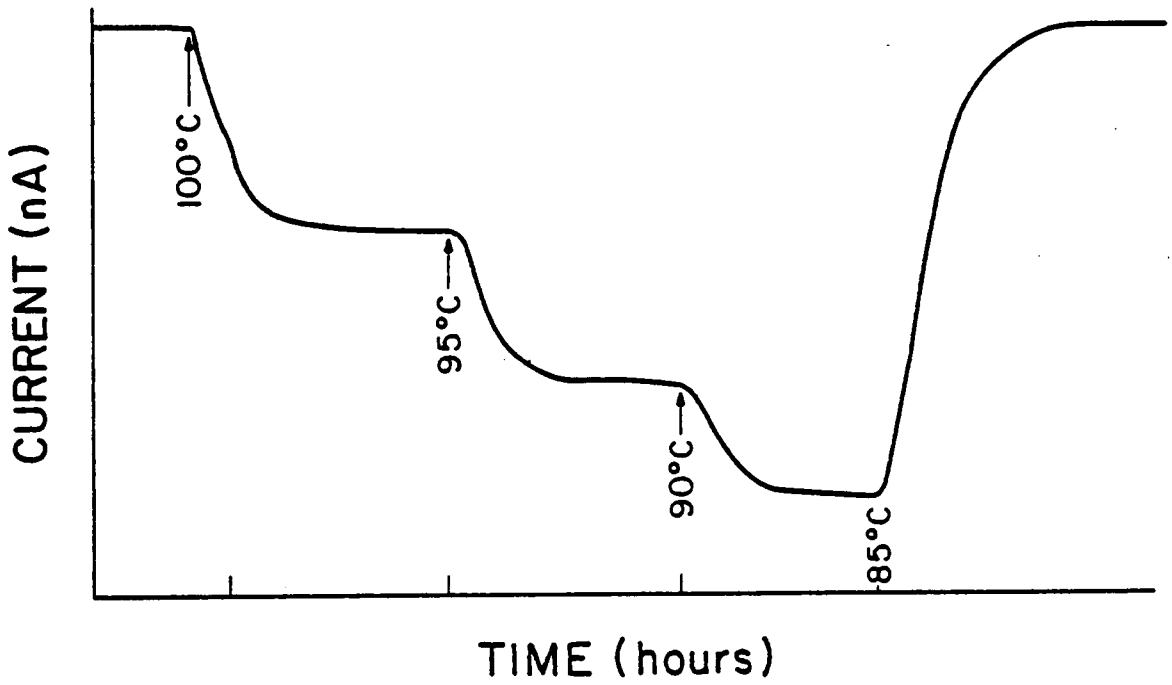

Figure 5.4 Current vs time plot showing the effect of temperature shifts for a Z5U type B capacitor. Electrometer output was fed to a chart recorder.

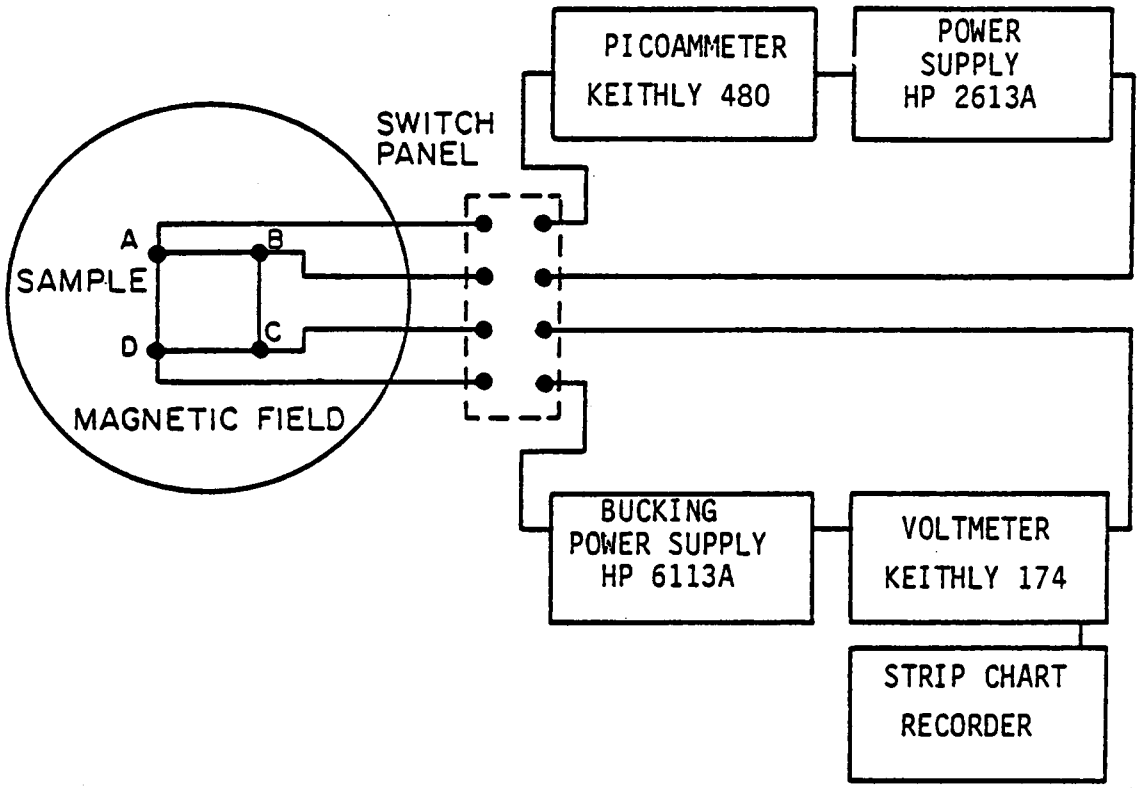

Figure 5.5 Van Der Pauw set-up used to measure Hall mobility.

800, 900 and 1000°C. Test specimens from each reduction lot were cross-sectioned to optically check for reduction uniformity and the outer (0.5 mm) layer of each sample was removed by polishing as an added precaution. Electrical contacts were made by vapor deposition of gold. Wires were connected to the contacts using silver epoxy. Samples were placed in an insulated copper box to minimize pyroelectric currents and electrical noise. Sample temperature was adjusted by means of two small heaters (mounted in the sides of the copper box) and connected to a rheostat. When these measurements failed to detect a Hall voltage, an AC setup with a three point probe was made (Figure 5.6), and further measurements were taken at 200°C on reduced samples.

5.3.4 Photoconductivity.

Photoconductivity measurements were made in an attempt to determine electron mobility and lifetime. X7R and Z5U capacitors were cross sectioned perpendicular to the electrodes and polished. Due to the pyroelectric nature of the samples, a Xenon strobelight system was used with a 1 μsec pulse and a dark/light ratio of at least 10000:1. Sample conductivity was monitored on a dual trace oscilloscope, displaying both sample current and strobe output, using the strobe as a trigger.

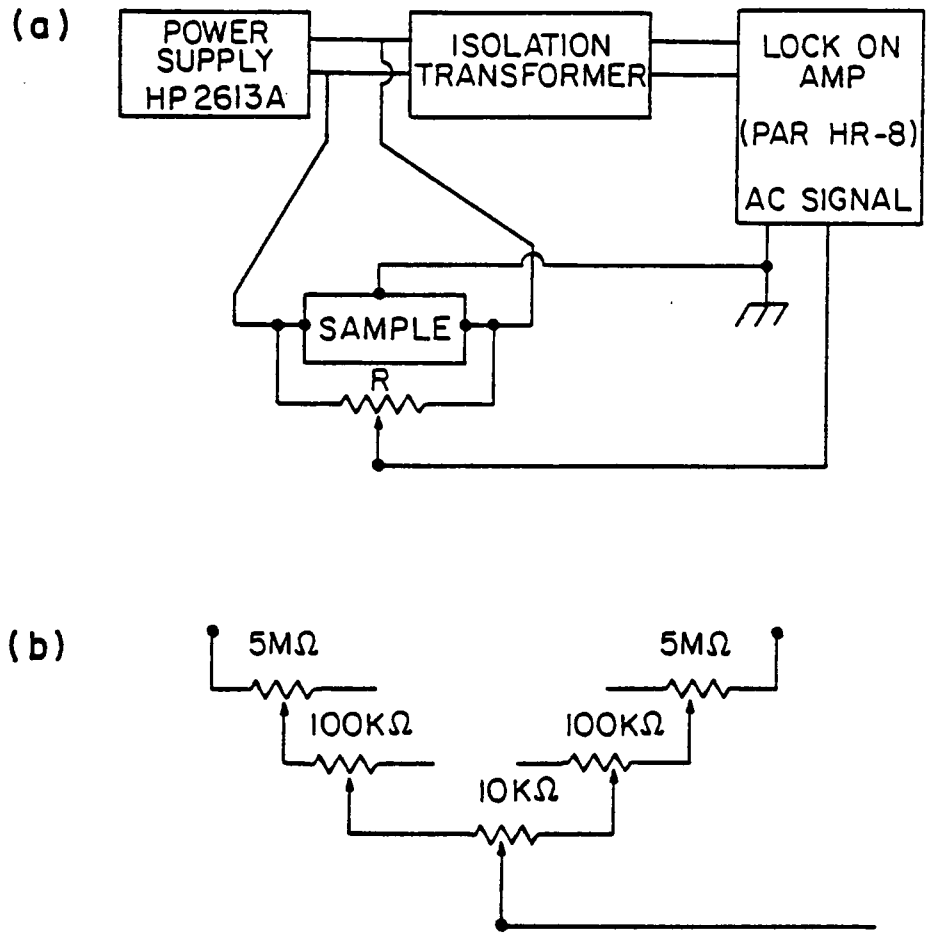

Figure 5.6 (a) AC setup used to measure Hall mobility, (b) detail of resistor.

Chapter VI

EXPERIMENTAL RESULTS

6.1 Microstructural Studies

The morphology of cross sectioned new and degraded capacitors revealed certain characteristic features. These features are typically in the form of:

a) electrode bulges, which arise during processing operation due to local non uniformities in dielectric sheet thickness. These are rounded depressions in the dielectric sheets which have been filled with electrode material during impregnation or silk screening.

b) electrode asperities, which arise due to electrode flow into voids between grains during impregnation, silk screening, and or sintering.

c) non uniform electrode spacing, which arise due to gradual variations in dielectric sheet thickness. This term is not meant to include operator error which results in two layers of dielectric without the electrode metal between layers.

d) dielectric color change with degradation. A

color gradient developed across the dielectric. This was observed for only one type of capacitor. Other type of defects were rare in the capacitors studied.

6.1.1 Z5U Capacitors

Comparison of the two types of Z5U capacitors showed a large difference in grain size and a slight difference in electrode spacing (Figures 6.1 and 6.2). Z5U type B capacitors showed much more grain growth and had an average grain size of 5.6 μm compared to 4.4 μm for Z5U Type A capacitors. Isolated fine grained regions were found in Z5U type B capacitors. These areas had large amounts of second phase surrounding the grains (Figure 6.3). Electrode spacing for Z5U type B capacitors averaged 25 μm (1.0 mil) versus 22 μm (0.88 mils) for Z5U type A capacitors. Since both brands have the same voltage rating and field strength is proportional to distance, type A capacitors are typically operating under a 13% greater electrical field than a type B capacitor. Both types of Z5U capacitors showed variations in electrode spacing greater than 20% (Figure 6.4). Z5U type A capacitors had large numbers of bulges and asperities, examples of which are shown in Figure 6.5. Bulges were less common and almost no asperities were found in Z5U type B

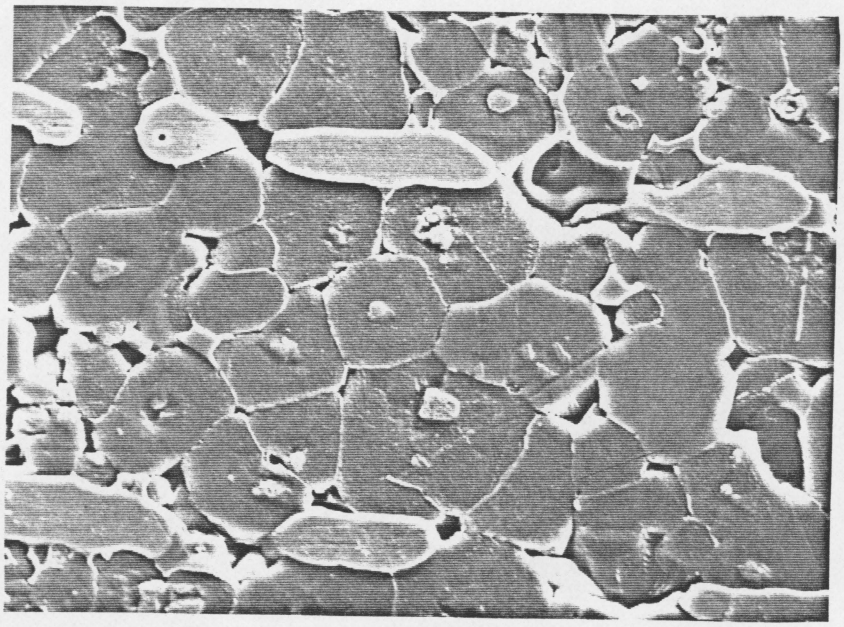

Figure 6.1 SEM micrograph of a Z5U type B capacitor showing typical grain morphology. Microprobe scans show the nodules in the grain centers were lower in dopants. (2000X)

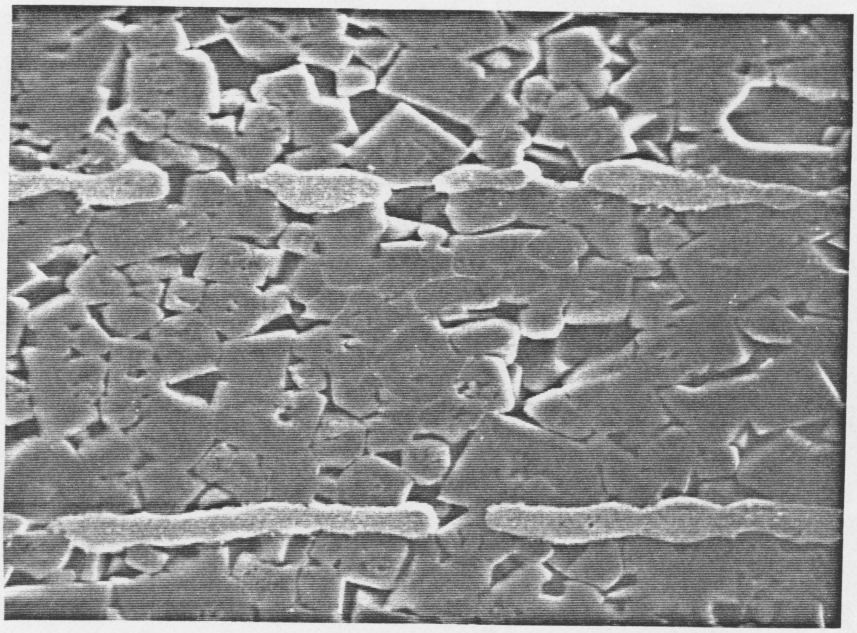

Figure 6.2 SEM micrograph of Z5U type A capacitor showing typical grain morphology. (2000X)

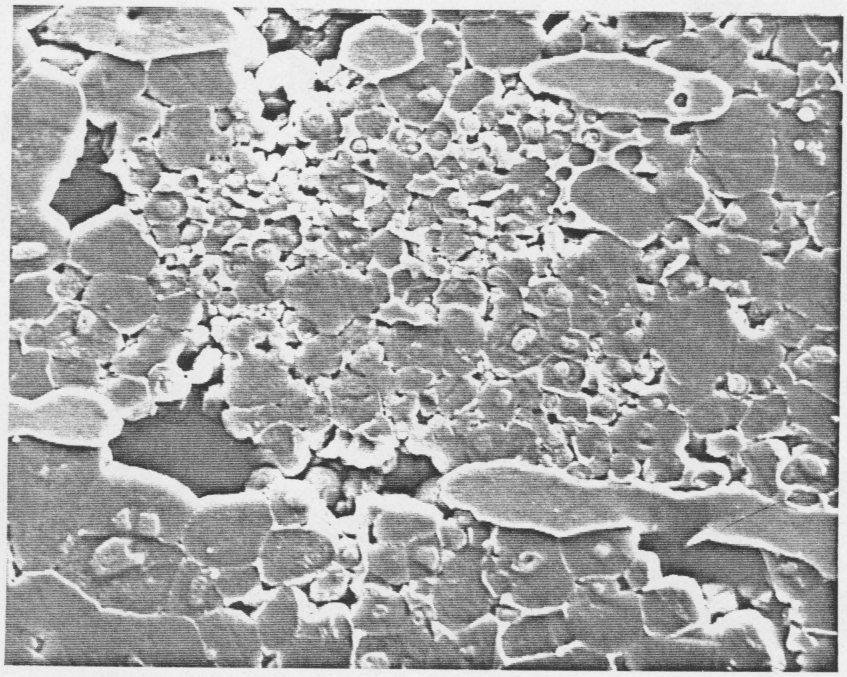

Figure 6.3 Example of one of the occasional fine grained regions found in Z5U type B capacitors. (2000X)

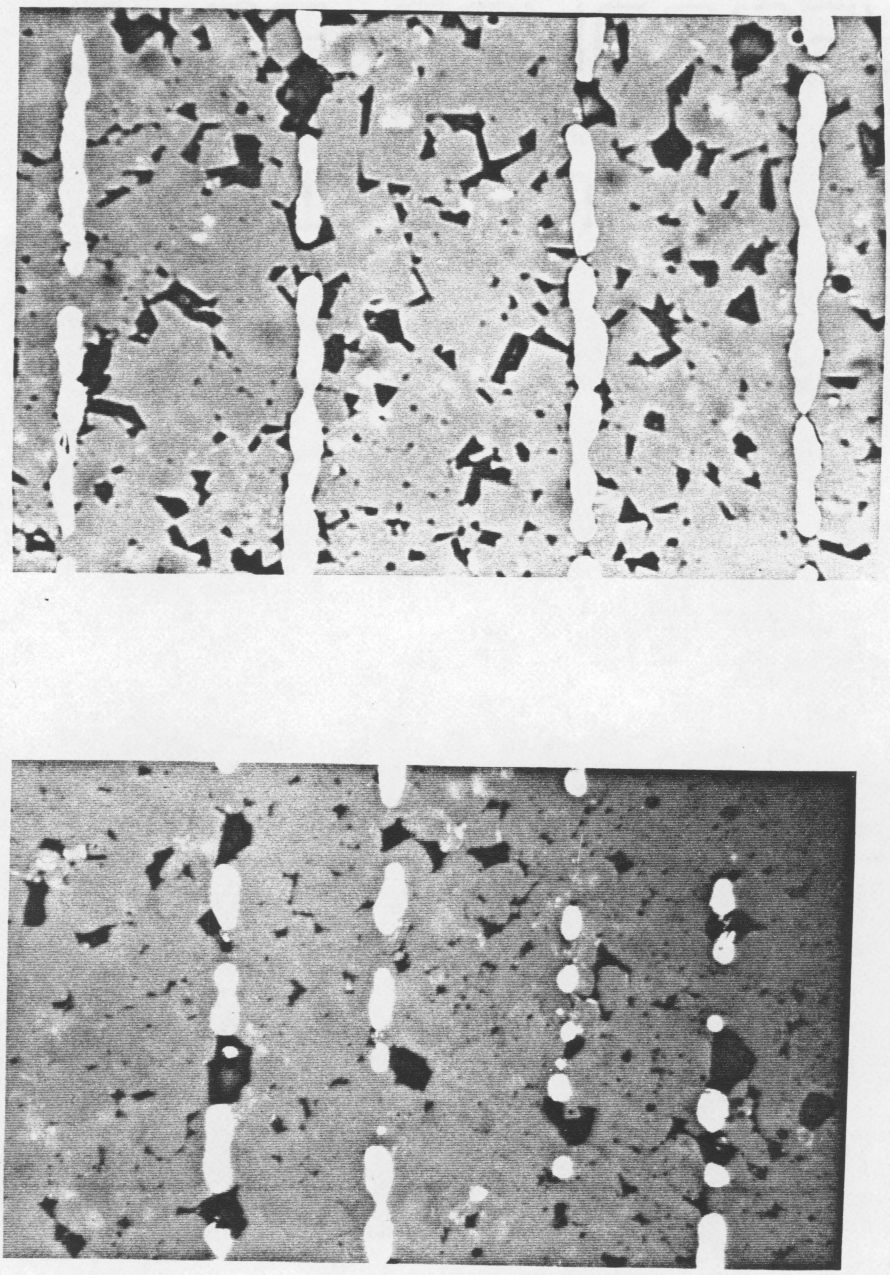

Figure 6.4 Examples of typical variations in electrode spacing, Z5U type A (upper, 1400X), Z5U type B (lower, 900X).

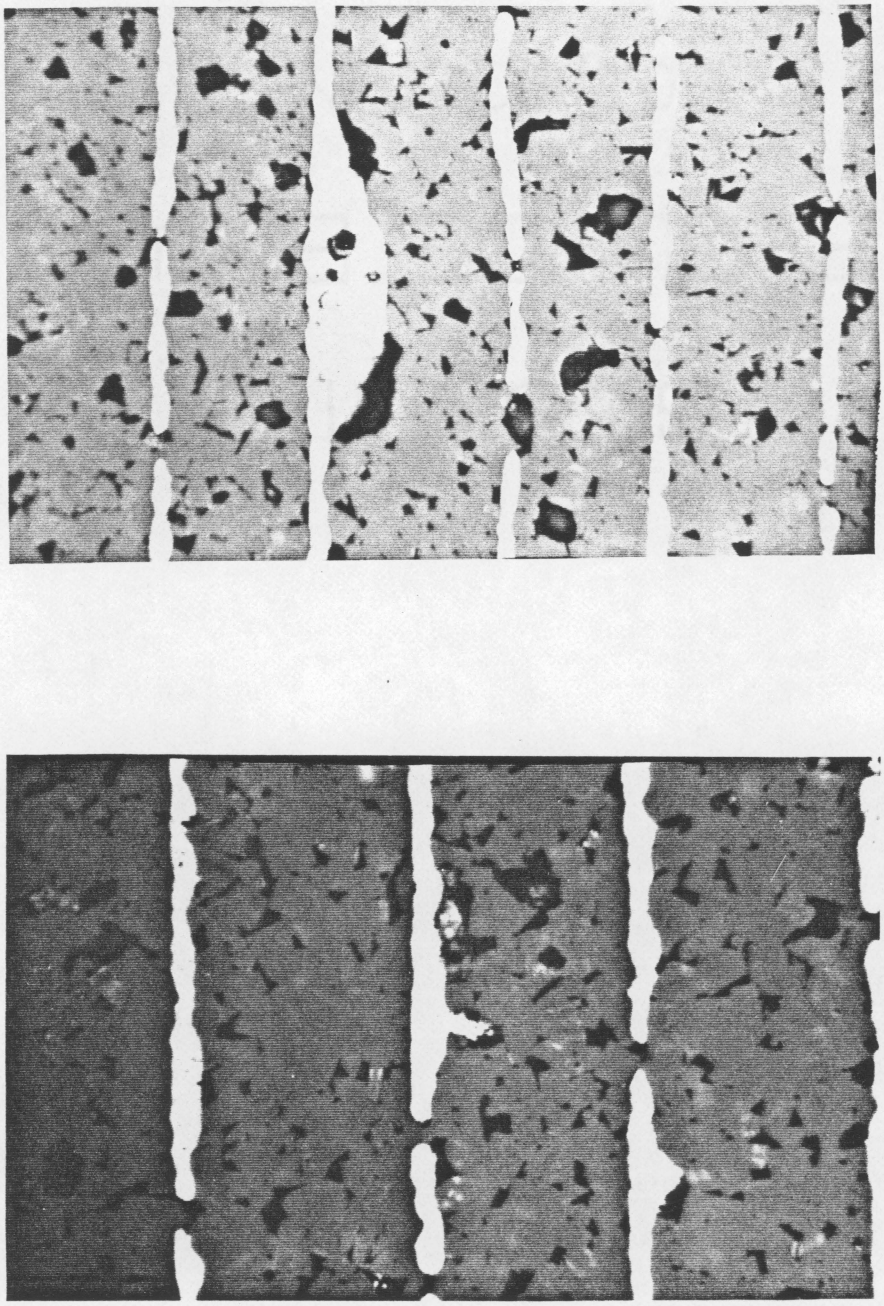

Figure 6.5 Examples of bulges and asperities found in Z5U type A capacitors, bulge (upper,900X), asperity (lower, 1400X).

capacitors. Examination of degraded Z5U type B capacitors in polarized reflected light showed a color gradient between electrodes. Using thin sections and transmitted light (polarized) revealed the color gradient much more clearly (Figure 6.6). No color gradient was observed in degraded Z5U type A capacitors.

6.1.2 X7R Capacitors.

Both of the X7R types examined have very fine grains in a continuous second phase matrix (Figure 6.7). An SEM photo helps illustrate the fineness of these grains (Figure 6.8). One of the items that should be noted from Figures 6.7 and 6.8 is that the relative electrode spacings for X7R type A capacitors are more than three times wider than X7R type B capacitors (76 µm for X7R type A, 25 µm for X7R type B). Variations in electrode spacing of approximately 15% were found in both X7R types. Bulges and asperities were also found on both types of X7R capacitors (Figure 6.9). In addition "spots" of metal were found between electrodes (Figure 6.10a). The metallic nature of these spots was confirmed by examination under an optical microscope using both polarized and unpolarized light (Figure 6.10b). These "spots" are connected by a continuous channel of metal to

Figure 6.6 Color gradient between electrodes of degraded Z5U type A capacitors.

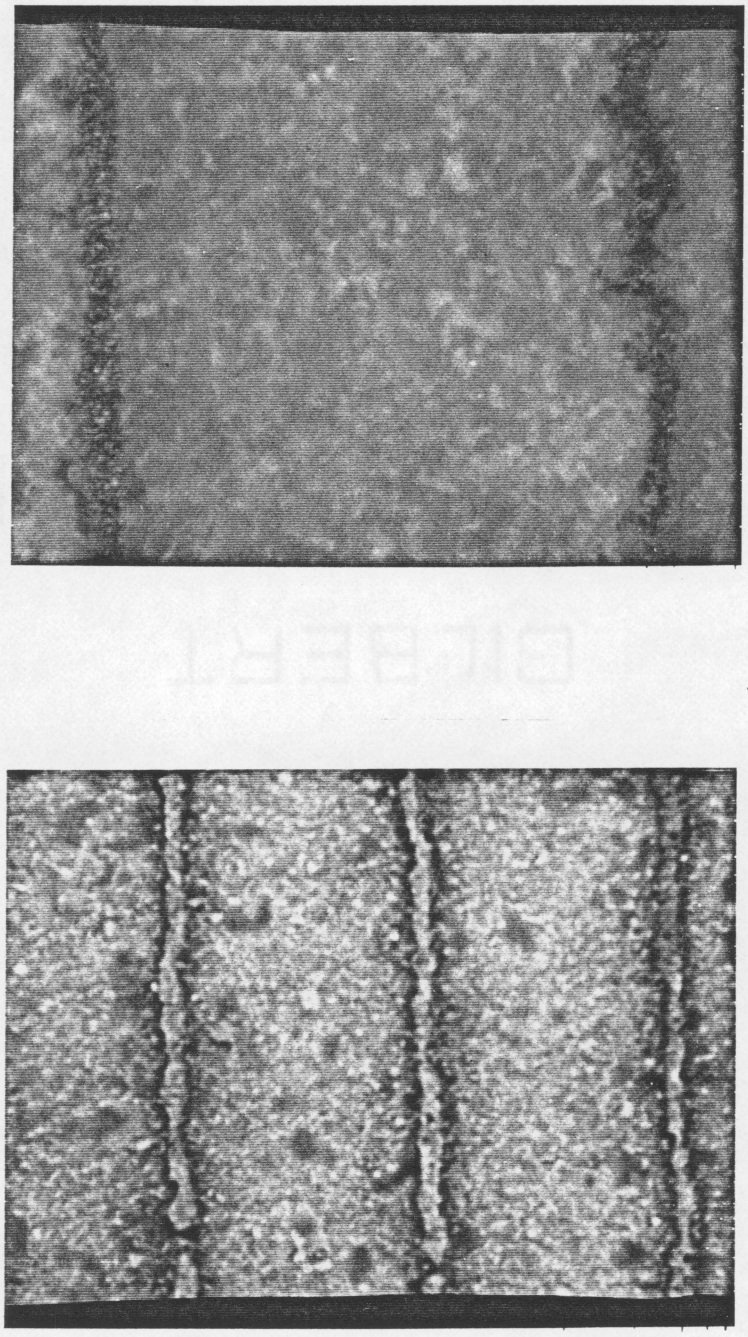

Figure 6.7 Optical micrographs of an X7R type A capactitor (upper,1400X), compared to an X7R type B capacitor (lower,1400X).

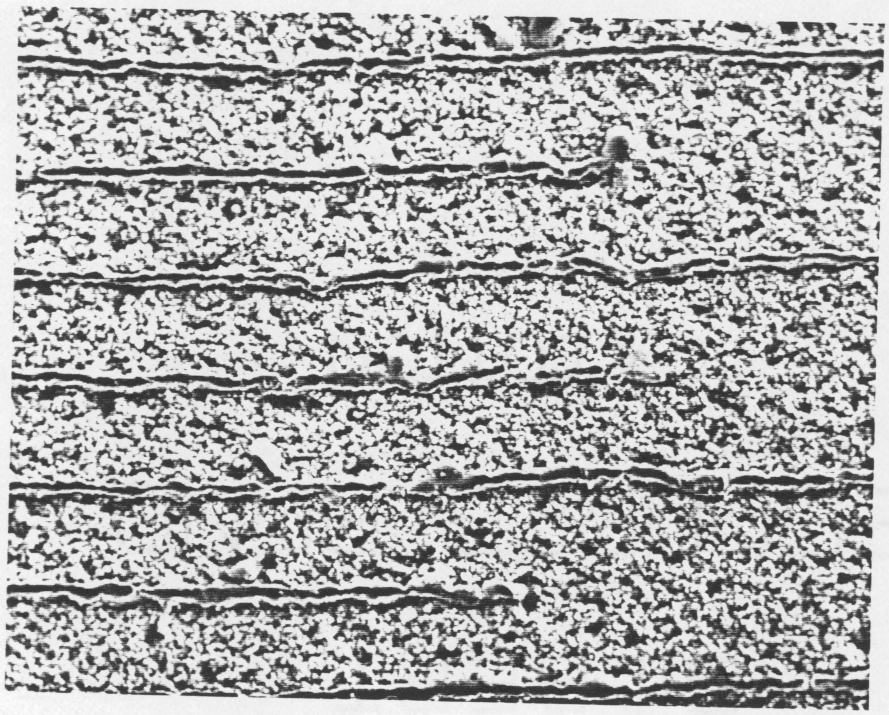

Figure 6.8 SEM micrograph of an X7R type B capacitor revealing an extremely fine grain size. Grains are surrounded by a continuous matrix of second phase. (500X)

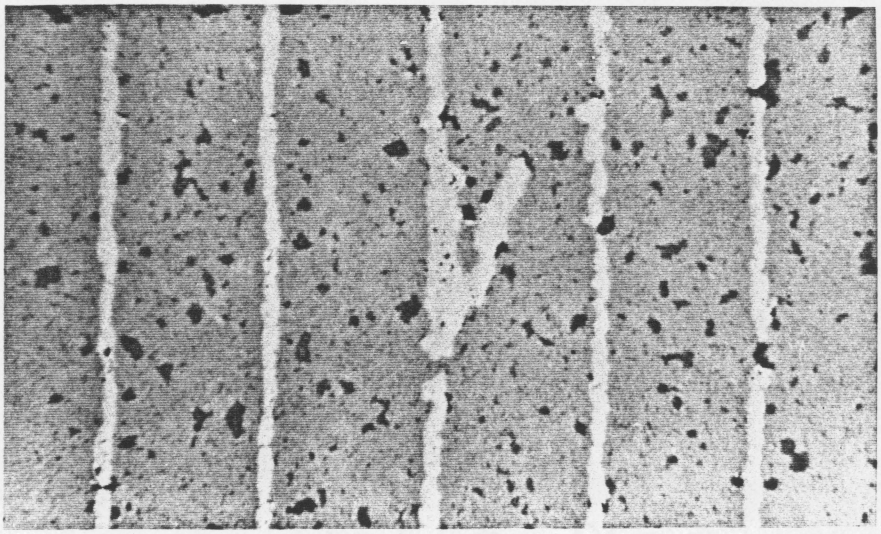

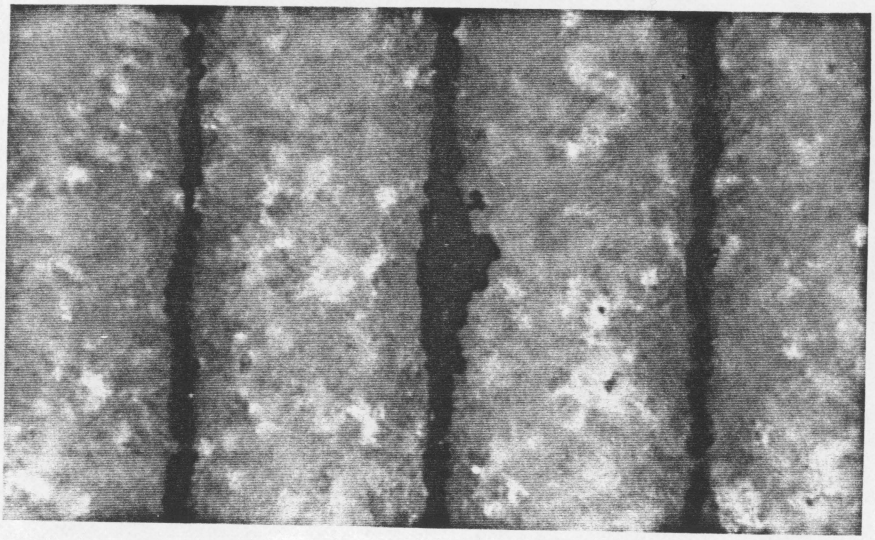

Figure 6.9 Examples of bulges and asperities found in X7R type B capacitors, asperity-(upper, 900X), bulge-(lower, 1400X).

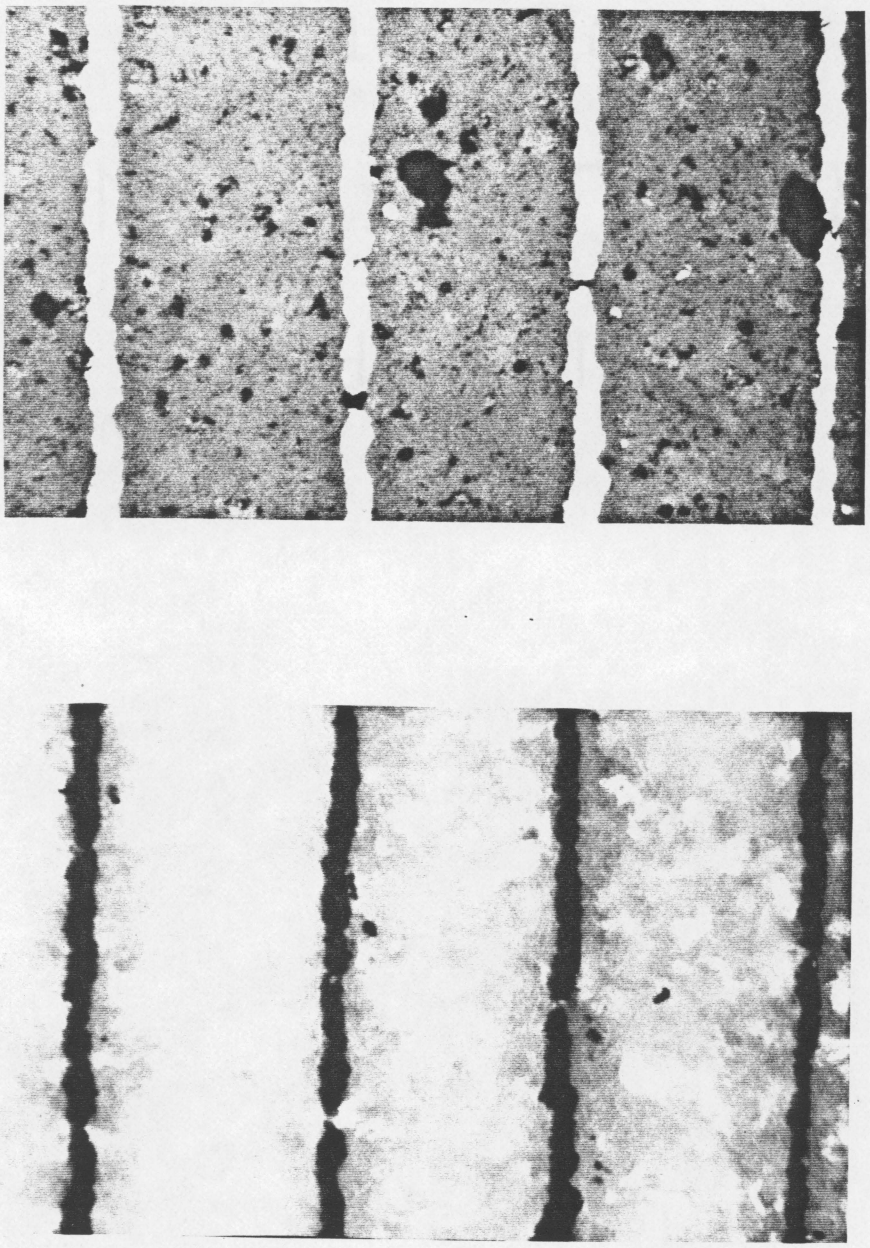

Figure 6.10 Spots of metal found between electrodes,
(a) reflected light (upper),
(b) polarized reflected light (lower).
(1400X)

the main electrode. The conducting path of the electrode was found by examining spots that were near occasional voids in the polished surface (due to pull out of grains during polishing). By focussing into the void, a fine path of electrode was observed between the grains along the sides of the void. Apparently the metal alloy used for the electrodes is very fluid during firing.

6.2 Compositional Studies

The composition of new and degraded capacitors was examined for localized changes in composition to determine if ion migration was analytically measurable and to determine the distribution of dopants. Compositional measurements were made using Auger, EDAX, and an electron microprobe. All tests for compositional differences were negative indicating that if ion migration is occurring, the levels are less than the detectable levels of the instrumentation (0.1 atomic percent).

6.2.1 Z5U Capacitors

Initial EDAX studies on multiple specimens of Z5U type B capacitors revealed the grains to be primarily barium

titanate with zirconium and calcium. It was found that composition varied across the grain and that grain centers had lower levels of dopants. EDAX on the second phase showed it to be barium titanate with higher levels of zirconium and calcium, with zinc also present (Figure 6.11). The electrodes are a palladium-silver alloy.

EDAX on Z5U type A capacitors showed a lower level of doping in the grains with large amounts of cadmium in the second phase (Figure 6.12). Figure 6.13 is an SEM photo showing a large region of second phase in the Z5U type A capacitor. The electrodes are a silver-palladium alloy. After the initial EDAX studies, EPMA and Auger analysis was performed on Z5U type B capacitors.

Emphasis was placed on Z5U type B capacitors since the observed color gradient and electrical characteristics of this type of capacitor strongly indicated ionic migration. Electron probe microanalysis showed the following elements present:

Zr	Ca
Sn	Ba
Zn	Ag
Ti	Pd

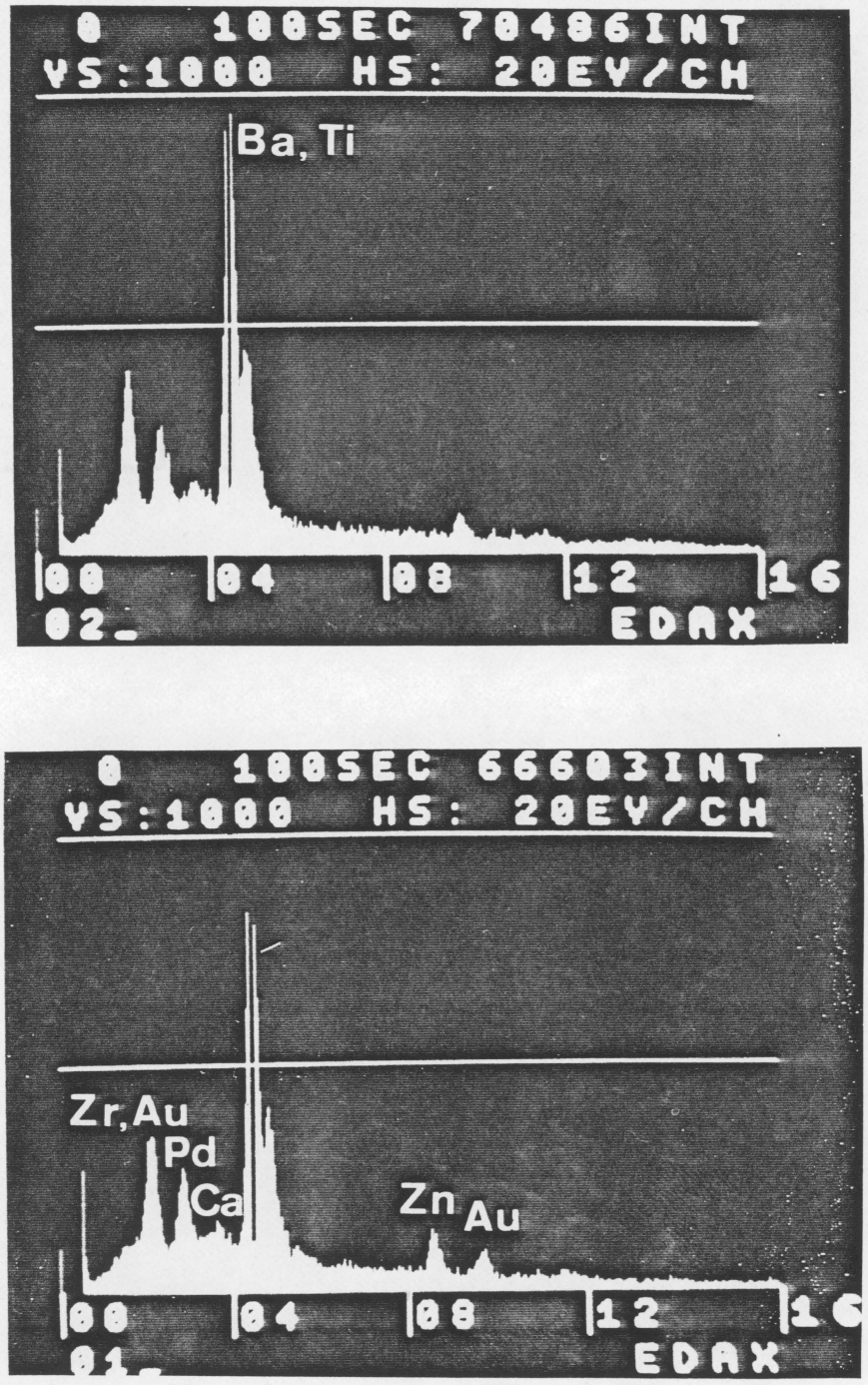

Figure 6.11 EDAX spectra for Z5U type B capacitors, composition of the grains (upper), and composition of the second phase (lower). (Au-Pd coating)

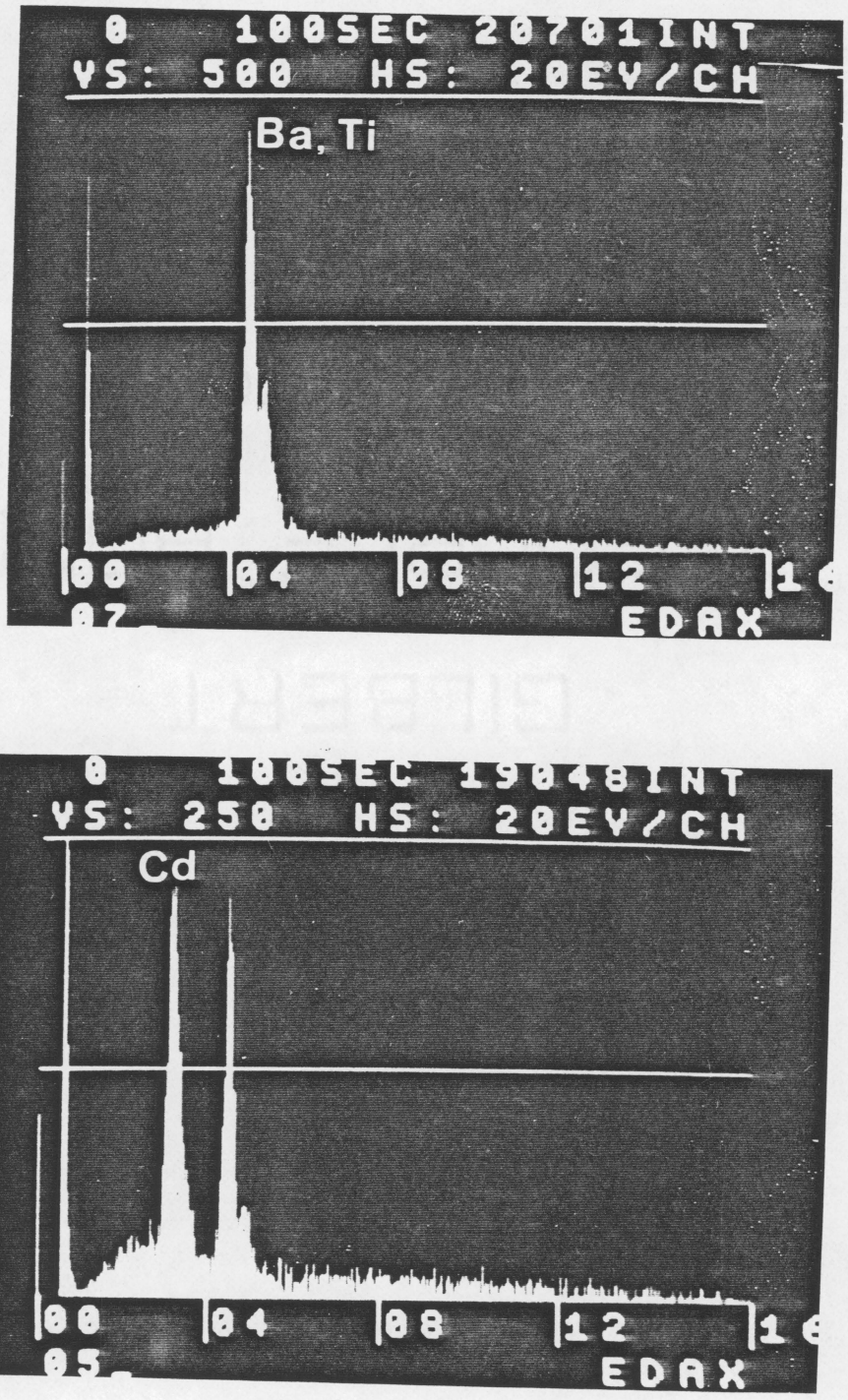

Figure 6.12 EDAX spectra for Z5U type A capacitors, composition of the grains (upper), and composition of the second phase (lower).

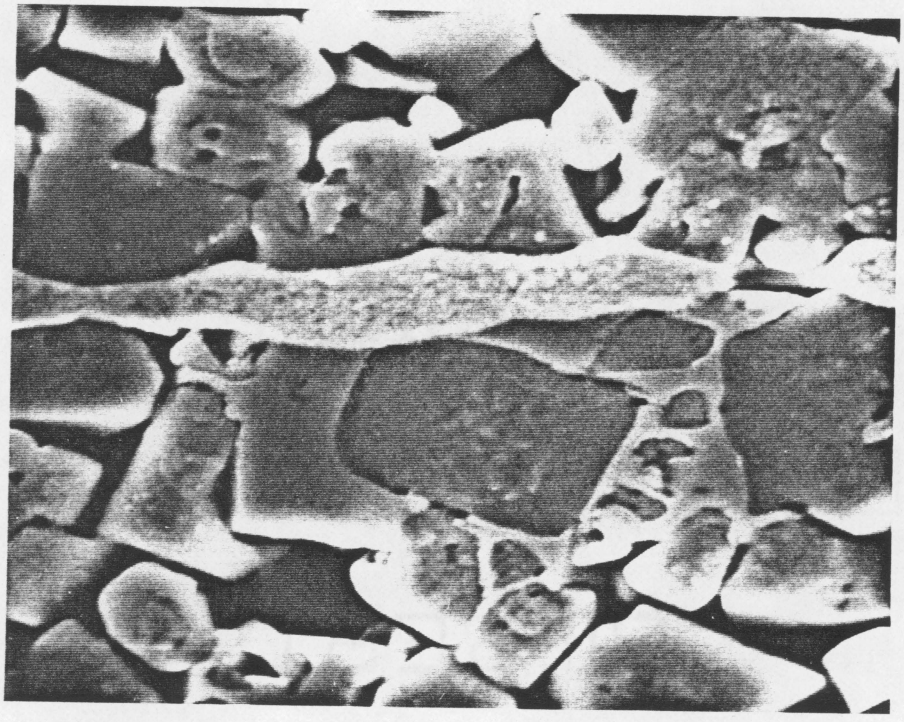

Figure 6.13 Section of a Z5U type A capacitor showing a large region of Cd rich second phase. Note the non uniform distribution of the second phase. (5000X)

EPMA maps were made for each of the dopants found. Only zinc and calcium were inhomogeneously distributed (Figures 6.14-6.16). Comparison of new and degraded devices did not show any composition gradients. To check for oxygen gradients, Auger analysis was used. Numerous measurements were made between opposing electrodes of a degraded Z5U type B capacitor with a visible color gradient. Silver, barium, titanium and oxygen counts were totalled and their ratios calculated. No statistical difference was found for any of these elements indicating the differences in localized composition were below 0.1 atomic percent. Sample spectra are shown in Figures 6.17 and 6.18.

6.2.2 X7R Capacitors

Since compositional analysis failed to detect a compositional gradient or difference between new and degraded Z5U capacitors, compositional studies on X7R capacitors were not performed except to check the composition of the electrodes. X7R type A capacitor electrodes are lead based. X7R type B capacitors have silver-palladium alloy electrodes.

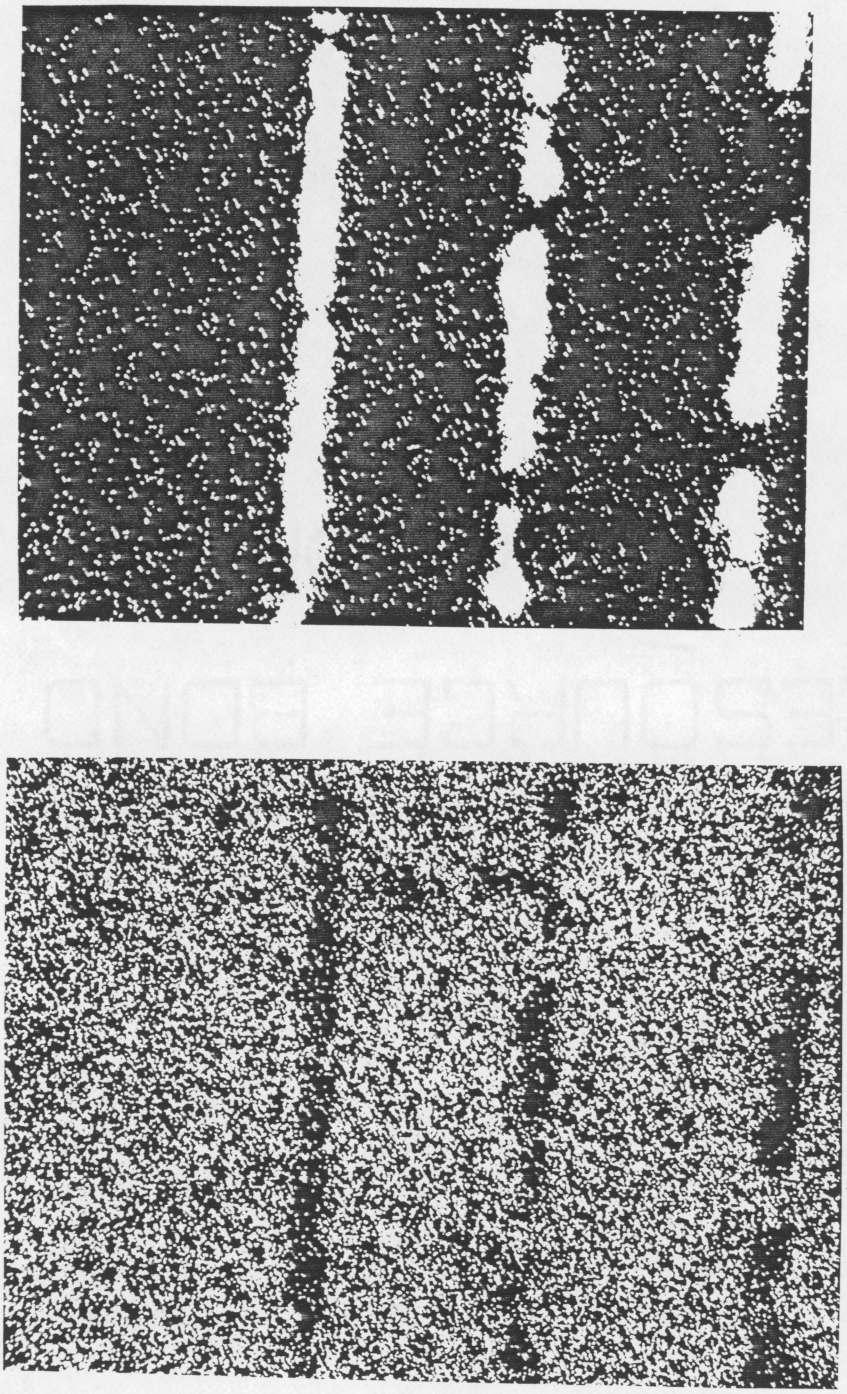

Figure 6.14 Microprobe maps for silver (upper) and tin (lower) - degraded Z5U type B capacitor.

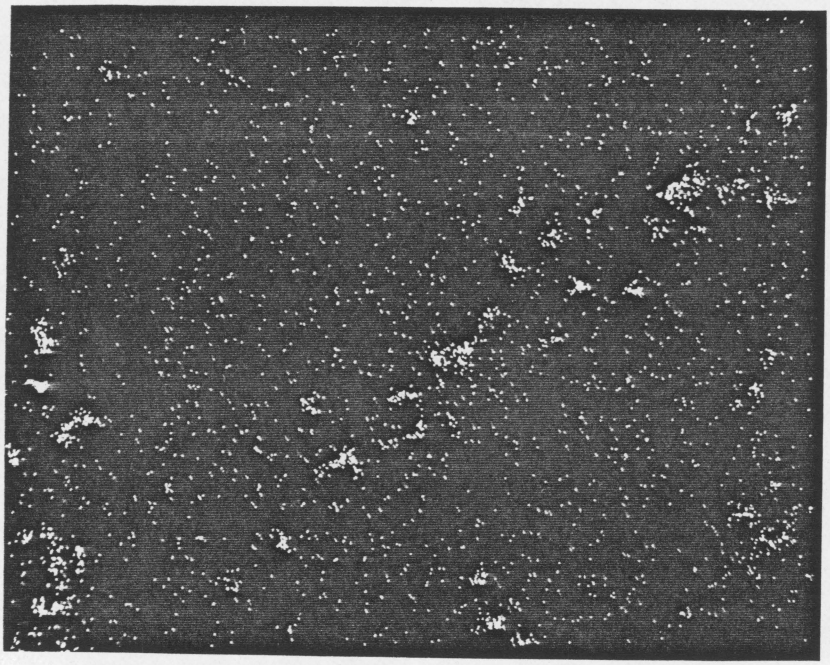

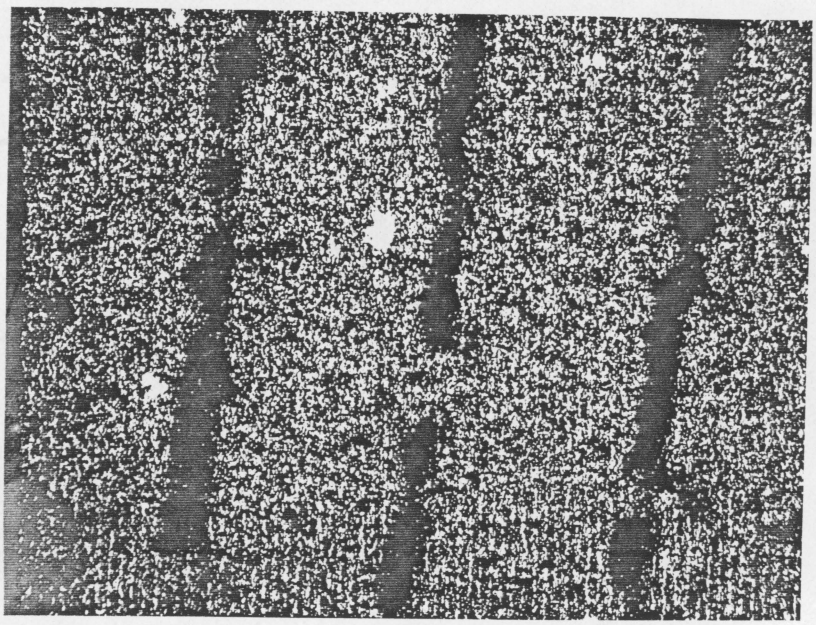

Figure 6.15 Microprobe maps for zinc (upper) and calcium (lower) - degraded Z5U type B capacitor.

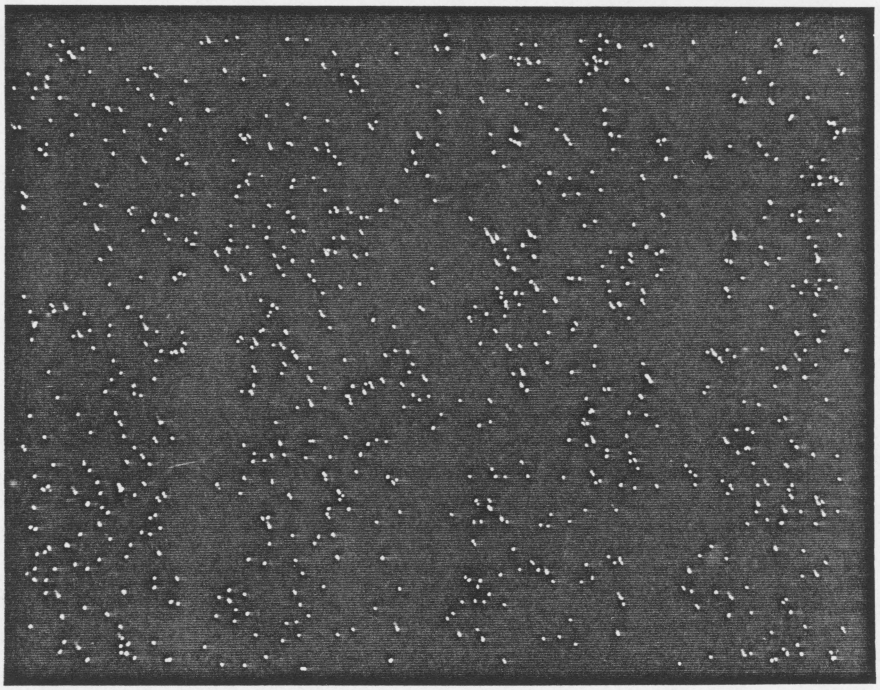

Figure 6.16 Microprobe map for zirconium distribution - degraded Z5U Type B capacitor.

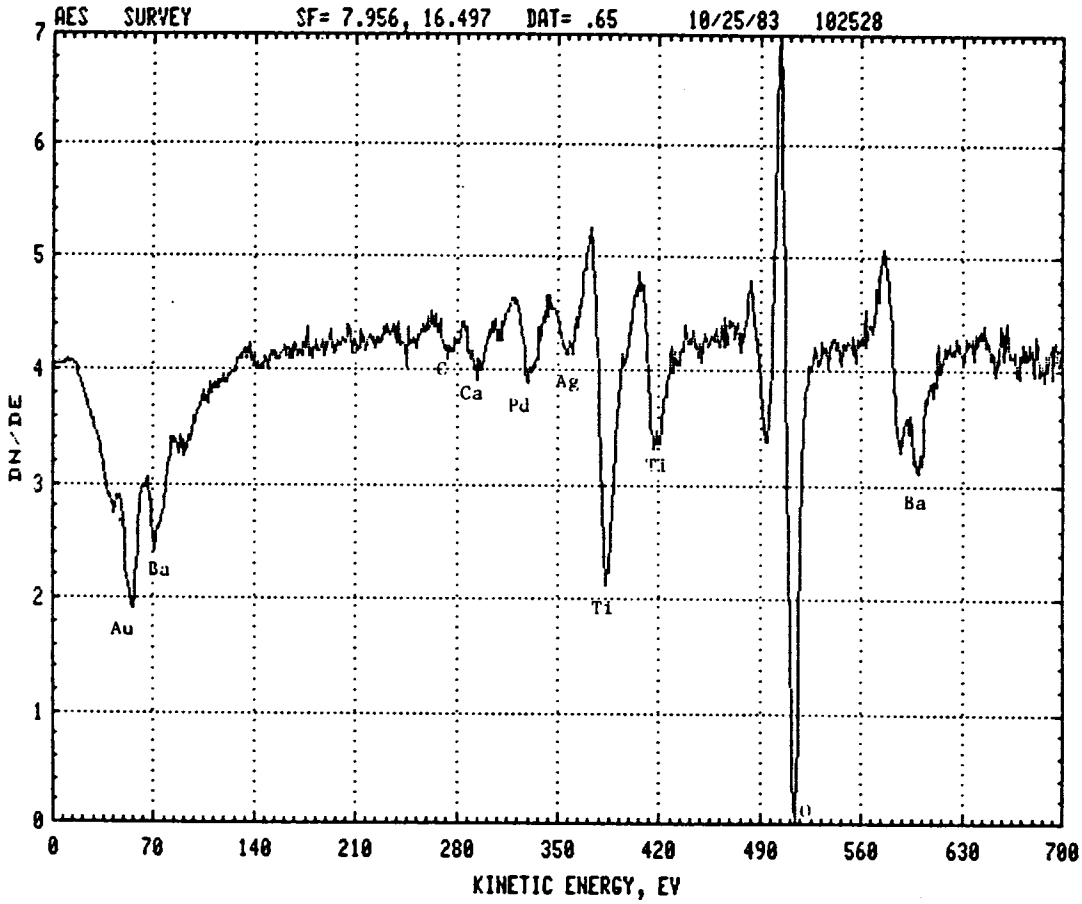

Figure 6.17 Auger survey spectrum on degraded Z5U type B capacitor dielectric near an electrode (compare to Figure 6.18).

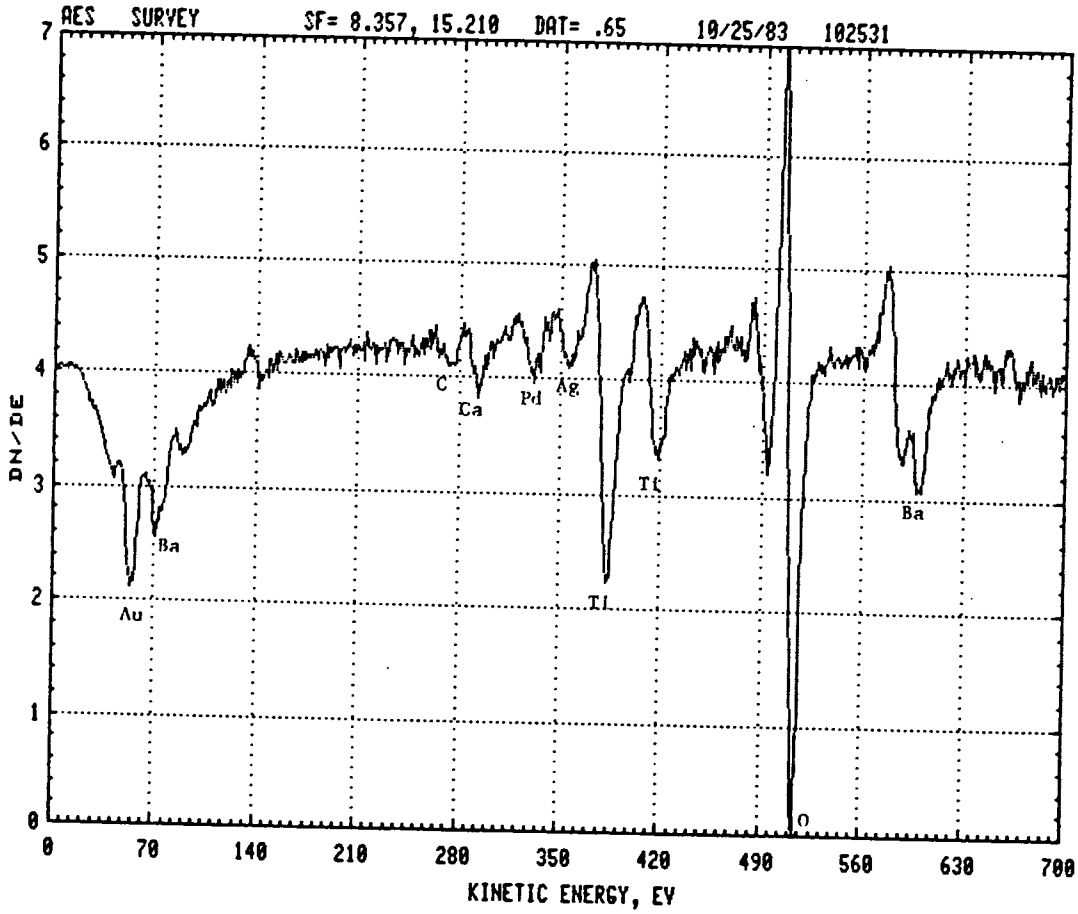

Figure 6.18 Auger survey spectrum on degraded Z5U type B capacitor dielectric near an opposing electrode. (opposing the one in Figure 6.17)

6.3 Leakage Currents and Activation Energy Studies.

Initial I-V measurements on both types of X7R capacitors revealed an approximately 3/2 dependance of current on voltage ($I \propto V^{3/2}$). Degraded capacitors exhibited a variety of current-voltage regimes typically ohmic at lower voltages shifting to a 3/2 power to quadratic space charge limited behavior at higher voltage stresses. Complimentary studies on non electroded new X7R chips[60] revealed that ohmic behavior does occur in new X7R capacitors but at lower field strengths than were tested in these studies. I-V measurements on Z5U capacitors revealed a near ohmic dependence for both types. All capacitors were found to have voltage independent activation energies.

6.3.1. I-V Curves.

Figures 6.19 and 6.20 are typical I-V characteristics for new X7R and Z5U capacitors showing the 3/2 power characteristic for X7R capacitors and the ohmic dependence for Z5U's. While these relations were followed by most capacitors tested, occasional X7R capacitors had dependences as low as n=1.2 ($I \propto V^{1.2}$). A potential source of error should be mentioned here: I-V characteristics should

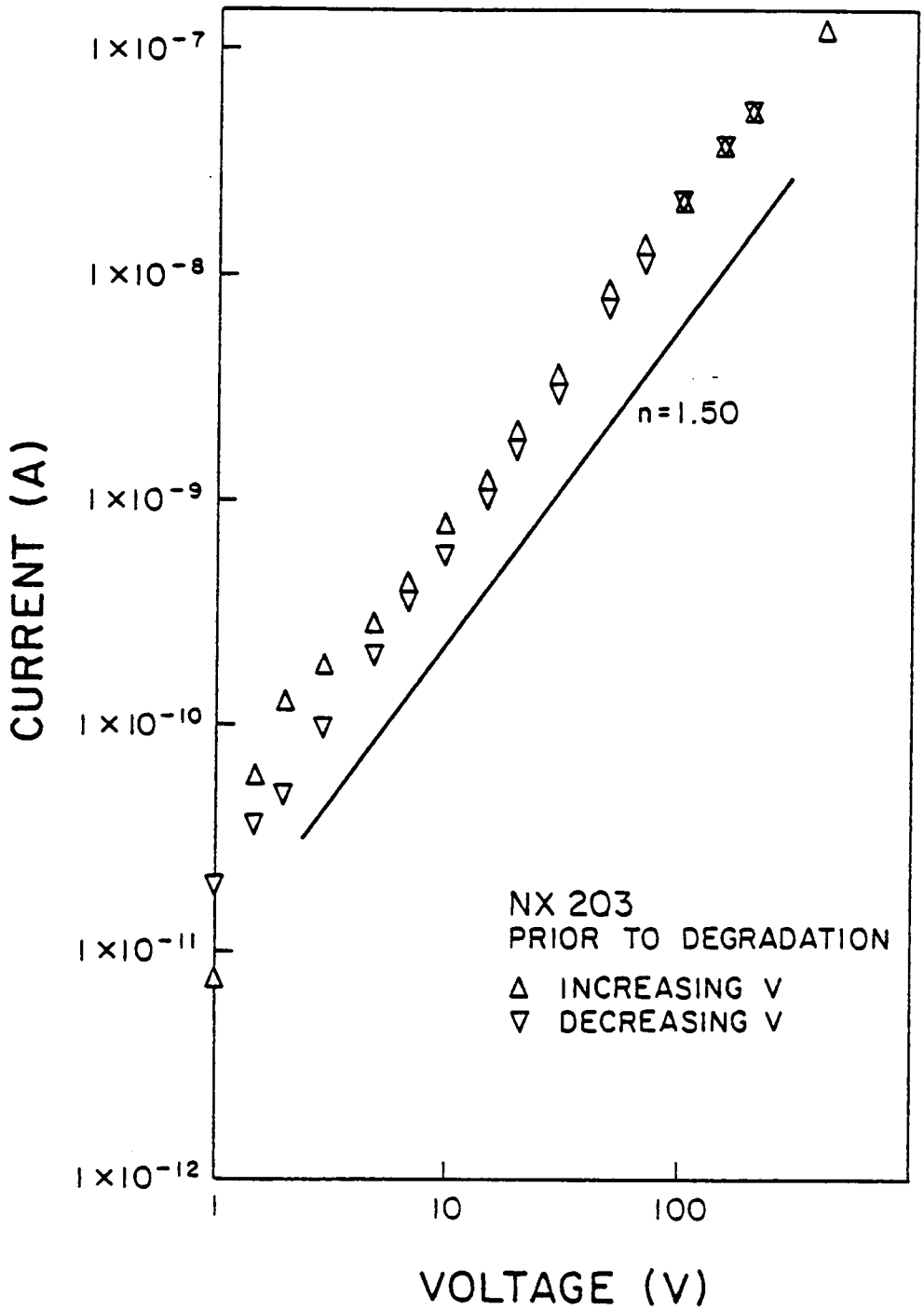

Figure 6.19 I-V curve for a new X7R type B capacitor at 150°C.

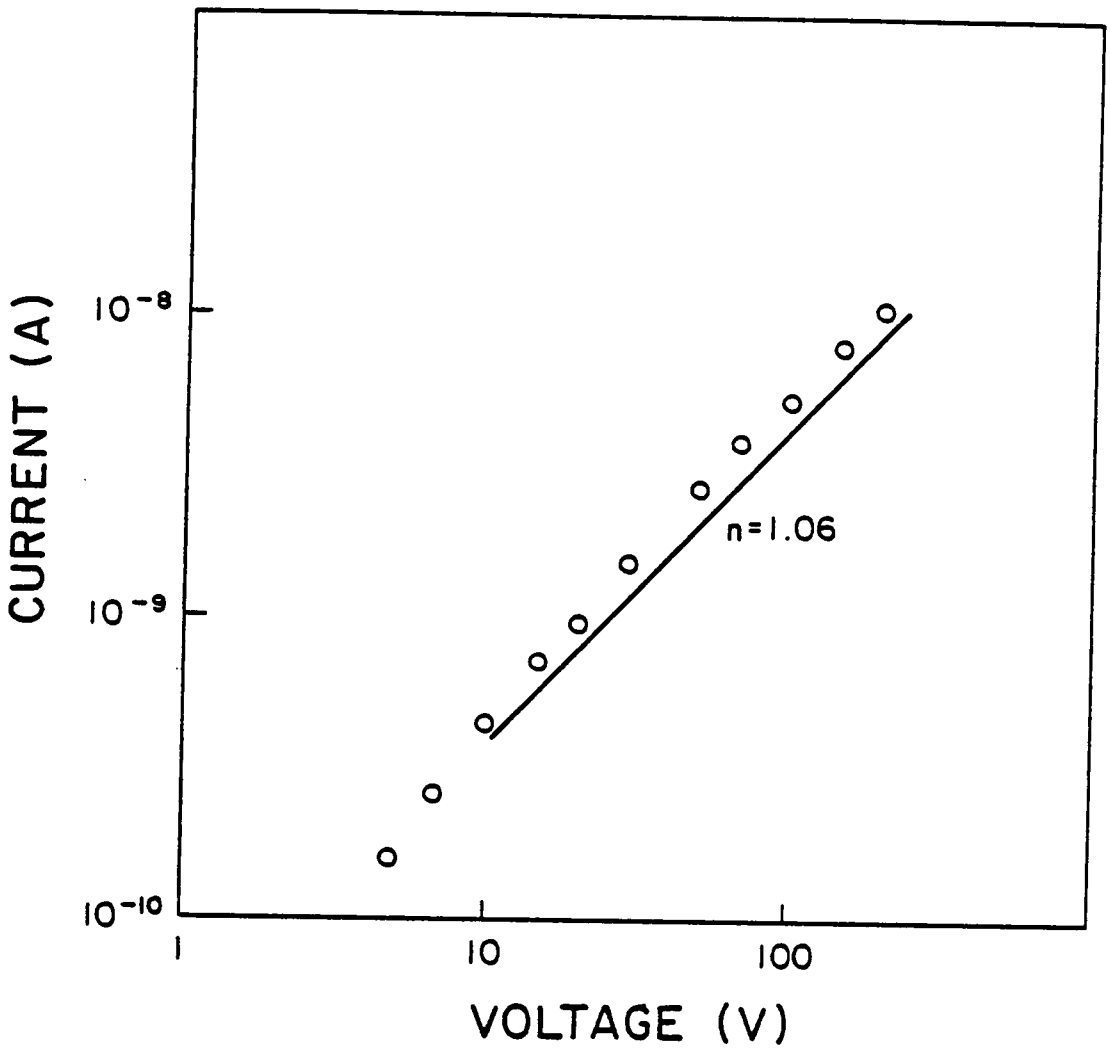

Figure 6.20 I-V curve for a Z5U type A capacitor at 150°C.

only be measured under conditions where the leakage current is stable with time. To ensure this, a plot of leakage current vs. time should be made at the highest voltage that will be used. The leakage current should not be noticeably changing after the first hour. Spurious results will occur if leakage currents are changing with time. This problem is detailed in section 6.3.3.1. When readings were taken on severely degraded capacitors three important changes were found:

a) Pyroelectric effects were greatly diminished,

b) an ohmic region appeared in the I-V curve, (X7R capacitors).

c) activation energies had dropped significantly.

This last finding is examined in section 6.3.2. Leakage current was used to determine capacitor condition. It was found that while leakage current rises by orders of magnitude, the change in I-V characteristics (with degradation) is gradual (Figure 6.21). The ohmic region, found in the X7R capacitors, shifts slowly to the right and a V^2 dependence of I may or may not appear at higher voltages. Current was used as the limiting factor in these measurements. To prevent sample heating, capacitor current was kept below 10^{-4} A on 1μF devices by limiting the applied voltage.

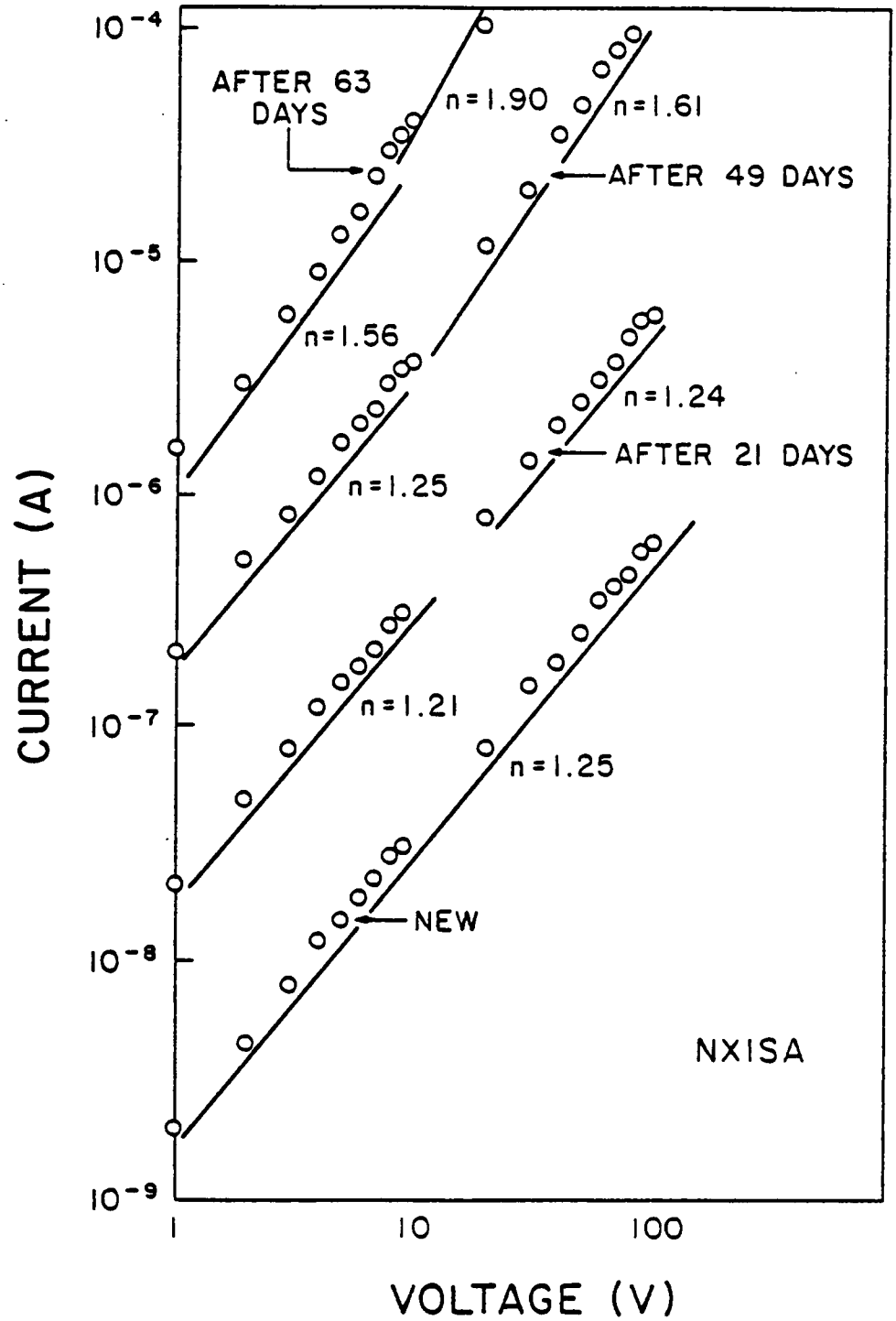

Figure 6.21 I-V curves for an X7R type B capacitor illustrating changes with degradation[61].

6.3.2 Activation Energies

Examination of the four capacitor types revealed that all four had voltage independent activation energies, as illustrated in Figure 6.22. The Z5U type A capacitors were found to have the highest activation energies, ≈1.5eV. Nominal values of thermal activation energies are given in Table 6.1. These values were checked throughout the voltage range of 1 to 200 volts except for the Z5U type B capacitors which were found to degrade rapidly at voltages above 50 volts in the temperature range used (130 to 150°C). Activation energies typically varied about 20% between new capacitors of the same type and often showed anomalous increases and decreases in activation energies across the lower portion of the voltage range (Figure 6.23). This effect appeared on both X7R and Z5U capacitors and tended to disappear if measuring temperatures were lower than 130°C. This temperature/voltage dependent change in the activation energy can be seen in an Arrhenius plot of leakage current versus temperature (Figure 6.24). This effect was not noticed at higher voltages (Figure 6.25).

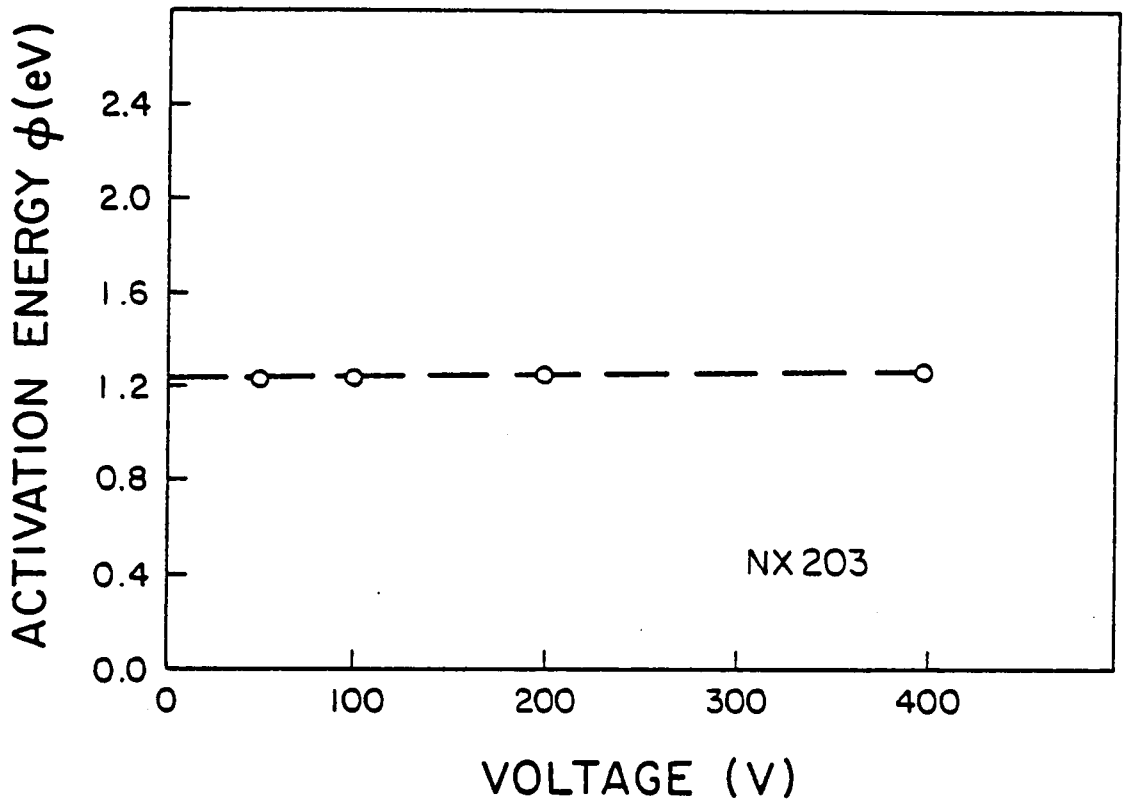

Figure 6.22 Activation energy as a function of voltage for an X7R type B capacitor.

Table 6.1. Nominal activation energies for new X7R and Z5U capacitors. Tested from 1 to to 200 volts using the temperature range of 150 to 130°C.

Capacitor type	Nominal activation energy
X7R type A	1.08 eV
X7R type B	1.10 eV
Z5U type A	1.48 eV
Z5U type B	0.95 eV *

* Only tested to 50 volts due to degradation rate at higher voltages.

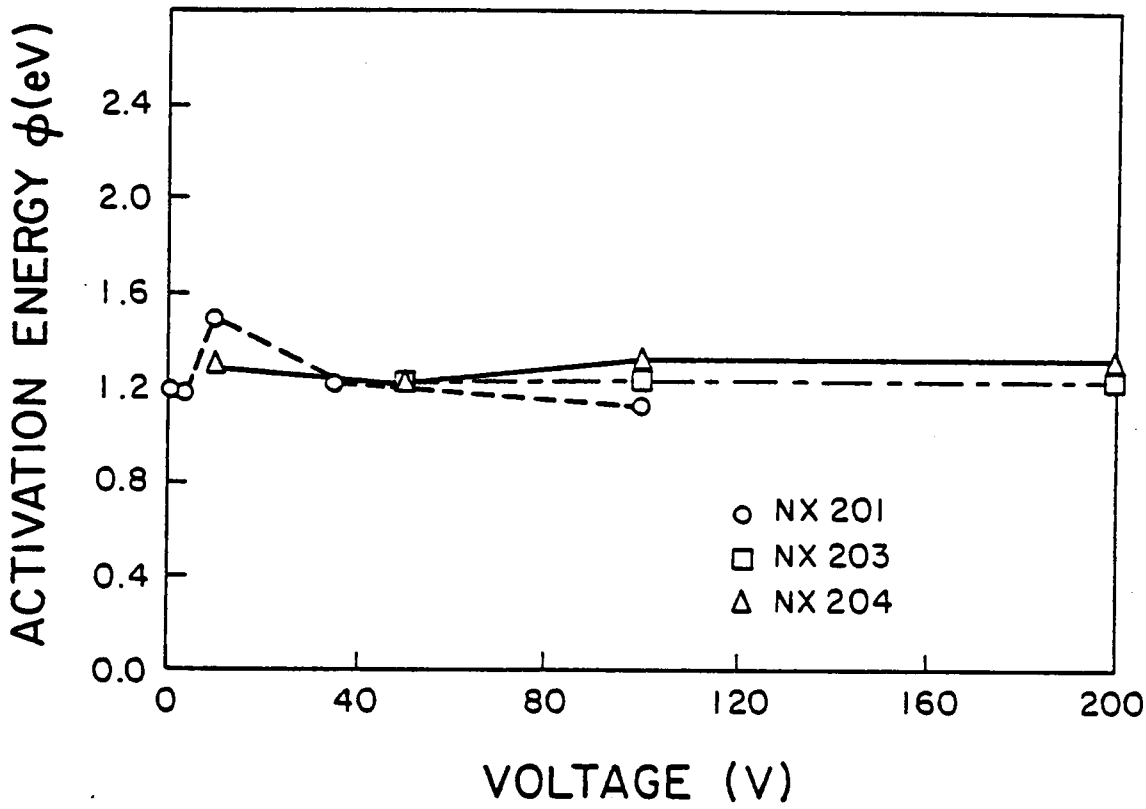

Figure 6.23 Plot of activation energy as a function of voltage for three X7R capacitors.

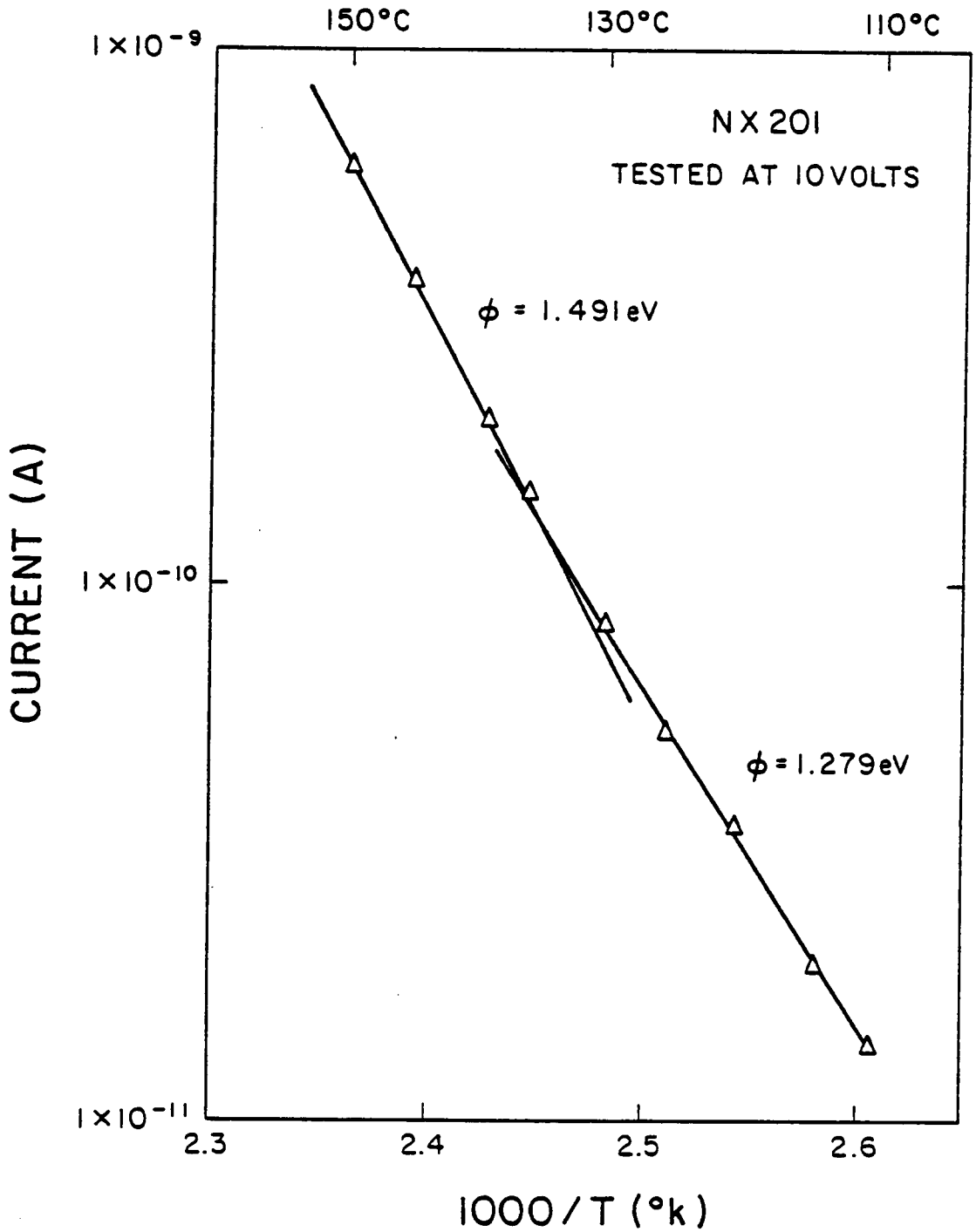

Figure 6.24 Arrhenius plot of leakage current vs. temperature showing a shift in activation energy with temperature. Compare to Figure 6.25.

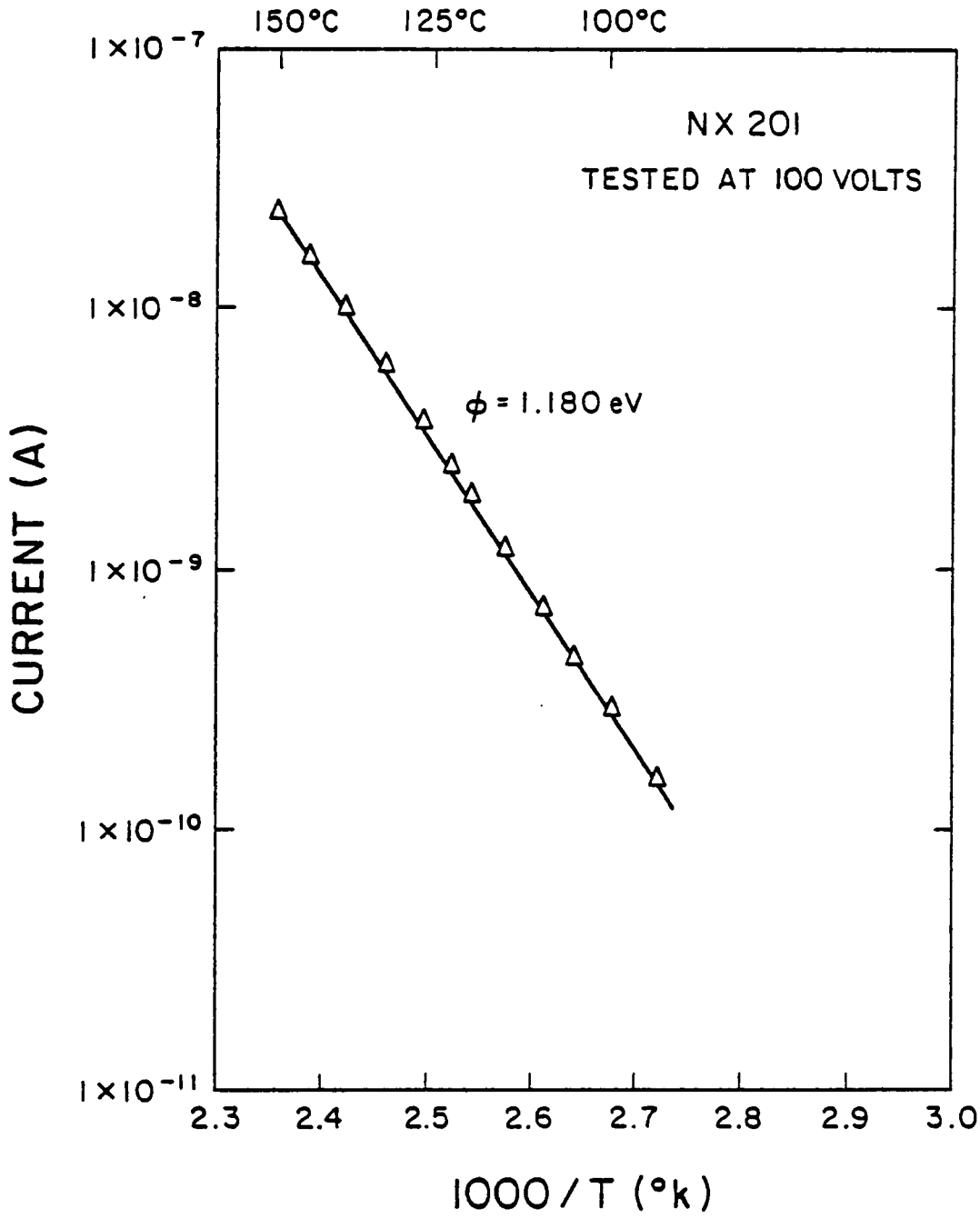

Figure 6.25 Typical Arrhenius plot of leakage current vs. temperature. Calculated activation energy is essentially temperature independent.

6.3.3 Degradation Studies.

Studies were made on the leakage current and activation energy characteristics over capacitor lifetimes. Tremendous differences were found in degradation characteristics under equivalent accelerated life test conditions. At 150°C and under 400 volts DC, Z5U type B capacitors were found to degrade in less than four hours. Z5U type A capacitors tested under the same conditions showed no signs of degradation after 30 days. The effects of polarity reversal and the capacitors ability to heal were examined. Activation energies were found to slowly decrease with degradation.

6.3.3.1 Leakage Current vs Degradation Time.

Studies of leakage current versus degradation revealed a number of interesting results. In addition to the effects of temperature (Figure 6.26), and voltage (Figure 6.27), on degradation rate, a tremendous difference in the degradation resistance of different capacitor compositions was found. The magnitude of this difference, shown in Figure 6.28, was unexpected. This result indicates that a large difference in the long term reliability of capacitors from one manufacturer to another exists. Figure 6.28 also shows the two general trends found for degrading capacitors.

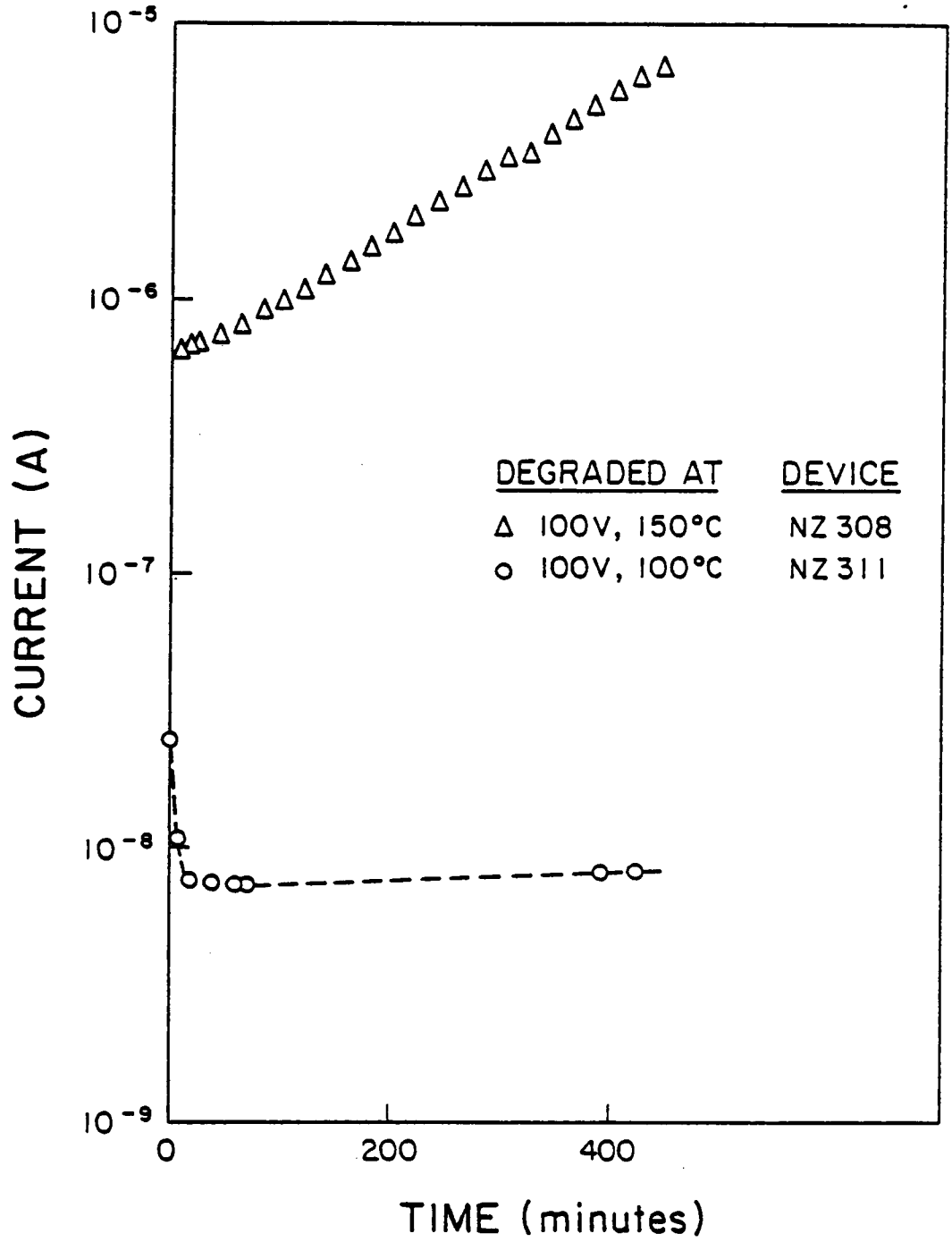

Figure 6.26 The influence of temperature on leakage current and degradation rate.

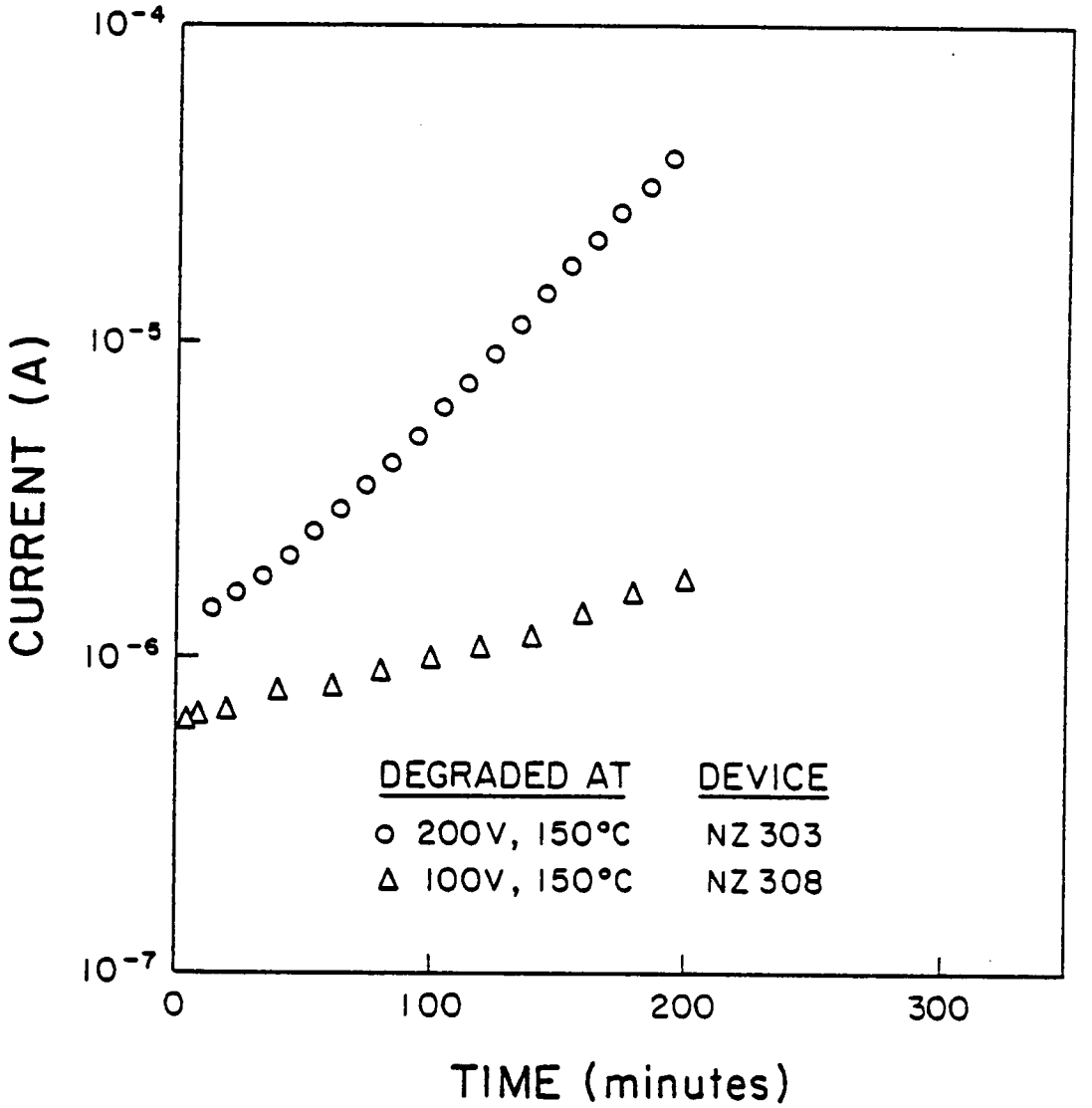

Figure 6.27 The influence of voltage on degradation rate.

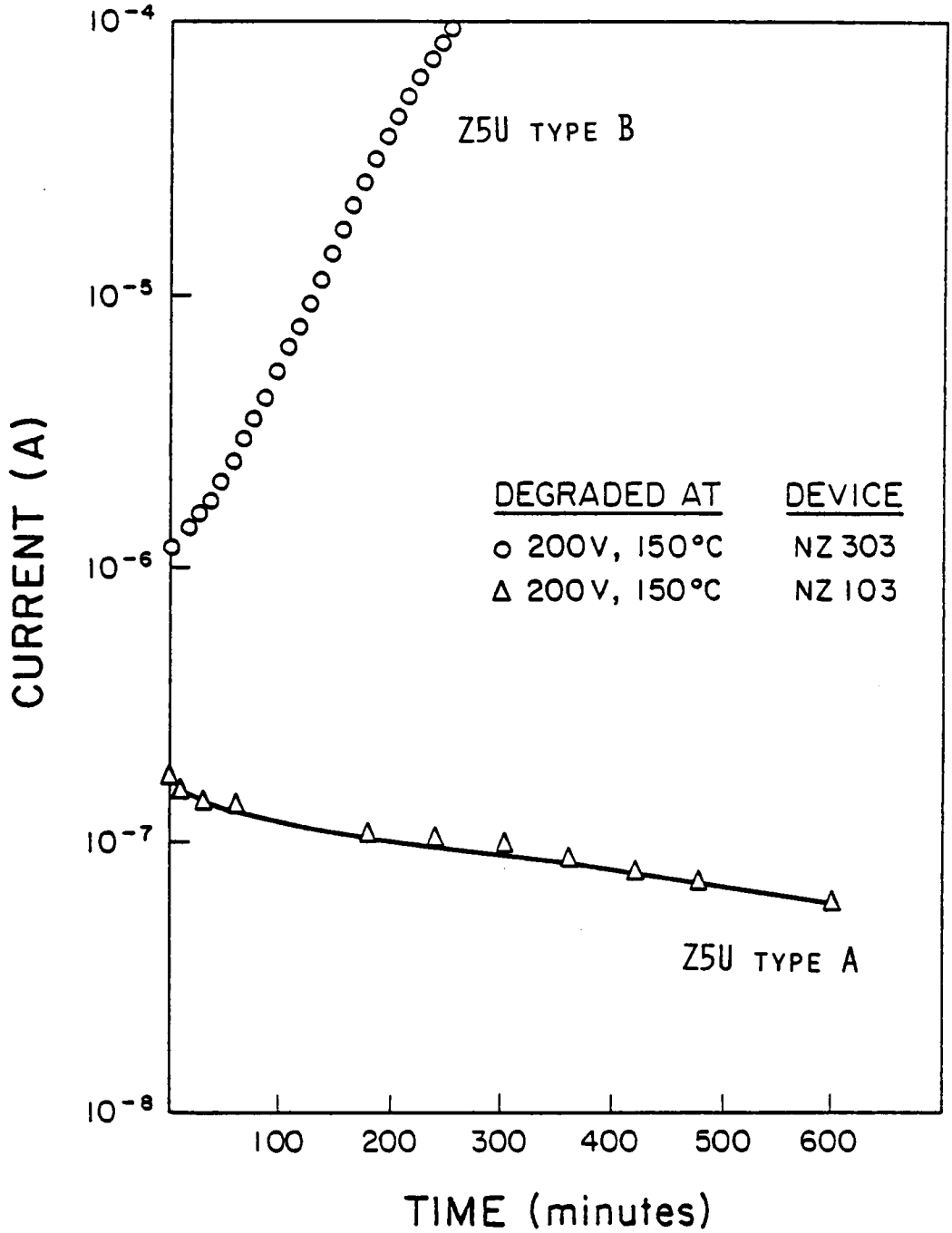

Figure 6.28 Comparison of life test curves for Z5U type A and type B capacitors under equivalent test conditions

At relatively lower temperature and voltage stresses the leakage current initially decreases and then either stabilizes or continues to slowly increase in resistivity over a long time period, behaving like capacitor NZ103. As the temperature and voltage stress is increased, the initial decrease in leakage current is seen. However, after the initial decrease, the leakage current will show an exponential rise with degradation time, as illustrated by NZ303. The slope of this exponential increase will rapidly rise with increasing temperature and voltage. This exponential rise in leakage current is what would be expected if leakage current is ionic or has a measurable ionic component. One of the major problems that was encountered when trying to degrade capacitors was the problem of finding the right ranges of voltage and temperature stress to degrade capacitors in a reasonable time span without having a large proportion of early failures due to extrinsic defects (Figures 6.29 and 6.30). Figure 6.31 illustrates the problem for X7R capacitors. Capacitors tested at 200 volts or less did not exhibit degradation, even when tested for 30 days. Raising the voltage to 400 volts was required for a reasonable degradation rate. However, due to a very high extrinsic failure rate at this voltage stress, several capacitors were

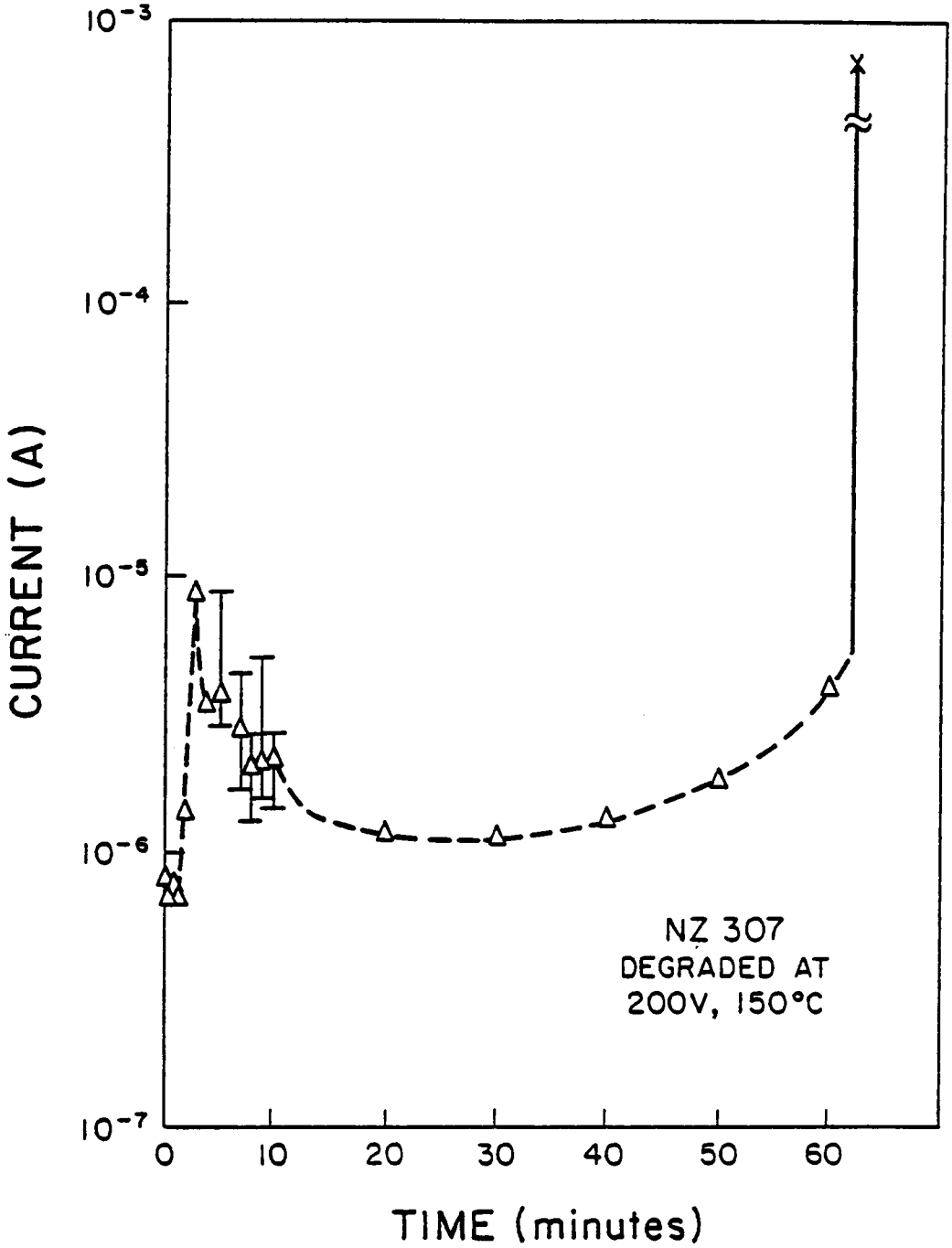

Figure 6.29 Typical life test curve for a capacitor that failed due to extrinsic defects. The current instability and instantaneous rise in current are characteristic of extrinsic failures.

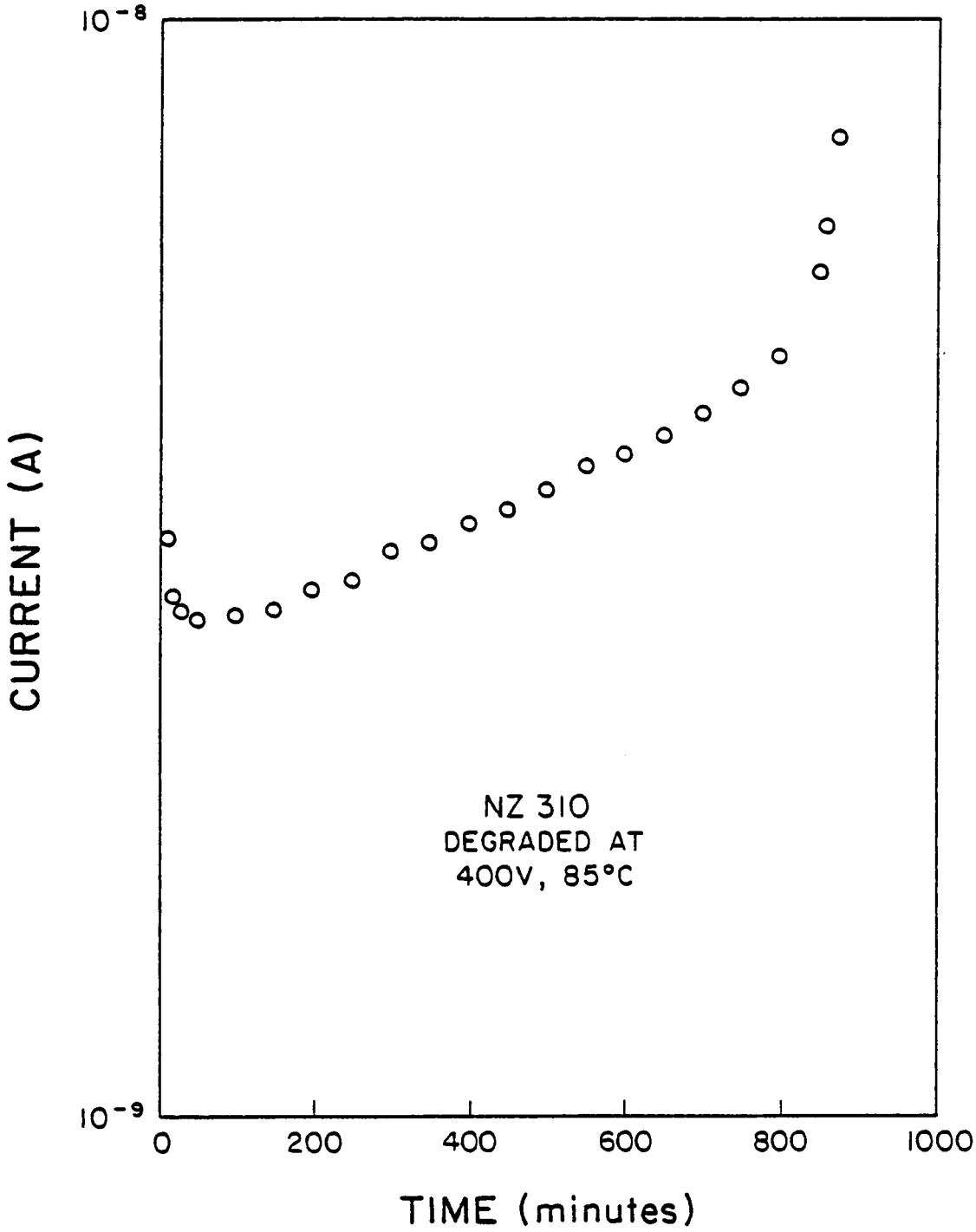

Figure 6.30 Z5U type B capacitor which failed due to an extrinsic defect. While current is fairly stable and thermal runaway is indicated by the tail of the curve, failure occurred at a current level four orders of magnitude below the normal level for this type of capacitor indicating a localized heating and consequent failure.

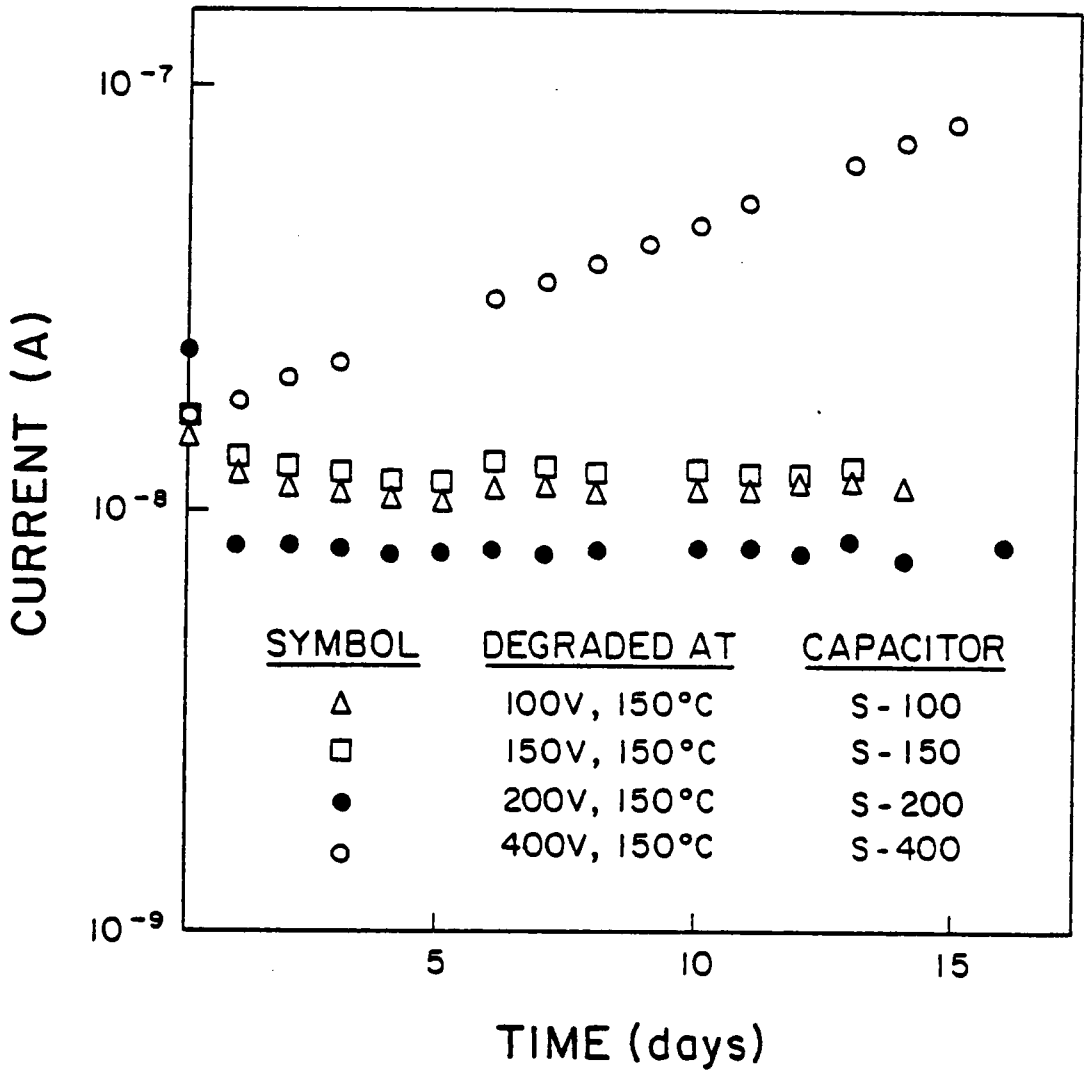

Figure 6.31 Leakage currents at 5 volts for X7R type B capacitors degraded at 100,150, 200, and 400 volts and 150°C. Only the capacitor tested at 400 volts had a measurable degradation rate.

tested before one degraded intrinsically at 400 volts. By comparison, Z5U type B capacitors could be degraded easily, at high degradation rates, and with a much lower incidence of extrinsic failures. Because of these characteristics, Z5U type B capacitors were chosen for two additional types of testing. These two tests were developed to further examine conduction and degradation mechanisms. The first test examined the capacitors ability to heal. Z5U type B capacitors were degraded at 150^{o}C under a DC voltage stress and then allowed to sit at temperature with the voltage stress turned off. After a period of time the stress was reapplied and the leakage currents measured. The results of this test showed that these capacitors can "heal" (Figure 6.32). The second test examined how reversing the polarity on a degraded capacitor changes the degradation characteristics. The results of this experiment were extremely interesting. When the polarity is reversed in a degrading capacitor the leakage current rapidly drops and then increases exponentially with time as before. If the polarity is switched again, the same thing happens (Figure 6.33). Two important aspects may be noted from this experiment:

1) the rapid drop in leakage current with polarity reversal.

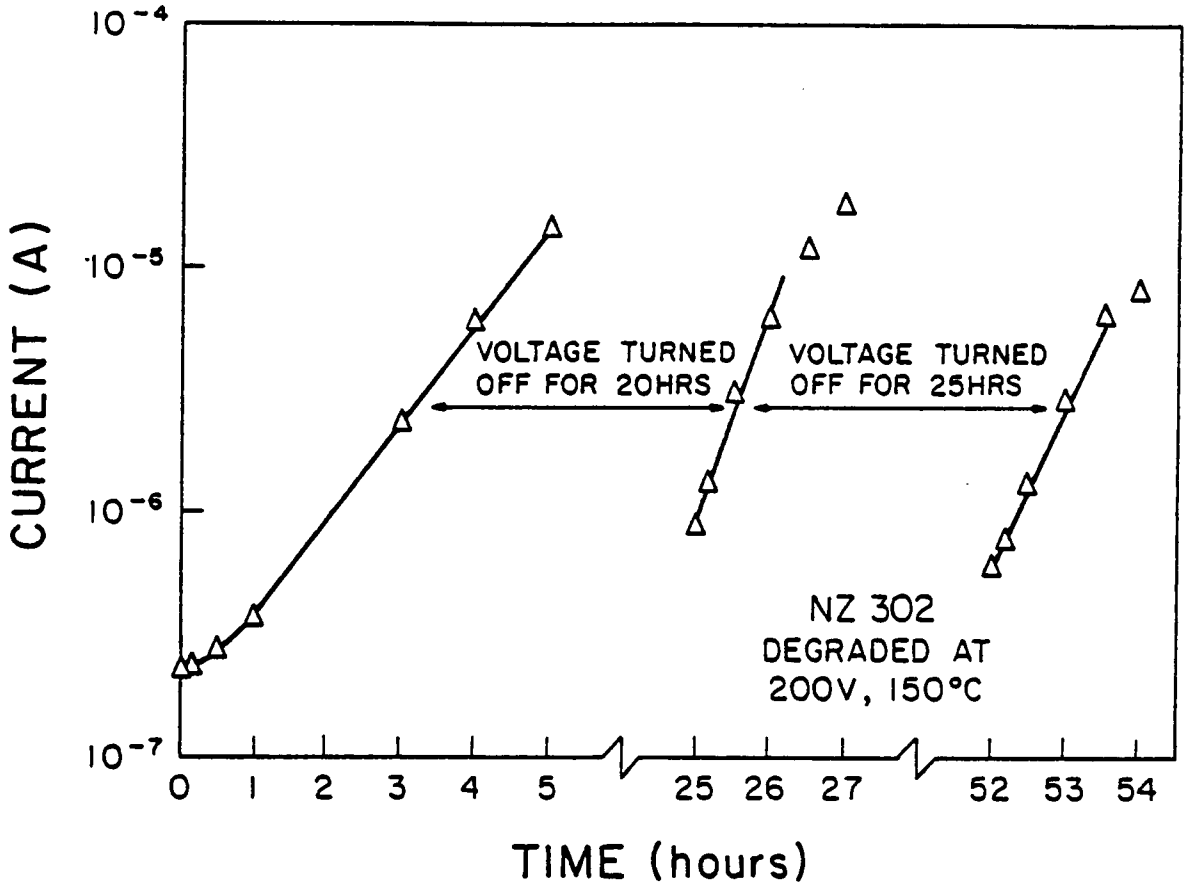

Figure 6.32 Life test curves for a Z5U type B capacitor illustrating their ability to heal when the voltage stress is removed.

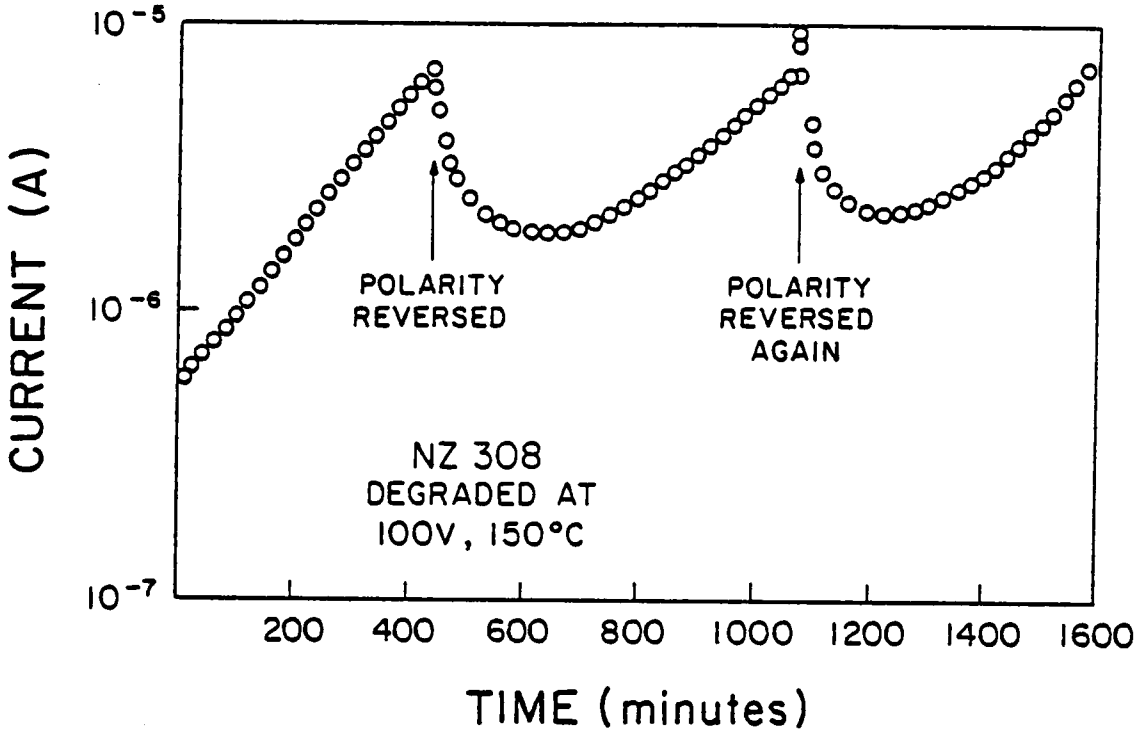

Figure 6.33 The effect of polarity reversal on capacitor leakage current. Note the decreasing slope with each polarity reversal.

2) the rate of current increase with time decreases with each polarity reversal. The importance of these results will be examined in the next chapter.

6.3.3.2 Activation Energies vs Degradation.

The leakage current vs degradation study on Z5U type B capacitors was repeated at a lower temperature (100°C), extending capacitor lifetimes and allowing periodic thermal activation energy measurements to be taken. Calculated thermal activation energies were found to decrease with degradation as shown in Figure 6.34. There is an initial drop and then a slow decrease with further degradation. These results are quite similar to those found for X7R capacitors, as illustrated in Figure 6.35. The trend of decreasing activation energy with time is quite uniform and was even noted for capacitors tested at lower temperature and voltage stresses where resistivity was not noticeably degrading.

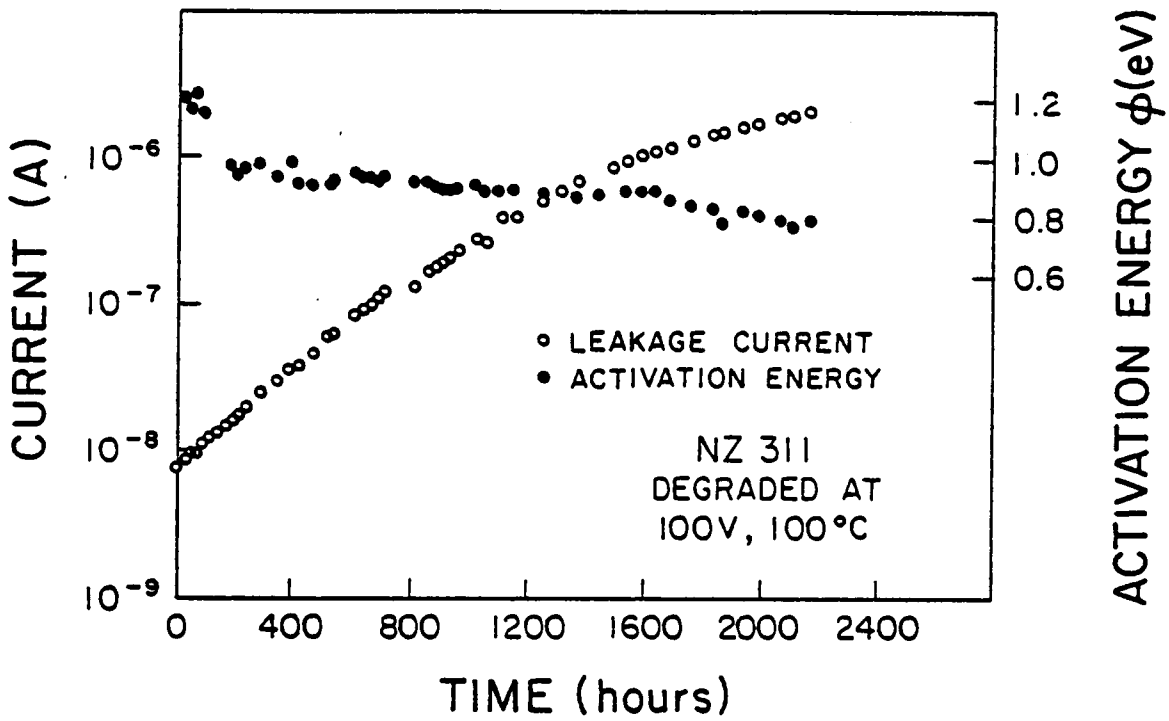

Figure 6.34 Activation energy versus degradation for a Z5U type B capacitor. Plotted with leakage current for comparison.

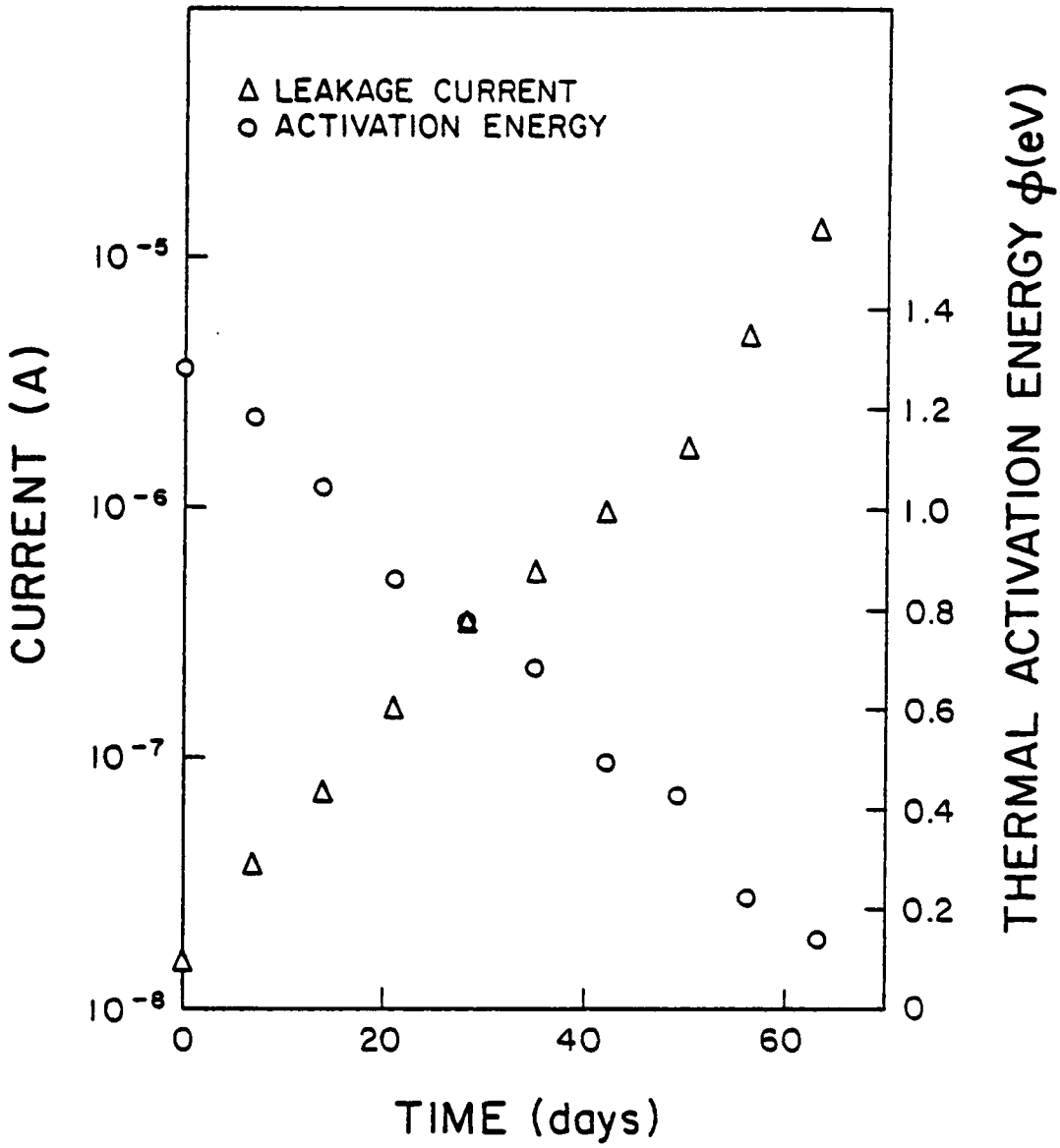

Figure 6.35 Activation energy versus degradation for an X7R type B capacitor. Plotted with leakage current for comparison[61].

6.4 Hall mobilities.

Hall mobilities were found to be less than 1 X $10^{-2}cm^2/V$ sec for both the new and hydrogen reduced samples. Figure 6.36 shows typical results for a hydrogen reduced specimen. No change in sample voltage was found for any of the X7R ceramic samples tested using the Van der Pauw method. Since the change in current was buried in the sample noise, the maximum value of 1 X$10^{-2}cm^2/V$ sec was deduced by calculating the maximum mobility that could be hidden in the sample noise. This Figure applies to the hydrogen reduced X7R type B ceramic over the temperature range of 35°C to 200°C, and to the new X7R ceramic from 100°C to 200°C. Problems with sample noise in the new ceramic prevented accurate measurements below about 90°C. The AC hall effect setup was plagued by an unknown source of noise and as a result this test was abandoned.

6.5 Photoconductivity

In the photoconductivity measurements on cross sectioned capacitors no change in conductivity was measured. It was felt that surface leakage currents were masking photoconductivity effects. Indications of surface effects on

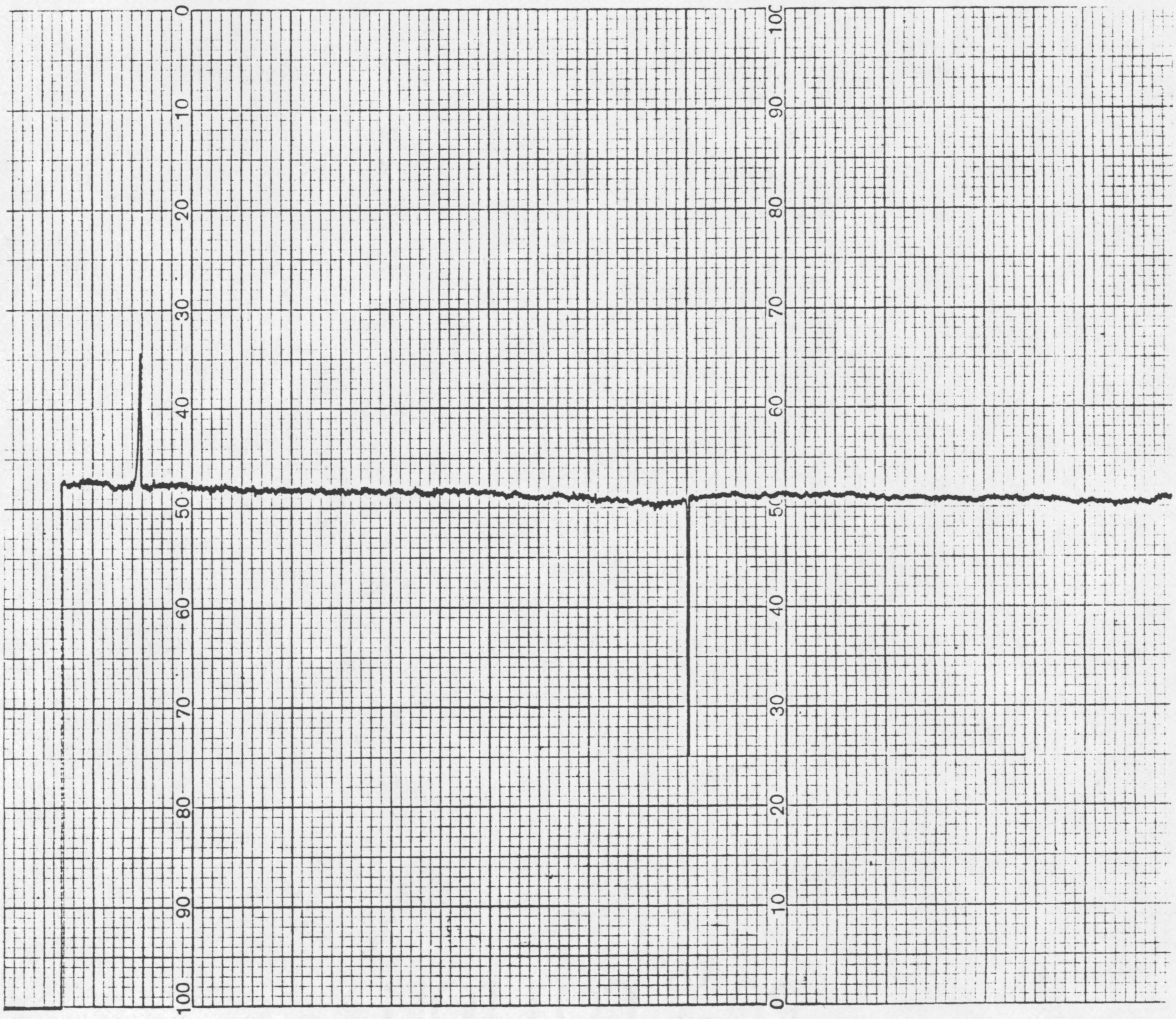

Figure 6.36 Chart recorder plot of voltage from picoammeter measuring hall voltage. Voltage spikes indicate the magnetic field being turned on (left) and off (right). No change in voltage appeared when the magnet was turned on (Hall voltage is buried in noise). Magnetic field strength: 13KG. Full scale is one millivolt.

conductivity were found in an applied voltage optical experiment. Optical studies of cross-sectioned capacitors under an applied voltage showed bright spots - areas of higher conductivity causing photon emission by luminescence or heating (Figure 6.37). (The applied voltage experiment was initially designed to study electrical degradation optically at room temperature. Capacitors were mounted in epoxy with their leads intact and cross-sectioned. These capacitors were then observed under the optical microscope before and during an applied voltage application. Due to arcing at high fields this test was dropped.)

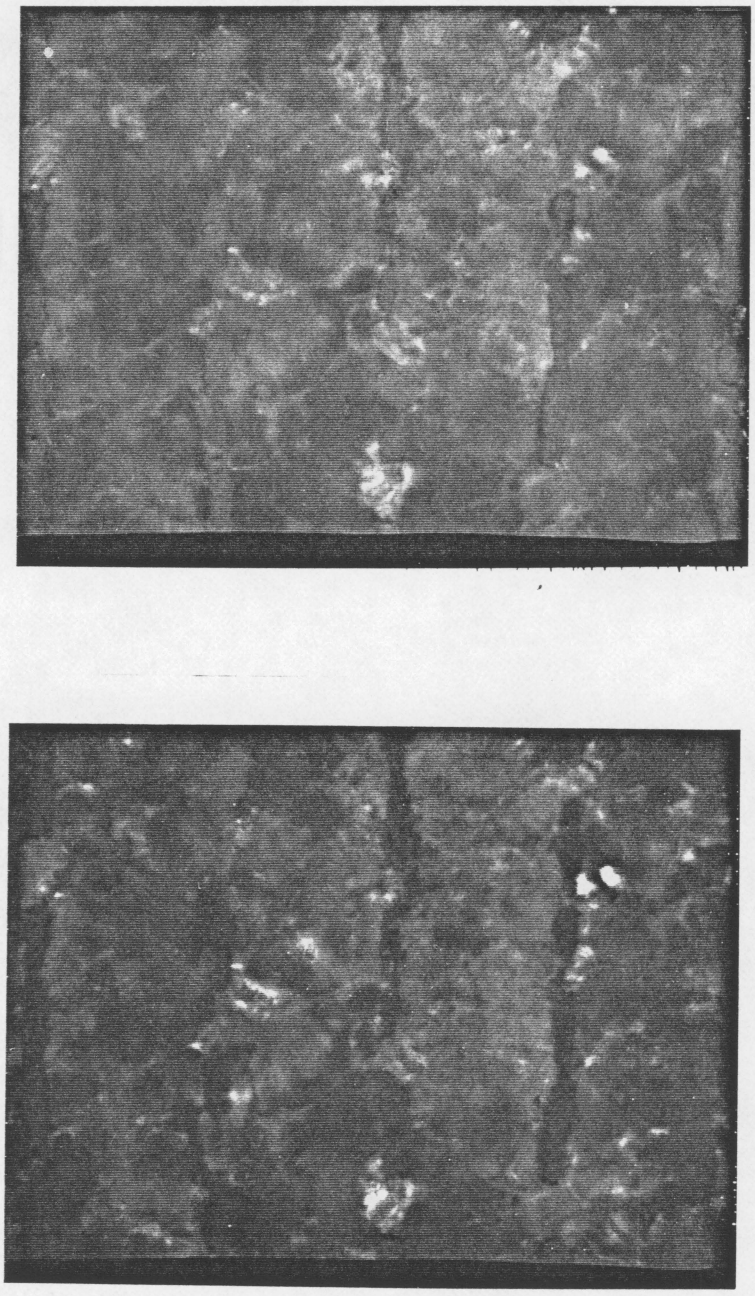

Figure 6.37 Comparison of a cross-sectioned Z5U type B capacitor with and without an applied voltage stress. (a) no voltage, (b) 200 volts applied. (900X)

Chapter VII

DISCUSSION

The degradation behavior seen in the Z5U type B capacitors and the other types is extremely interesting. Analysis of the electrical behavior of degrading capacitors will be divided into two parts:

a) Changes in I-V curves and activation energy with degradation,

b) Changes in resistance with degradation.

The first part explains how conduction is occurring. The second explains the conduction mechanism and why leakage current changes with time.

7.1 I-V Curves and Activation Energies.

The I-V curves and activation energy studies yield valuable insights into conduction in MLC's. There were three items of interest noted in the I-V curves of X7R capacitors:

1) an ohmic region which slowly increases with degradation.
2) an approximately 3/2 power law behavior above the ohmic region.

3) a shift from Child's law behavior ($I \propto V^{3/2}$) to a square law dependance when capacitors become severely degraded.

The slow shift upwards in the ohmic region indicates that a gradual increase in the donor density is occurring with degradation. The linearity of the I-V curves with a slope n between 3/2 and 2 indicates space charge limited conduction. Schottky or Poole-Frenkel emission can be eliminated as possible conduction mechanisms for the capacitors tested here, since their I-V curves are linear. One possible explanation for the 3/2 power law in the X7R capacitors, is space charge injection from electrode protuberances, as was explained in Chapter 4. The large numbers of bulges and asperities found in the capacitors examined generally support this postulation. The shift to a quadratic dependance from a 3/2 power law can be readily explained if oxygen diffusion is accepted as the cause of degradation. The movement of oxygen vacancies to the cathode with degradation would produce a lower resistivity region around the protuberances and blunt their effect on conduction (Figure 7.1). This observation compliments the idea of a moving cathode, which has been explained in detail by Huebner and Anderson [58].

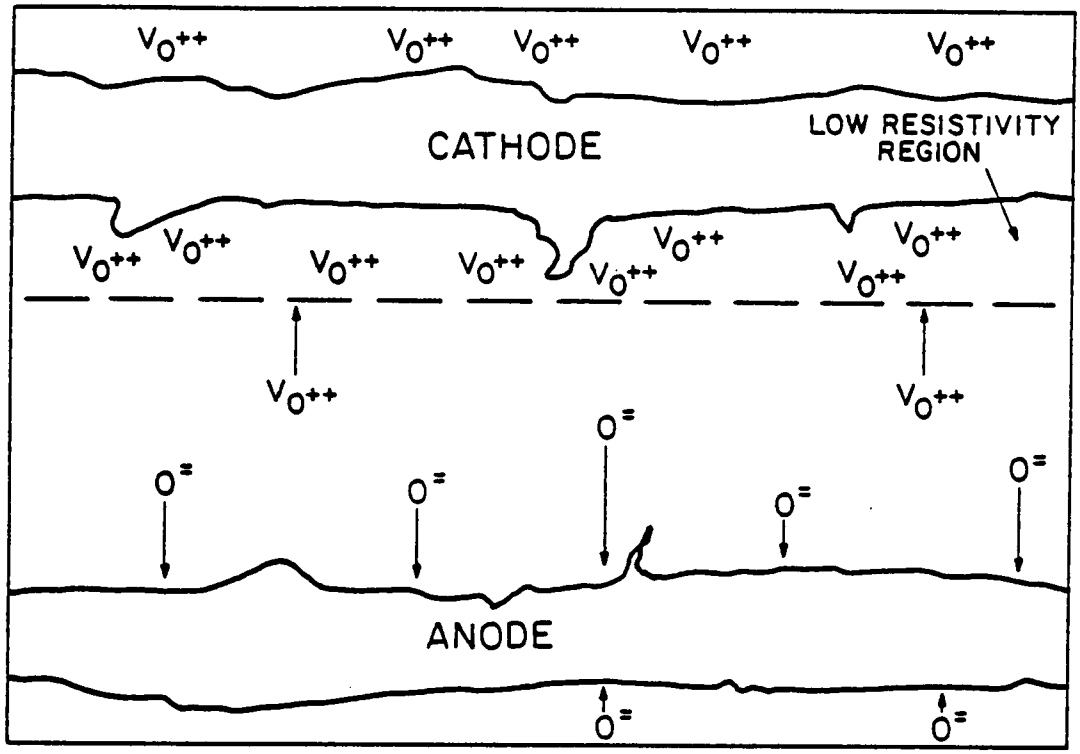

Figure 7.1 Diagram showing the proposed effect of oxygen migration to the cathode. The decreased resistivity would blunt the effect of electrode protuberances.

The thermal activation studies revealed two important features:

1) activation energies were voltage independent.
2) activation energies slowly declined with degradation.

In MLC's thermal activation energies may measure any one of four possible work functions:

a) contact potential between the electrode and ceramic (Schottky barrier).
b) contact potential between grains (Poole-Frenkel Barrier).
c) grain boundary potential barrier.
d) a hopping potential.

Since none of the capacitors tested here exhibited Schottky or Poole-Frenkel type currents a and b may be eliminated. While tests were not performed to differentiate between small polaron hopping and grain boundaries, it is suggested here that the work function is due to grain boundaries. Since grain boundaries have been shown to influence capacitor lifetimes and dielectric breakdown strength, it is probable that grain boundaries affect current flow. Hopping potentials are related to the barrier

height between jump sites and imply that grain boundaries do not present a significant barrier to conduction.

If activation energies in these capacitors are due to grain boundary potential barriers, the voltage independent activation energy indicates that the barrier height is clamped at the grain boundary. This may be due to an intrinsic region near the grain boundary or a high resistivity second phase between the grains (Figures 2.2b and c).

7.2 Conduction - Ionic or Electronic.

One of the big questions that has been occasionally raised and never satisfactorily answered is whether conduction in $BaTiO_3$ based dielectrics is ionic or electronic. The studies performed here have shown that both are present and the predominance of one or the other is time, temperature, and field dependant.

A calculation of the number of oxygen vacancies that would be required for completely ionic conduction showed that an oxygen vacancy density $\approx 1 \times 10^{20}$ per cm^3 would be required for an X7R type B capacitor degraded at 200V and 150°C for 15 days (Appendix A). Calculation of the oxygen

density in $BaTiO_3$ gives $\approx 2\times10^{22}$ oxygen atoms/cm^3. Given the information that the oxygen density is only two orders of magnitude larger than the density of vacancies required, and the fact that the observed current levels are completely stable under these conditions, a model proposing totally ionic conduction would be inappropriate, at least in the X7R capacitors.

All experimental results for Z5U type B capacitors point to ionic conduction:

a) observed color gradient in degraded capacitor.
b) the exponential dependance of leakage current with time.
c) the capacitors ability to heal with time.
d) the ability to almost completely reverse degradation by reversing the polarity.

That a color gradient develops between electrodes of opposite polarity is in itself a strong indicator of ionic conduction. This argument is strengthened further by the observation that this type of color gradient may be reversed by reversing the polarity[46]. The charge carriers here are most probably oxygen vacancies even though the level of the gradient was not measurable. If ionic conduction is responsible for electrical degradation then why aren't color

gradients visible on all degraded capacitors? The major factor is apparently whether the capacitor failed intrinsically or extrinsically. Only Z5U Type B capacitors which failed by thermal runaway showed signs of a color gradient in polarized reflected light. Z5U type B capacitors which "popped" or failed by avalanche breakdown did not exhibit color gradients. Since the other types of degraded capacitors studied here were typically life tested at 8 times the rated voltage and 180°C it is quite probable that almost all these capacitors all failed by avalanche breakdown since the probability (or percentage) of extrinsic failures appears to rise exponentially with increasing voltage (This observation was found by plotting statistical failure analysis data from reference 53 as shown in Figure 7.2). A examination of the life test data (where available) supported this rationalization.

The next question to be answered is: If all capacitors have similar degradation mechanisms, why are capacitor life curves so different for the Z5U type B capacitors, compared to the Z5U type A capacitors under equivalent life test conditions? Both of these curves are actually variants of a generic life test curve. The difference between the two

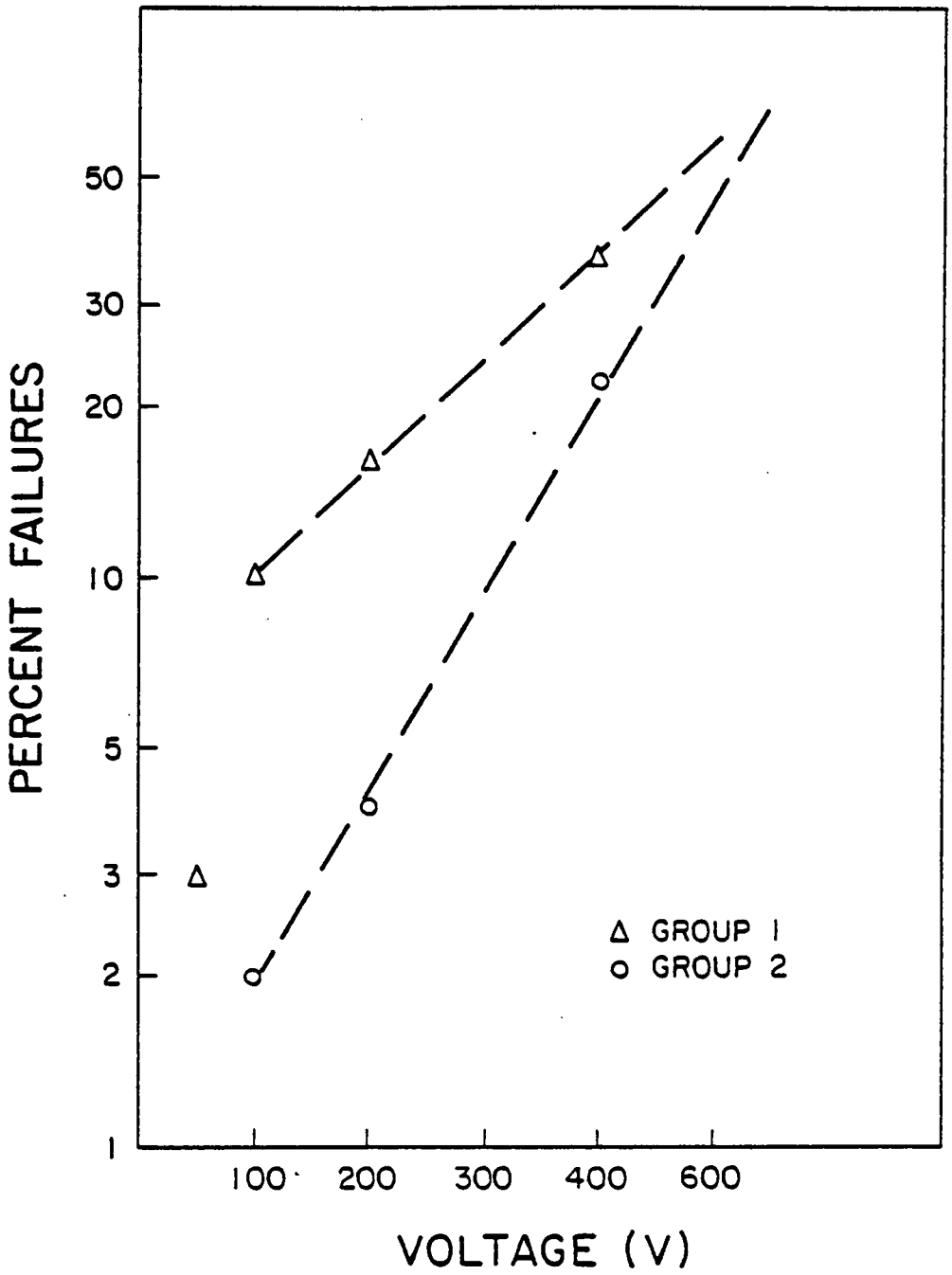

Figure 7.2 Plot of statistical life test data suggesting an exponential increase in extrinsic failures with increasing voltage stress above some minimum voltage. Data taken from reference 53.

curves is due to different compositions which have different levels of ionic and electronic conduction. The predominance of electronic or ionic conduction in a device may be easily determined by observing the time dependance of the current. If electronic conduction is the source of leakage current then the level of current will not be time dependant (Figure 7.3a). However, if ionic conduction is the major source of current flow then a plot of current versus time will be an exponentially increasing function (Figure 7.3b). This time dependant increase in leakage current, due to ionic conduction, plus the increased electronic conduction, due to the decreasing stoichiometry, is termed here as "ionically induced current". Although life test data has been plotted in a number of different ways: log I versus log $t^{(39)}$, I versus $t^{(53,62)}$, I versus log $t^{(37)}$, log J versus $t^{(58)}$, upto this point no one has proposed a model to explain capacitor life test curves. Analysis of capacitor leakage currents as a function of time has resulted in proposing the following model to explain the shape of capacitor life test curves. A general model is proposed first, followed by an explanation of the modifying factors and their influence on capacitor lifetime and the shape of the curve.

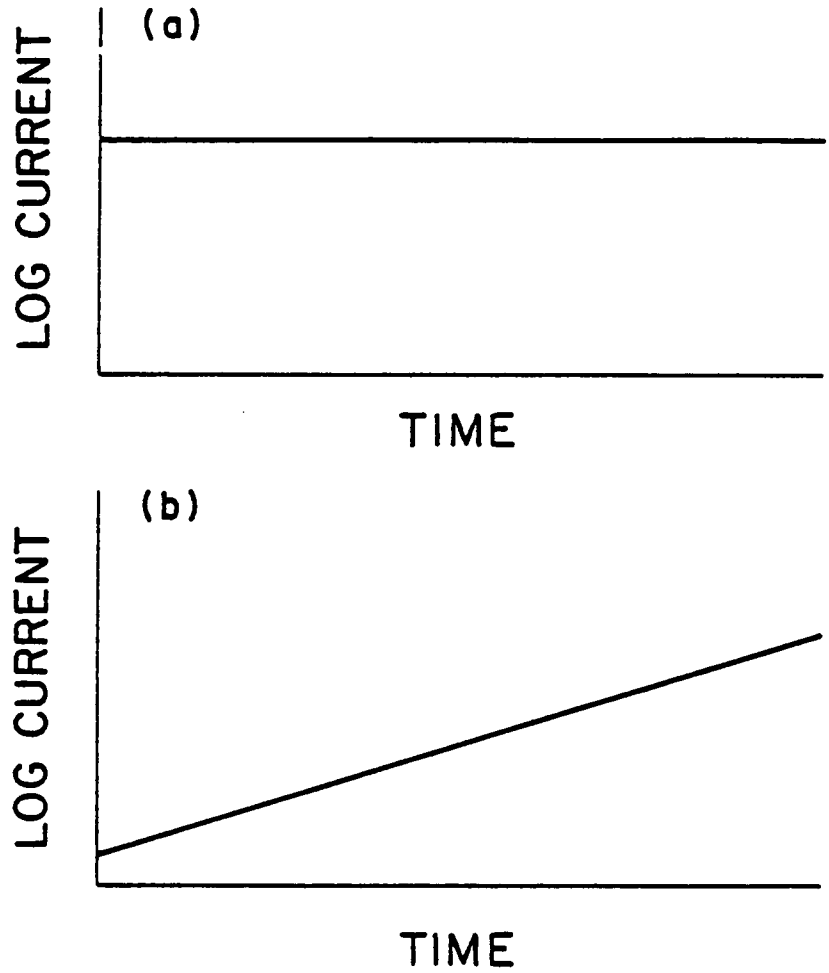

Figure 7.3 Plots of leakage current as a function of time, (a) for electronic conduction only, (b) for ionically induced current.

The key to understanding capacitor behavior is not to look at current at one point in time and decide if conduction is ionic or electronic. Conduction in MLC's may be understood by examining what would happen in a capacitor with both electronic and ionic components of conduction, where the ionic component is initially orders of magnitude below the electronic component (Figure 7.4). Initially the small ionic component of conduction is swamped out by the large electronic component and leakage current remains essentially constant with time (region I). However, eventually the ionically induced component will become measurable and leakage current will then exponentially increase with time (region II). At some point in time the current density will rise to a point where Joule heating will become noticeable and this rise in temperature will cause a synergistic reaction with the ionic reaction resulting in a super exponential rise in leakage current with time until the capacitor burns out (region III). If an initial exponentially decaying function is superimposed on this graph (Figure 7.5) we have a fair approximation of a capacitors leakage current as a function of degradation time. The reason for this exponentially decaying function is not completely understood, it may be a result of the electric field polarizing the dielectric and reducing the

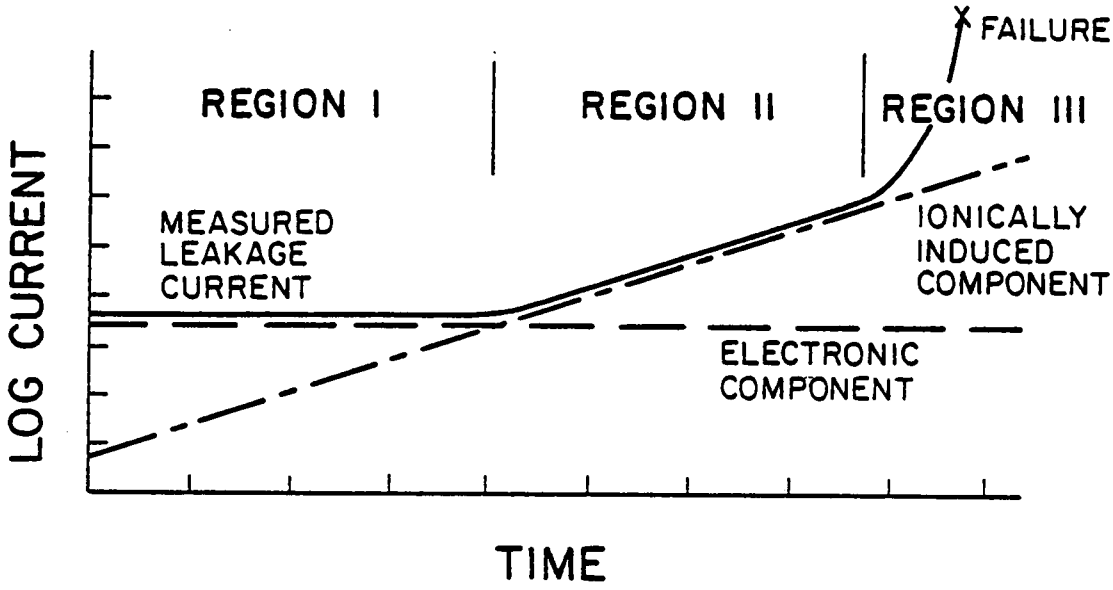

Figure 7.4 Plot of leakage current as a function of time showing the effect of an ionically induced component of current flow on the measured value of leakage current.

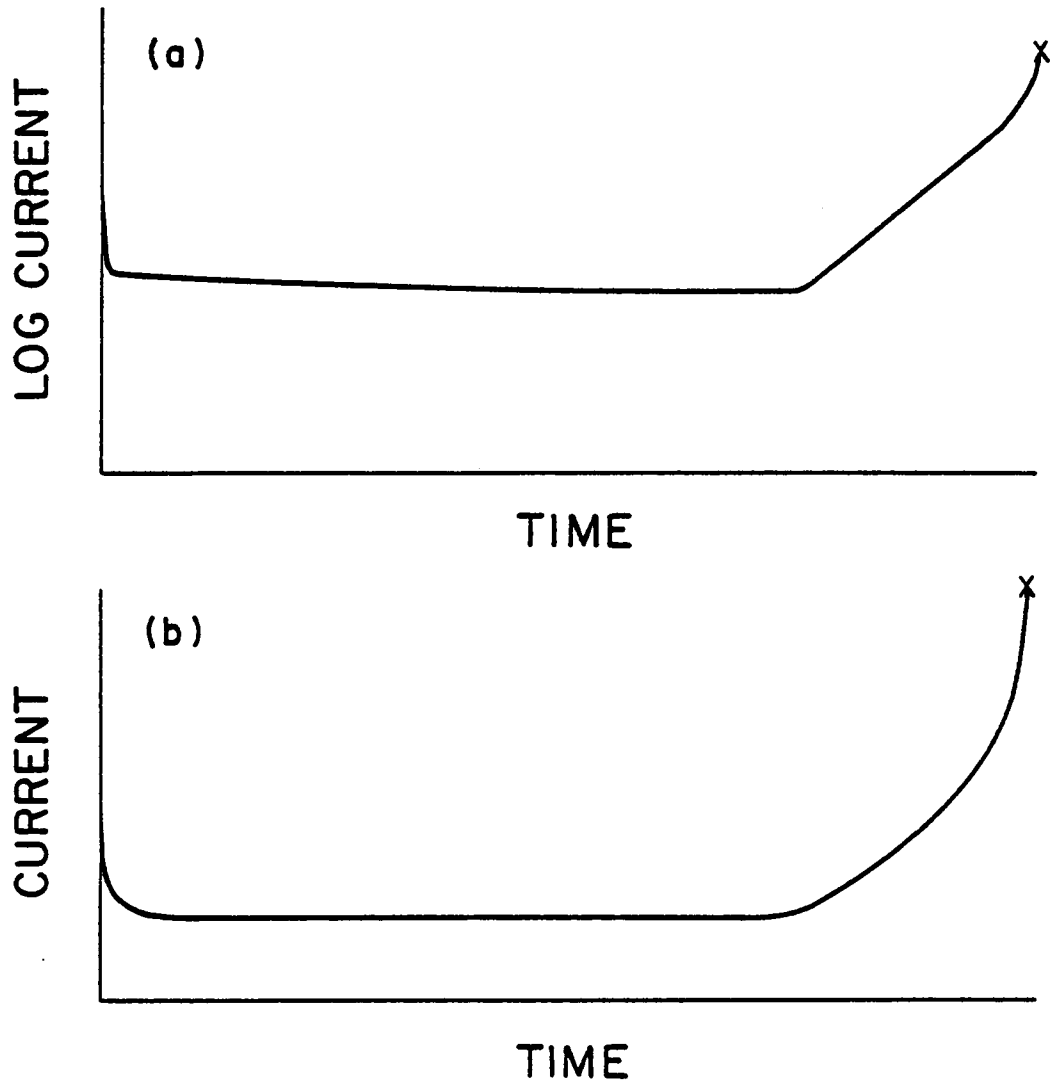

Figure 7.5 Generic life test curve for a MLC capacitor, (a) Ln current vs. time, (b) current vs. time.

effective field, or it may be due to an initial change in the dielectric constant affecting SCLC resulting in a reduction in leakage current. The longer term slight decrease in leakage current with time (as observed in some life tests), may possibly be due to an increase in the oxygen vacancy concentration since certian dielectric compositions show an increase in resistivity when fired in reducing atmospheres. The actual appearance of a capacitors life test curve (leakage current vs degradation), depends on three interrelated factors:

a) Capacitor Composition

b) Test Temperature

c) Applied Field

The capacitor composition determines the initial value of ionic current, slope of the current increase, and the level of electronic current at a given temperature and voltage stress. Temperature will cause a shift upwards in both the curves and increase the slope of the ionic current. The effect of raising either temperature or voltage stress is illustrated in Figure 7.6.

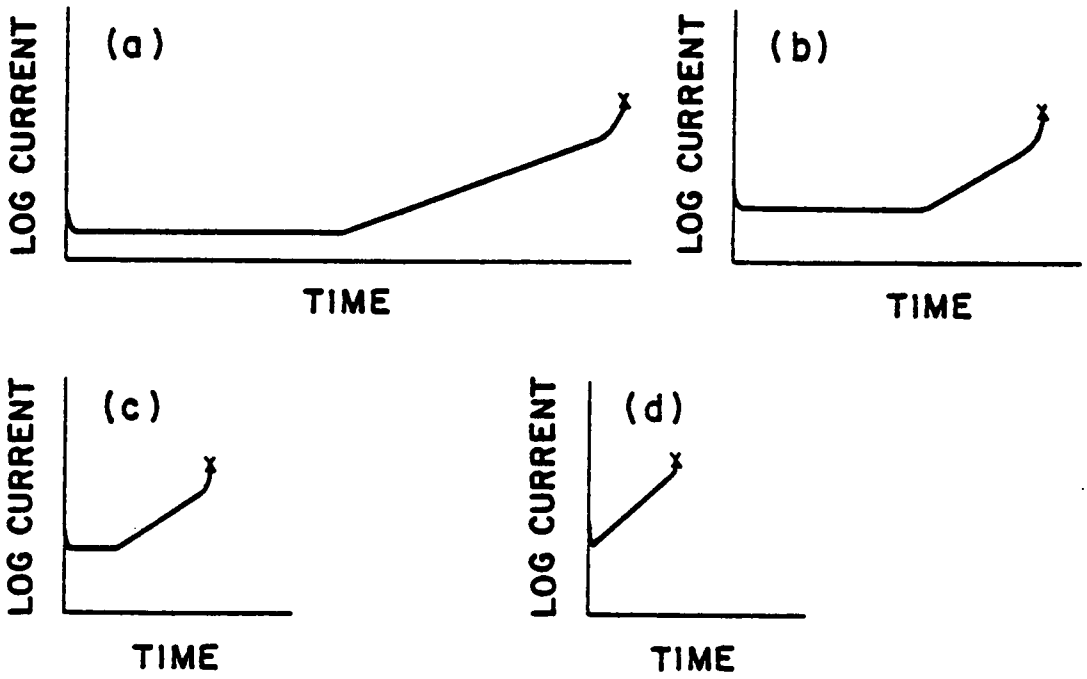

Figure 7.6 Plots of leakage current versus time showing the effects of raising either temperature or voltage. (increasing from a to d)

Chapter VIII

SUMMARY AND CONCLUSIONS

The main objectives of this research were: to examine capacitor microstructures; to examine electrical characteristics of capacitors, and how they change with degradation; to check for compositional changes in capacitors due to degradation; and to understand why capacitors degrade intrinsically. This research has demonstrated how capacitors current-voltage characteristics, activation energies, and leakage currents change with degradation and has provided information leading to the development of a model for capacitor life test characteristics. The important observations of this study were:

1) DC leakage currents in new X7R capacitors follow a near 3/2 power dependence above ≈1 volt, with ohmic behavior at lower voltages.
2) With degradation the range of the ohmic region increases and the Childs law behavior shifts to a square law dependence (X7R's).
3) The increase of the ohmic range can be attributed to an increased donor density (X7R's).

4) The 3/2 power and square law current-voltage behavior can be modelled after space charge limited currents. The 3/2 case can be attributed to electrode protuberances and geometry. The square law dependence can be attributed to emission from planar electrodes (X7R's).
5) DC leakage currents in Z5U capacitors have a nearly ohmic dependence.
6) Schottky or Poole-Frenkel currents were not found.
7) Large numbers of electrode protuberances were seen in cross-sectioned devices - these were correlated to the $I \propto V^{3/2}$ dependence found in X7R's.
8) Symmetric color gradients were found between positive and negative electrodes in degraded capacitors. The color gradient is ascribed to oxygen vacancy migration to the cathode. The shift to a V^2 dependence is attributed to the consequent formation of a low resistivity region at the cathode.
9) Compositional gradients were not detected in degraded capacitors, indicating gradients (if present), are less than 0.1 atomic percent.

10) Activation energies were found to be voltage independent in X7R and Z5U capacitors. This finding also indicates that Schottky or Poole-Frenkel currents are not present.
11) Activation energies were observed to slowly decline with degradation.
12) Tremendous differences in degradation resistance were observed for different commercial capacitor compositions, indicating large differences in long term reliability exist between manufacturers.
13) Electrical degradation was observed to follow an exponential curve with time ($\ln I \propto t$) leading to a model for conduction in MLC's.

Chapter IX

REFERENCES

1. K.Rothschild, *Electronic News*, Aug 13, 5, 1984.

2. E.I.A.Standard, *RS-469*, Electronic Industries Association, Washington D.C. 1980.

3. W.J.Minford, *IEEE-CHMT*, Vol.5, p 297, 1982.

4. *The Reliability of Multilayer Ceramic Capacitors*. Publication NMAB-400, National Academy of Sciences, Washington, D.C. 1983.

5. G.Goodman, *J.Am. Cer. Soc.*, Vol.46, p 48, 1963.

6. W.R.Buessem and T.I. Prokopowicz, *Ferroelect.*, Vol.10, p 225, 1976.

7. K.R.Choudary and E.C.Subbarao, *Ferroelect*, Vol.35, p 689, 1981.

8. D.Kolar, S.Gaberscek, Z.Stadler and D.Suvorov, *Ferroelec*, Vol.27, p 269, 1980.

9. E.C.Subbarao, V.C.S.Prasad and K.Veerabhadra Rao, *Preparation and Characterization of Materials* Edited by J.Honig and C.N.R.Rao, Academic Press, New York.

10. A.M.J.H.Seuther, *Phillips Research Report Supplement*, Vol.3, p 210, 1979.

11. J.B.MacChesney, P.K.Gallagher, and F.U.Dimarcello, *J.Am.Cer.Soc.*, Vol.46, p 197, 1963.

12. W.R.Bratschum, *J.Am.Cer.Soc.*, Vol.45, p 161, 1962.

13. F.W.Ainger and J.M.Herbert, *Trans. Brit. Cer. Soc.*, Vol.58, p 410, 1976.

14. N.H.Chan and D.M.Smyth, *J.Electrochem Soc.*, Vol.123, p 1584, 1979.

15. S.B.Desu and E.C.Subbarao, *J.Mat.Sci.*, Vol.15, p 2113, 1981.

16. Kiyoshi Okazaki and Hideji Igarashi, *Ferroelec*, Vol.27, p 263, 1980.

17. I.Ihrig, *J.Phys. C.Solid State Physics*, Vol.11, p 819, 1981.

18. I.Burn and J.M.Maher, *J.Mat Sci.*, Vol.10, p 633, 1976.

19. Yukio Sakabe, Kuchi Minai and Kikuo Wakino, *Japan J.Appl. Phys.*, Vol.20, p 147, 1981.

20. E.C.Subbarao, *Ferroelec*, Vol.35, p 143, 1981.

21. D.A. Payne, *The Role of Internal Boundaries upon the Dielectric Properties of Polycrystalline Ferrroelectric Materials*. Pennsylvania State University, 1976.

22. W.Heywang, *J.Mat.Science*, Vol.6, p 1214, 1971.

23. B.A.Rotenberg, Y.U.L.Danilyuk, E.I.Gindin and V.G.Prokhatilov, *Fizika Tverdogo Tela*, Vol.7, p 3048 1965, Soviet Phys. Solid State, Vol.7, p 2465, 1966.

24. G.H.Jonker, *Solid State Electronics*, Vol.7, p 895, 1964.

25. H.Schmelz, *Phys.Stat. Sol.* Vol.35, p 219, 1969.

26. W.Heywang, *J.Am.Cer.Soc.*, Vol.47, p 484, 1964.

27. Hiroshi Ikushima and Shigeru Hayakawa, *Japan J.Appl.Phys.*, Vol.4, p 328, 1967

28. Tatsuo Fukami, and Hidetoshi Tsuchiya, *Japan J.Appl.Phys.*, Vol.18, p 735, 1979.

29. M.Kahn, *Effects of Sintering and Grain Growth Reactions on the Distribution of Niobium Additives in Barium Titanate Ceramics*. Pennsylvania State University, 1969.

30. T.Ashida, and H.Toyoda, *Japan J.Appl.Phys.*, Vol.5, No.4, p 269, 1966.

31. H.Nemoto and I.Oda *J.Am.Cer.Soc.* Vol.63, p 398, 1980.

32. P.Gerthsen and K.H.Hardtl, *Z.Naturf.* Vol.18a, p 423, 1963.

33. H.Rehme, *Phys. Stat. Sol.*, Vol.18, K 101, 1966.

34. H.B.Haanstra and H.Ihrig, *Phys. Stat. Sol.* Vol.a39, K7, 1977.

35. H.Ihrig and M.Klerk *Appl. Phys. Letters*, Vol.35, p 307, 1979.

36. K.Lehovec and G.A.Shirn, *J.Appl.Phys.* Vol.33, p 2036, 1962.

37. Y.Goto and S.Kachi, *J.Phys. Chem. Solids*, Vol.32, p 889, 1971.

38. C.Schaffirn, *Phys. Stat. Sol.*, Vol.35a, p 79, 1976.

39. W.A.Schulze, L.E.Cross and W.R.Buessem *J.Am.Cer.Soc.*, Vol.63, p 83, 1980.

40. D.A.Payne, *Sixth Annual Proceedings, Reliability Physics Symposium*, October 1973.

41. J.V.Biggers and G.J.Gardopee, *Cer. Bull.* Vol.53, p 853, 1974.

42. K.Sato, Y.Ogata, K.Ohno, and H.Ikeo,. *IEEE*, p 205, 1980.

43. K.V.Ya, A.N.Tsikin and N.Shturbina, *A.Soviet Phys-Solid St.* Vol.11, p 598, 1969.

44. M.S.Kosman and E.V.Bursian, *Soviet Phys-Dokl*, Vol.2, p 354, 1957.

45. L.Benguigui, *J.Phys.Chem.Solids*, Vol.34, p 573, 1973.

46. Y.Goto and S.Kachi, *J.Phys.Chem.Solids*, Vol.32, p 889, 1971.

47. H.Arend,P.Coufova and J.Novak, *J.Am.Cer.Soc.*, Vol.50, p 22, 1967.

48. S.Ikegami and I.Ueda, *J.Phys.Soc.Japan*, Vol.19, p 159, 1964.

49. P.Coufova and H.Arend, *Czech.J.Phys.*, Vol.11, p 416, 1961.

50. K.Okazaki, *Recent status of Ceramic Multilayer Capacitors in Japan*, Amer.Cer.Soc.-31st Pacific Coast Regional Meeting,1978.

51. T.I.Prokopowicz and A.R.Vaskas, *ECOM-90705-F, NTIS, AD-864068*, p 175, 1969.

52. W.J.Minford, *Proceedings of Symposium on Capacitor Technologies - Applications and Reliability*. p 93, 1981.

53. B.S.Rawal and N.H.Chan, *AVX Technical Bulletin*.

54. P.Nagels, *The Hall Effect and Its Applications* (C.L.Chien and C.R.Westgate, editors), Plenum Press, 1980.

55. M.A.Lambert and P.Mark, *Current Injection in Solids*, Academic Press, 1970.

56. M.A.Lambert and P.Mark, *Semiconductors and Semimetals*, Vol.6, Academic Press, 1970.

57. T.W.Hickmott, *J.Appl.Phys.*, Vol.51, p 4269, 1980.

58. W.Huebner, H.U.Anderson and D.E.Day, *Reliabilty Studies of Ceramic Capacitors* Progress Report for the period of July 1983-Oct.1984, ONR, 1984.

59. P.Gerthsen, K.H.Hardtl and A.Csillag, *Phys.Stat.Sol.(a)* Vol.13, p 127, 1972.

60. Hee Young Lee, *unpublished research*, VPI&SU, 1985.

61. Sanjai Agarwal, *unpublished research*, VPI&SU, 1985.

62. E.Loh, *J.Appl.Phys.*, Vol.53, p 6229, 1982.

Appendix A

Calculation of Oxygen Vacancy Concentration for X7R type B Capacitors

Sample calculation for an X7R type b capacitor degraded at 200V and 150°C. (device S-200)

For ionic conduction, the number of vacancies required is given by the expression:

$$V_o = \frac{\int I \, dt}{2 q} \qquad (1)$$

where V_o = oxygen vacancy concentration

I = leakage current

q = charge on an electron

t = time

Since current was stable with time for this capacitor, equation (1) reduces to:

$$V_o = \frac{I \, t}{2 q} \qquad (2)$$

$$V_o = \frac{(1.17C/s)(15days)(24Hrs/day)(60min/Hr)(60s/min)}{(2)(1.602\times10^{-19}C)}$$

Which yields

$V_o = 4.73\times10^{18}$ for 15 days

The density of V_o produced is given by the expression:

$$D_v = \frac{V_o}{A\ d} \qquad \text{or} \qquad D_v = \frac{V_o}{V_{eff}}$$

where D_v = density of oxygen vacancies

A = total cross-sectional area between electrodes

d = dielectric thickness

V_{eff} = effective volume

The effective volume of a capacitor may be determined by either measurements on cross-sectional area or from the capacitance and dielectric constant, using the equation:

$$C = \frac{\varepsilon\ A}{d} \qquad (3)$$

This formula may be rearranged to give

$$A = \frac{C\ d}{\varepsilon}$$

For X7R type B capacitors:

$C = 1\mu F$

$d = 25\mu m$

$\varepsilon = 1800\varepsilon_o$

where ε_o = permittivity of free space

these values yield: $A = 15.99\ cm^3$

Substituting A and d into equation (2) yields:

$$D_v = \frac{4.73\times10^{18}(\text{oxygen vacancies})}{(15.99\ cm^2)(25\mu m)}$$

or

$$D_v = 1.2\times10^{20}\ \text{oxygen vacancies}/cm^3$$

This may be compared to the density of oxygen atoms in $BaTiO_3$:

$$D_o = \frac{\text{density}(BaTiO_3)\times\text{Oxygen atoms/molecule}}{\text{atomic wt}} \times N$$

where D_o = density of oxygen atoms

N = Avagadro's number of molecules

For $BaTiO_3$:

atomic wt = 137.34+204.37+(3)(16.00)

= 389.71 g/g·mole

assuming the dielectric is 95% dense:

$$\text{density}(BaTiO_3) = 5.7\ g/cm^3$$

$$D_o = \frac{(5.7 g/cm^3)(3)(6.023\times10^{23} mole^{-1})}{389.71\ g/g\ mole}$$

Which yields:

$$D_o = 2.65\times10^{22}\ atoms/cm^3$$

The vita has been removed from the scanned document

The vita has been removed from the scanned document